Biochemical and Biological Characterization of the ADP-Ribosylhydrolase 3

Dissertation

zur

Erlangung der naturwissenschaftlichen Doktorwürde

(Dr. sc. nat.)

vorgelegt der

Mathematisch-naturwissenschaftlichen Fakultät

der

Universität Zürich

von

Jeannette Abplanalp

von

Innertkirchen BE und aus Dänemark

Promotionskommission

Prof. Dr. Dr. Michael O. Hottiger
(Leitung der Dissertation)
Dr. Petr Cejka
Prof. Dr. Oliver Zerbe
Prof. Dr. Andreas Marx

Zürich, 2018

Summary

Post-translational modifications (PTMs) of proteins regulate their structure, cellular localization and function. ADP-ribosylation is a PTM catalyzed by ADP-ribosyltransferases (ARTs), which attach one (mono-ADP-ribose, MAR) or several (poly-ADP-ribose, PAR) consecutive ADP-ribose moieties from NAD^+ onto a protein. ADP-ribosylation is involved in various cellular stress responses and human pathologies such as cancer, inflammatory and neurodegenerative diseases. Understanding how proteins are ADP-ribosylated and again demodified is crucial for understanding the molecular mechanisms underlying these disease processes. The known nuclear ADP-ribose acceptor amino acids are arginine, lysine, glutamic and aspartic acid and serine, with serine being the most prominent one. Degradation of PAR is catalyzed by poly-ADP-glycohydrolase (PARG) and ADP-ribosylhydrolase 3 (ARH3). In contrast, ARH1, macrodomain-containing proteins 1 and 2 (MACROD1, MACROD2) and C6ORF130 degrade MAR linked to arginine or aspartic and glutamic acid, respectively. However, an enzyme capable of releasing MAR from serines has so far not been described. Therefore, the aim of this thesis was to identify and characterize an enzyme capable of hydrolyzing the ADP-ribose-serine linkage *in vitro* and *in vivo*.

Using state of the art *in vitro* modification assays and mass spectrometry, we identified ARH3 as a novel serine-mono-ARH *in vitro* and *in vivo* that localized to chromatin. ARH3 knockout (KO) MEFs showed an increase in total ADP-ribosylated proteins compared to wild type MEFs under basal conditions and upon oxidative stress induced by H_2O_2. *ARH3* KO mice were viable, fertile and exhibited largely a WT phenotype except for a body weight gain in females observed upon aging. Western blot and mass spectrometric analysis revealed an increase in MARylated proteins particularly in the spleen of *ARH3* KO animals. Many of the identified putative ARH3 targets within the spleen were nuclear proteins involved in DNA- and RNA-associated processes.

Together, these results revealed that ARH3 is the only enzyme known to date that hydrolyzes both PAR and MAR attached to serine residues. Our data suggest ARH3 as an important regulator of nuclear ADP-ribosylation turnover and main opponent of ADP-ribosyltransferase diphtheria-toxin 1 (ARTD1), the major enzyme responsible for serine-ADP-ribosylation in the nucleus.

Zusammenfassung

Die Struktur, zelluläre Lokalisation und Funktion von Proteinen wird durch Posttranslationale Modifikationen (PTMs) reguliert. ADP-Ribosylierung ist eine PTM, welche durch ADP-Ribosyltransferasen (ARTs) katalysiert wird und NAD^+ als Substrat benötigt. Bei der Reaktion werden eine (Mono-ADP-Ribose, MAR) oder mehrere ADP-Ribosegruppen (Poly-ADP-Ribose, PAR) an ein Protein gebunden. Die ADP-Ribosylierung ist an verschiedenen zellulären Stressantworten und Humanpathologien wie Krebs, entzündlichen und neurodegenerativen Erkrankungen beteiligt. Das Verständnis, wie Proteine ADP-ribosyliert und wieder demodifiziert werden, ist entscheidend für das Verständnis der molekularen Mechanismen, welche diesen Krankheitsprozessen zugrundeliegen. Im Zellkern findet man ADP-ribosylierte Arginine, Lysine, Glutamin- und Asparaginsäuren sowie, am häufigsten, Serine. Der Abbau von PAR wird durch Poly-ADP-Glycohydrolase (PARG) und ADP-Ribosylhydrolase 3 (ARH3) katalysiert, wohingegen ARH1, die Makrodomänen-Proteine 1 und 2 (MACROD1, MACROD2) und C6ORF130 MAR entfernen, welche an Arginin beziehungsweise Asparagin- und Glutaminsäure gebunden ist. Bisher ist jedoch kein Enzym bekannt, das MARylierte Serine demodifiziert. Ziel dieser Arbeit war es daher, ein solches Enzym zu identifizieren und zu charakterisieren.

Mittels *in vitro* Modifikationsassays und Massenspektrometrie wurde ARH3 *in vitro* und *in vivo* neu als Serin-Mono-ARH im Zellkern identifiziert. ARH3-Knockout (KO) MEFs zeigten einen Anstieg der gesamten ADP-ribosylierten Proteine im Vergleich zu WT MEFs, sowohl unter basalen Bedingungen als auch während H_2O_2-induziertem oxidativem Stress. *ARH3* KO Mäuse waren lebensfähig, fruchtbar und hatten einen vergleichbaren Phänotyp wie WT Mäusen, mit Ausnahme einer altersbedingten Gewichtszunahme bei Weibchen. Western Blot und massenspektrometrische Analysen zeigten einen Anstieg an MARylierten Proteinen vor allem in der Milz von *ARH3* KO Tieren. Viele dieser Proteine sind im Zellkern lokalisiert und an DNA- und RNA-assoziierten Prozessen beteiligt.

Zusammenfassend zeigten diese Ergebnisse, dass ARH3 das einzige bisher bekannte Enzym ist, das ADP-Ribose vollständig von Serinen entfernt. Unsere Daten deuten darauf hin, dass ARH3 ein wichtiger Regulator von ADP-Ribosylierung im Zellkern ist und als Antagonist der ART Diphtherie-Toxin 1 (ARTD1) wirkt, dem Hauptenzym verantwortlich für Serin-ADP-Ribosylierung im Zellkern.

Table of contents

1 Introduction

1.1 ADP-ribosylation

In both eukaryotic and prokaryotic organisms, the DNA encodes genes, which upon transcription and translation give rise to intra- and extracellular proteins. The complexity of a single cell or an entire organism is enhanced by various regulatory mechanisms on the DNA and mRNA level, which include initiation of transcription at alternative promoters, differential termination, or alternative splicing of a certain transcript. Additionally, one important way of introducing a certain complexity to a cell on the protein level is a post-translational modification (PTM).

PTMs include the addition of one or several chemical groups, e.g. methyl- or acetyl-groups, as well as the attachment of small proteins, such as ubiquitin or small ubiquitin-related modifier (SUMO), onto targets. These modifications have been shown to impact different properties of a protein, ranging from structural to functional changes. PTMs allow a cell to quickly react to external and internal cues as compared to e.g. changes in transcription, or splicing[1].

As opposed to rather small modifications, such as methylation or acetylation, the modification discussed in this thesis, ADP-ribosylation, is a rather bulky modification, harboring two negative charges per unit of ADP-ribose (Figure 1).

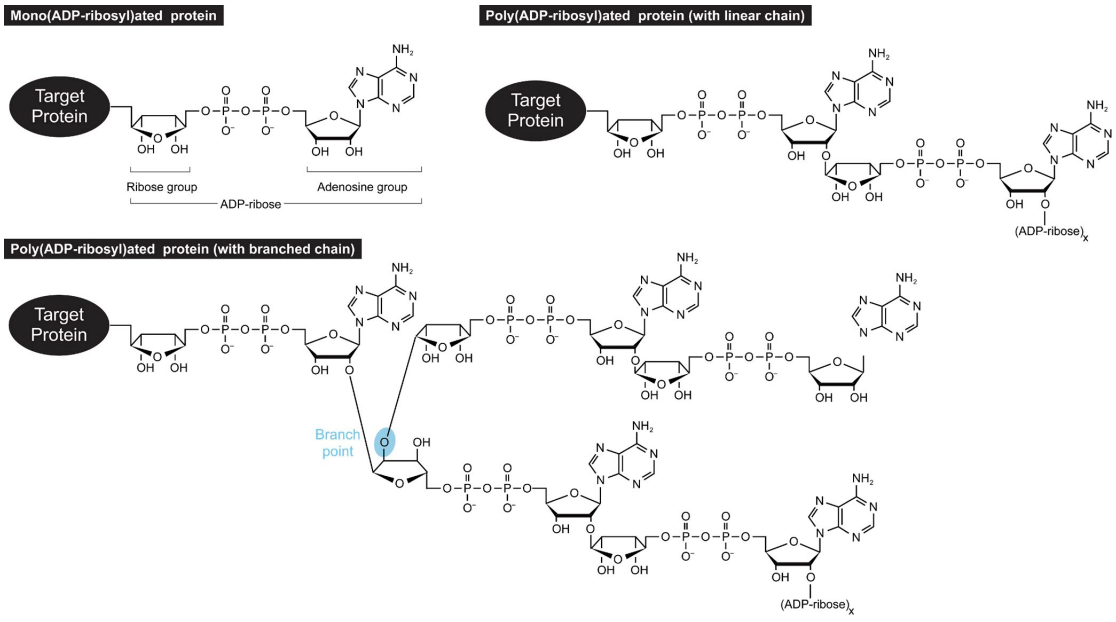

Figure 1: Structure of ADP-ribose in its monomeric and polymeric form. Taken from[2].

It is thus not surprising that adding ADP-ribose in either a monomeric or polymeric form influences a wide array of cellular functions, such as DNA repair and transcription, and is at work in various pathological processes including inflammatory and antiviral responses[3].

The earliest reports of ADP-ribosylation date back to the mid 1960s, where poly-ADP-ribose (PAR) was first detected in nuclei of mammalian cells[4]. Soon after, the attachment of mono-ADP-ribose (MAR) onto mammalian proteins by bacterial toxins was discovered[5]. Since these first findings, various research groups have worked on the identification of the writers, readers and erasers of ADP-ribosylation, as well as the targeted proteins and the respective amino acid acceptor sites, which will be discussed in more detail below.

1.2 Writers of ADP-ribosylation

All enzymes with the capability of synthesizing MARylation or PARylation consume nicotinamide adenine dinucleotide (NAD^+). NAD^+ is an abundant cellular metabolite, and functions in various pathways[6]. Its main role lies in energy metabolism, where NAD^+ forms the reducing agent NADH upon accepting two electrons, thereby fueling the mitochondrial electron transport chain[7]. Synthesis of NAD^+ can happen either *de novo*, which requires tryptophan uptake through food, or via various salvage pathways, where nicotinic acid (NA), nicotinamide (NAM), or nicotinamide riboside (NR) are taken up and further catalyzed by the enzymes nicotinamide phosphoribosyltransferase (NAMPT) and nicotinamide mononucleotide adenylyltransferase (NMNAT)[8].

The main families synthesizing extracellular and intracellular MAR and PAR are Clostridium toxin- and diphtheria toxin-like ARTs (ARTCs and ARTDs, respectively). They use the ADP-ribose moiety of NAD^+ and attach it to their targets. Writers of ADP-ribosylation compete for cellular NAD^+ with other enzymes. E.g. cyclic ADP-ribose (cADPR), a messenger molecule important in calcium signaling, is produced by cADPR synthases, which also use NAD^+ as a substrate[9]. Sirtuins require NAD^+ as a co-substrate for the deacetylation of lysines (or removal of larger PTMs such as malonyl- and succinyl-groups) by transfer of the acetyl group to the ADP-ribose of NAD^+[10]. Some sirtuins have recently been shown to be capable of using the

ADP-ribose moiety of NAD^+ to act as ADP-ribosyltransferases (ART) as well, but will not be discussed further[10].

ADP-ribosyltransferases, clostridium toxin-like (ARTCs)

The ARTC family is characterized by sequence homology to clostridium toxin and its members are membrane-bound and act extracellularly[11]. ARTCs have been shown to specifically mono-ADP-ribosylate arginines (R), and the amino acid motif arginine-serine-glutamic acid (R-S-E) in the catalytic cleft is necessary for this activity[12]. In human tissue, mRNAs for ARTC1, 3, 4, and 5 are expressed, whereas in mice, mRNAs from ARTC1-5 are identified[13].

Enzymatic activity has been shown for ARTC1, 2, and 5, while ARTC3 and 4 are inactive, presumably due to the lack of the aforementioned catalytic R-S-E triad. Interestingly, the analysis of mRNA expression patterns for the enzymatically active ARTCs revealed tissue-specific expression, with ARTC1 being abundant in muscle and cardiac cells, and ARTC5 in testes[13].

ADP-ribosyltransferases, diphtheria toxin-like (ARTDs)

The ARTD family is characterized by homology to diphtheria toxin and catalyzes intracellular ADP-ribosylation[11]. Which ARTD modifies which amino acid is so far largely unknown (see further below). Catalytically active ARTDs harbor a different triad in the catalytic cleft compared to ARTCs, namely histidine-tyrosine-glutamic acid (H-Y-E)[11]. A total of 18 different members have been identified in humans (Table 1).

Table 1: **ARTD family members**: Activity taken from[14], localization information retrieved from www.proteinatlas.org, table continues on the next page.

New nomenclature	Old nomenclature	Activity	Localization in unstimulated cells
ARTD1	PARP1	PAR	Nucleus
ARTD2	PARP2	PAR	Nucleus, nucleoli
ARTD3	PARP3	MAR	Nucleoli, cytosol
ARTD4	PARP4, vPARP	MAR	Cytosol
ARTD5	PARP5a, TNKS	PAR	Nucleoplasm, nuclear membrane
ARTD6	PARP5b, TNKS2	PAR	Microtubules
ARTD7	PARP15, BAL1	MAR	Mitochondria

ARTD8	PARP14, COAST6, BAL2	MAR	Cytosol
ARTD9	PARP9, BAL1	MAR	Nucleoplasm, cytosol, mitochondria
ARTD10	PARP10	MAR	Nucleoli, cytosol
ARTD11	PARP11	MAR	Not available
ARTD12	PARP12	MAR	Nucleus
ARTD13	PARP13, ZAP, ZC3HDC1	Presumably inactive	Cytosol, Golgi
ARTD14	PARP7, TIPARP	MAR	Uncertain
ARTD15	PARP16	MAR	Not available
ARTD16	PARP8	MAR	Nucleoplasm, cytosol
ARTD17	PARP6	MAR	Plasma membrane
ARTD18	TPT1	Presumably inactive	Cytosol

In contrast to ARTCs, ARTD1, 2, 5, and 6 are capable of producing not only monomeric ADP-ribosylation, but can form linear or branched chains of PAR[15]. The other family members are thought to either be inactive, due to a lack of the catalytic H-Y-E triad, or known to catalyze MAR[16]. Interestingly, besides their catalytic domain, ARTDs carry various other domains, e.g. RNA-recognition motifs, macro-domains which bind ADP-ribose, zinc finger domains known to bind DNA, to name just a few[11]. These domains regulate various aspects of the respective ARTD family member, such as intracellular localization, target binding, activation and function.

ADP-ribose amino acid acceptor sites

For a long time, the potential amino acids to be modified by ARTDs were thought to be aspartic (D) and glutamic acids (E) (via an ester linkage), as well as lysines (K) and arginines (R) (via a ketoamine linkage).

One approach used to identify ADP-ribosylated sites is the reanalysis of already existing phosphoproteomics data, because the phosphopeptide enrichment protocols potentially also isolate ADP-ribosylated peptides. Indeed, intracellular targets modified at Rs were identified by this approach[17].

Recently, new ADP-ribosylation enrichment protocols and mass spectrometric techniques emerged which allow the direct detection of ADP-ribosylated peptides. Mass spectrometric analysis of the so far most studied PAR writer ARTD1 and its targets provided evidence for the ADP-ribosylation of Ds, Es, and Ks *in vitro*[18-20].

ARTD10, the best-known MAR writer, *auto*- and *trans*-ADP-ribosylated acidic amino acid residues Ds and Es[21].

Proteome-wide analysis using boronate-affinity chromatography for enriching ADP-ribosylated peptides confirmed Ds and Es to be modified *in vivo*[22]. An enrichment method using Af1521, a protein from *Archaeglobus fulgidus* with high affinity for ADP-ribose, has recently been established as a tool for enriching ADP-ribosylated proteins and peptides and can be used in combination with mass spectrometry to identify tissue- and cell-specific ADP-ribosylomes, confirming Ds, Es, Ks and Rs as ADP-ribose acceptor sites[23,24].

The accuracy of this data has recently been challenged by the development of more precise and reliable mass spectrometry methods, which revealed that the most prominently ARTD-modified sites *in vivo* are serines[25-27].

1.3 Readers of ADP-ribosylation

As for other protein modifications, ADP-ribose binding proteins are necessary to recognize and translate an ADP-ribose mark into a signal and are, thus, so called readers of ADP-ribosylation (Figure 2).

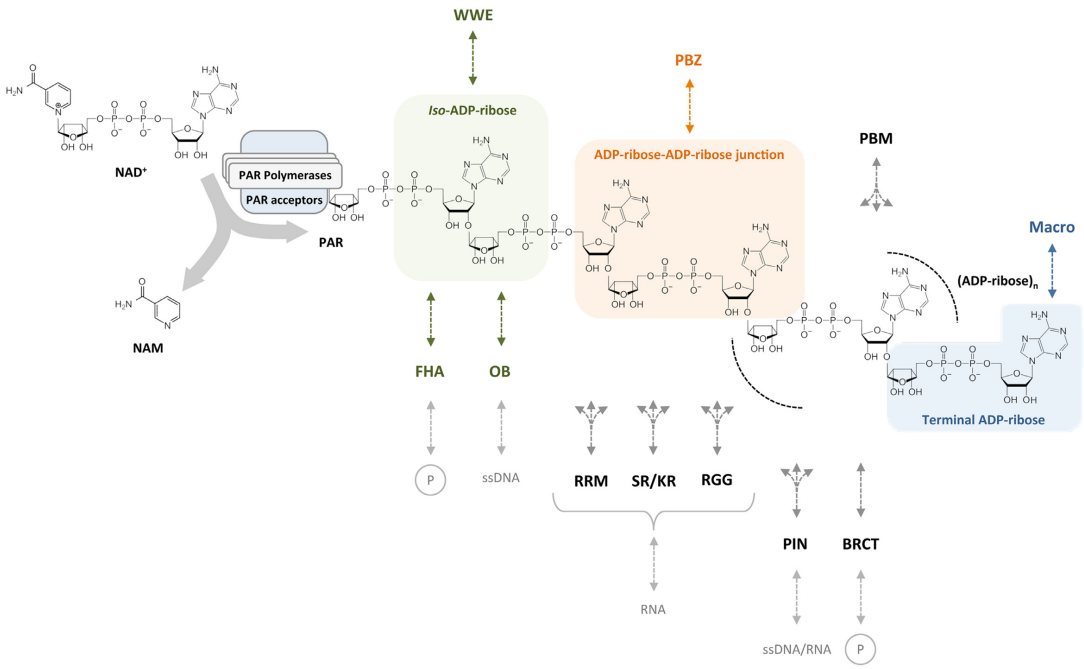

Figure 2: Readers of PAR. Binding modules and their respective binding site are shown, multi-branched arrows indicate that the binding sites have so far not been identified. Taken from[28].

Macrodomain

The macrodomain is a rather large domain of around 130-190 amino acids, and got its name by homology to the core histone macroH2A, whose non-histone sequence is a macrodomain[29]. The macrodomain has been shown to have high affinity for ADP-ribose and binds both MAR and the terminal ADP-ribose moiety of PAR[30]. To date, eleven human proteins have been identified to have one or more macrodomains, including several ARTs, namely ARTD7, ARTD8, and ARTD9, as well as the proteins macrodomain containing 1 and 2 (MACROD1, MACROD2) and terminal ADP-ribose glycohydrolase (TARG, also C6ORF130)[31]. The latter three have been found to possess macrodomains with hydrolase activity, which will be discussed in more detail below[21,32,33]. Having binding ability and in some cases enzymatic activity against MAR makes the macrodomain a versatile module. The macrodomain-containing protein Af1521 from *Archaeglobus fulgidus* has recently been established as a tool for enriching ADP-ribosylated proteins and peptides for instance for mass spectrometry approaches to identify tissue- and cell-specific ADP-ribosylomes[23,24]. In contrast to the other known ADP-ribose binding domains, the macrodomain is the only one binding MAR.

WWE

The WWE domain contains around 90 amino acids and is named after its conserved amino acid triad consisting of two tryptophans (W) and one E. The WWE domain exclusively binds to PAR, as it recognizes *iso*-ADP-ribose, a structure unique for two consecutively bound ADP-ribose units in a linear PAR chain[34]. The few proteins found to possess a WWE domain can be categorized as either ARTD or ubiquitin ligase family members, pointing towards a potential interplay of the two PTM systems[35]. Similar to the macrodomain, the WWE domain has recently been used as a biotechnological tool, in this case to establish a chromatin affinity purification (ChAP) protocol to identify ADP-ribosylated loci in the genome[36].

Poly-ADP-ribose-binding motif (PBM)

The PBM has been identified as an around 20 amino acid long consensus sequence containing a hydrophobic stretch[37]. It is unknown which exact part of the PAR chains the PBM binds to. With the development of more advanced

bioinformatics tools, several hundred proteins with a potential PBM have been identified[38]. No other PAR binder is equally well represented in the proteome. Functionally, the PBM is present in proteins involved in DNA repair, replication and chromatin remodeling, as well as in cell cycle regulation and RNA binding[38].

PAR-binding zinc finger (PBZ)

The PBZ is an around 30 amino acid long stretch[39]. It binds to two ADP-ribose units in a PAR chain, the so-called ADP-ribose-ADP-ribose junction[39,40]. The PBZ was found in two proteins so far, APFL and CHFR, suggesting a specialized role of this binding domain in non-homologous end- joining (NHEJ) and cell cycle control, respectively[41]. Checkpoint kinase 1 (CHK1) contains a potential variation of the PBZ allowing PAR binding[42]. The presence of other PBZ-containing proteins is unknown.

FHA and BRCT domains

The fork-head associated (FHA) or breast cancer 1 C-terminal (BRCT) domains span around 90 amino acids. Formerly known to bind phosphorylated targets, these domains have been shown to be capable of also recognizing ADP-ribosylated proteins[43]. Similar to the PBM, the exact binding mode to PAR is missing so far. Various proteins have been identified to possess FHA or BRCT domains and all are found to function in DNA damage response pathways[43].

RNA- and DNA-binding domains

PAR resembles nucleic acids in that it is highly negatively charged and contains phosphate and ribose groups. Considering this similarity, it is not surprising that recent studies revealed several domains and motifs so far mainly associated with DNA- or RNA-binding to also exhibit a certain affinity for PAR[28]. For most of these domains, their exact binding mode and functions are not known, and will therefore only be shortly introduced:

- The most widely spread RNA-binding motif is the RNA recognition motif (RRM), with over 50'000 copies found in all domains of life[44].
- Serine/arginine repeats (SR) are mainly associated with SR proteins. Those are involved in the regulation of splicing, and additionally to their SR motif also contain an RRM[45].

- Arginine- and glycine-rich regions (RGG) carry various positive charges which allow the binding to PAR[46]. They are found abundantly in the human proteome[46].
- The oligonucleotide/oligosaccharide-binding fold (OB-fold) and the PilT N-terminal (PIN) domain bind single-stranded nucleic acids and oligosaccharides, and were recently found to also bind PAR[47,48].

1.4 Erasers of ADP-ribosylation

As opposed to the many known ARTs (described above), only a few proteins with hydrolytic activity towards the ADP-ribose bonds within PAR or the ADP-ribose-amino acid linkage have been identified so far (Table 2)[49].

Table 2: Erasers of ADP-ribosylation. Activity taken from[49], localization information retrieved from www.proteinatlas.org.

Eraser	Hydrolase activity (amino acid)	Localization in unstimulated cells
ARH1	MAR (R)	Nuclear membrane, nucleus
ARH2	Inactive	Nucleoplasm
ARH3	PAR	Nucleoplasm
MACROD1	MAR (D/E)	Nucleoplasm
MACROD2	MAR (D/E)	Nucleus, nucleoli
TARG (C4ORF130)	PAR/MAR (D/E)	Nucleus, nucleoli
PARG	PAR	Nucleus, vesicles

ARH family

Around 30 years ago, the first mammalian hydrolase with the ability to reverse arginine-ADP-ribosylation has been purified from turkey erythrocytes[50,51]. The 39 kDa protein was later named ADP-ribosylhydrolase 1 (ARH1) and was the founder of the ARH family of ADP-ribosylhydrolases. In parallel, the bacterial protein dinitrogenase-activating glycohydrolase (DRAG) was identified as an arginine-specific ARH regulating nitrogen fixation in *Rhodospirillum rubrum*[52,53]. Several

years later, bioinformatic searches identified three DRAG-homologous proteins in the mammalian genome, one of which was the already identified ARH1, and two additional proteins, ARH2 and ARH3[13].

ARH1

ARH1 specifically hydrolyzes the *N*-glycosidic bond linking the mono-ADP-ribose to the guanidine group of arginine [54]. *In vitro*, ARH1 has been shown to have a very weak hydrolase activity towards the *O*-glycosidic bond of PAR and 2'-*O*-acetyl adenosine diphosphate ribose (OAADPR), the metabolite released by sirtuins upon deacetylation of their respective targets[55]. However, due to the much higher activity of PARG and ARH3 on these substrates, this catalytic activity of ARH1 can probably be neglected *in vivo*. Other ADP-ribose-amino acid linkages synthesized by bacterial toxins, such as ADP-ribose-cysteine, -asparagine-, and diphthamide were resistant to ARH1 treatment[56]. ADP-ribose seems to be the only substrate for ARH1, as only ADP-ribose but no derivatives or structurally related molecules, e.g. ribose 5-phosphate, adenosine monophosphate (AMP), adenosine diphosphate (ADP) or NAD^+, inhibits its activity[51,56].

At position 60 and 61, the human ARH1 protein harbors two catalytically important aspartic acids, keeping two magnesium ions (Mg^{2+}) in place, and when mutating these residues to alanine, enzymatic activity but not binding to ADPr is greatly reduced[57]. A recent study revealed several sites on ARH1 that are subject to phosphorylation and that phosphorylated ARH1 is more orderly structured[58].

Generation and investigation of an *Arh1* knockout mouse revealed an essential function of ARH1 in the organismal response to cholera toxin, as both cells and intestinal loops isolated from knockout mice showed a higher sensitivity towards cholera toxin application[59]. *ARH1* knockout animals were also shown to develop spontaneous lymphomas, adenocarcinomas and metastases more frequently than wildtype age-matched control animals, establishing ARH1 as a tumor suppressor[60,61].

ARH2

ARH2 is the least studied member of the ARH family. ARH2 is presumably catalytically inactive, even though capable of binding ADP-ribose. Presumably, its

inactivity is due to the lack of the two catalytic aspartic acids present in both ARH1 and ARH3[55].

ARH2 is exclusively expressed in the heart of developing mammals, and recently, knockdown of all ARH2 variants in *Xenopus laevis* revealed that ARH2 is needed for myofibril assembly and both outgrowth and functionality of heart ventricles[62].

ARH3

ARH3 degrades PAR via hydrolysis of the *O*-glycosidic bond[56,63]. Additionally, ARH3 efficiently hydrolyzes OAADPR[55,64]. This seems puzzling, as the high structural similarity to ARH1 would suggest ARH3 to have an activity towards mono-ADP-ribosylated Rs. However, neither activity towards MARylated Rs nor towards any bacterially caused MARylation could be experimentally confirmed[56]. As for ARH1, ARH3 activity is inhibited by ADPr, but not by ribose-5-phosphate, AMP, ADP, or NAD^{+}[56].

Catalytic activity of ARH3 requires two Mg^{2+} ions, and the aspartic acid residues at position 77 and 78 of human ARH3 are thought to mediate the binding to these ions[56,63]. As for ARH1, mutation of these conserved residues abolishes catalytic activity of ARH3[56]. Several ARH3 mutants were generated *in vitro* and revealed various amino acids which are enzymatically and/or structurally important[63].

ARH3 is mainly found in the nucleus, but was also detected in the cytoplasm and mitochondria[65]. Functionally, ARH3 was found to be the main enzyme degrading mitochondrial PAR[66]. In another study focusing on oxidative stress, ARH3 has also been found to play a protective role in that its enzymatic activity degrades PAR, thereby inhibiting PAR-dependent cell death (parthanatos)[65]. Even though mouse embryonic fibroblasts from Arh3 knockout mice were used in the previous studies, no phenotypic data has been published so far. In humans, the expression of ADPRHL2 (gene name of ARH3) correlates with decreased survival of breast cancer patients[67].

Macrodomain-containing erasers

Macrodomain-containing proteins are not only capable of binding to MARylated proteins, but some of them have been identified also as potent erasers of MAR. MACROD1 and MACROD2 have been shown to specifically release MAR

from acidic amino acid residues[21,33]. The structurally related TARG possesses a unique catalytic activity with respect to the fact that it does not only release MAR from targets comparable to MACROD1 and MACROD2, but also cleaves off entire PAR chains by hydrolyzing the ADP-ribose-amino acid-linkage[32]. Discovery of these MAR erasers proved that ADP-ribosylation of acidic amino acids is reversible.

Macrodomain-containing erasers are mainly localized to the nucleus, with MACROD1 also found in the mitochondria and MACROD2 in the cytoplasm. Physiologically, MACROD1 and MACROD2 were shown to be mutated or differentially expressed in various cancers, pointing towards a tumor suppressor function similar to ARH1[68,69]. TARG mutations were shown in individuals with severe neurological dysfunctions[32].

PARG

PAR glycohydrolase (PARG) was the first enzyme identified in cell extracts of calf thymus to hydrolyze the *O*-glycosidic bond of PAR chains[70,71]. PARG is inactive towards the ADP-ribose-amino acid linkage, thus leaving a MAR modification on target proteins[72]. The catalytic cleft of PARG was found to share homology with macrodomains[72].

Several splice variants of PARG exist, and the respective proteins localize to the nucleus, cytoplasm and mitochondria[73]. The knockout of murine PARG leads to embryonic lethality, due to accumulation of PAR, providing evidence that PARG is the main responsible protein for PAR degradation in cells and is required during embryogenesis[74].

1.5 Functional relevance of ADP-ribosylation

Functions of MAR

The physiological relevance of MARylation has so far been poorly studied and only recently, technological advances allow unraveling the function of specific mono-ARTDs.

ARTD3 is an important player in the maintenance of genome integrity. It is recruited to DNA double-strand breaks (DSB) and is necessary for mitotic progression by stabilizing the mitotic spindle[75]. Further studies on the role of ARTD3 in the DNA damage response revealed it to be a key factor in the cell's choice

between homologous recombination (HR) and non-homologous end-joining (NHEJ), promoting NHEJ upon DSBs and limiting DSB end resection during HR[76]. Recent evidence implies a role for ARTD3 in single-strand breaks (SSB), where it binds to mononucleosomes containing nicked DNA and MARylates the histones[77].

ARTD4, together with the major vault protein (MVP) and telomerase-associated protein 1 (TEP1), is a component of barrel-shaped cytoplasmic ribonucleoprotein particles, so called vaults[78]. The knockout of ARTD4 in mice leads to enhanced susceptibility to carcinogen-induced tumors and germline ARTD4 mutations were found in cancer patients, indicating a role for ARTD4 in cancer development[79,80]

ARTD7 (BAL3) along with ARTD8 (BAL2 or CoaSt6) and ARTD9 (BAL1) constitute the B-aggressive-lymphoma (BAL) protein family[81]. The family shares some distinct feature in that all members harbor several macrodomains and an ART domain[81]. The function of ARTD7 remains unknown to date.

ARTD8 is an interaction partner of STAT6, a transcription factor activating gene transcription in the IL-4 signaling pathway[82,83]. Under non-stimulated conditions, ARTD8 is found at promoters of STAT6 responsive genes, and bound to HDAC2 and 3, working as a repressor[84]. Upon stimulation with Il-4, STAT6 gets phosphorylated, dimerizes and shuttles to the nucleus[84]. In parallel, ARTD8 gets activated in the nucleus by a so far unknown mechanism, and ADP-ribosylation of the HDACs and ARTD8 leads to their release from chromatin, allowing STAT6 to bind and activate transcription[84]. MARylation is crucial for these events, as treatment with unspecific PARPi blocks transcription and a catalytically inactive ARTD8 mutant fails to activate STAT6 target genes[85].

ARTD9 has long been thought to be catalytically inactive, as it has never been capable of *auto*-ADP-ribosylation *in vitro*[14]. However, a recent publication has shown that a heterodimer of ARTD9 and Dtx3L functions in ubiquitin ADP-ribosylation, thereby hindering ubiquitination of substrates[86].

ARTD10 was shown to interact with several kinases, and the validation of these findings with GSK3β, has shown that *in vitro* ADP-ribosylation reduced its activity[87]. Knocking down ARTD10 in cells leads to an increase in kinase activity, similar to overexpression of the eraser MACROD2[21]. Furthermore, ARTD10 was reported to MARylate NEMO, an important protein in the inflammatory NF-κB

pathway, which interferes with its poly-ubiquitination and further downstream signaling, thereby preventing the transcription of target genes such as IκB and IL-8[88].

ARTD11 plays a role in nuclear pore complex organization, as revealed by a recently developed mass spectrometry approach[89]. The technique involves the overexpression of an engineered ARTD capable of only metabolizing a clickable NAD^+ analog, and modified targets can easily get enriched and subjected to mass spectrometry measurements[89].

ARTD12 function is not fully understood. Transcriptome analysis revealed it to be expressed upon interferon treatment of cells, where it is recruited to stress granules to block mRNA translation[90]. In contrast, lipopolysaccharide (LPS) stimulation of cells leads to binding of ARTD12 to proteins of the NF-κB pathway, which increases inflammatory signaling[90].

ARTD14 is induced by treatment of cells with 2,3,7,8-tetrachlorodibenzo-*p*-dioxin (TCDD), a toxin produced as a byproduct in industrial processes[91]. Upon TCDD binding to the aryl hydrocarbon receptor (AHR), the receptor translocates to the nucleus where it binds to the AHR nuclear translocator (ARNT), and leads to the transcription of various genes, including ARTD14[91,92]. ARTD14 regulates the pathway as a transcriptional repressor[93]. AHR has been shown to be ADP-ribosylated by ARTD14, and MACROD1 reverses this reaction *in vitro*, such that overexpression of MACROD1 in cells leads to the loss of ARTD14-mediated repression of AHR signaling[94].

MARylation in the ER by ARTD15 seems to impact the unfolded protein response (UPR). Under ER stress, ARTD15 MARylates IRE1α and PERK, and thereby increases their kinase activity, leading to enhanced downstream effects such as the inhibition of translation and the transcription of chaperones[95].

ARTD16 is a so far completely uncharacterized protein of the ARTD family.

ARTD17 functions in neuronal development, where it is crucial for hippocampal dendrite morphogenesis, and its MARylation activity is needed for the development of dendritic complexity in primary hippocampal neurons[96]. ARTD17 expression is associated with poor prognosis in various cancers, and its expression promotes growth and survival of colorectal adenocarcinoma cells[97].

Functions of PAR

Some ARTDs have been shown to catalyze the formation of PAR chains with a length of up to 200 ADPr units[98]. Adding two negative charges per ADPr, this drastically changes the electrostatic characteristics of a modified protein, changing its structure and function. Additionally, PAR might provide an extensive scaffold for recruiting proteins.

ARTD1 is the most-studied member of the ARTD family and will therefore be discussed in more detail. ARTD1 inhibitors (PARP inhibitors (PARPi)), have recently been used in the treatment of BRCA-mutated cancers because of the crucial role of ARTD1 in the DNA damage control[99,100]. The three zinc finger (ZF) domains of ARTD1 help to bind DNA and to recognize both SSB and DSB and mediate ARTD1 homodimer formation[101,102]. ARTD1 has therefore been implicated in SSB repair, where it serves as a detector and, through activation and *auto*-PARylation, recruits repair factors such as XRCC1, APE1, DNA ligase 3 and PCNA[103]. Therefore, inhibition of ARTD1 causes replication fork stalling at unrepaired SSBs, which in turn causes the formation of DSB[104]. Tumor cells, which have mutations in the BRCA genes, are incapable of repairing DSBs via HR. Hence, treatment of such tumors with PARPi leads to genomic instability and eventually tumor cell death[105].

ARTD1 has also important functions in inflammatory responses. ARTD1-deficient mice are resistant to septic shock induction by LPS-induced septic shock[106]. Similarly, ARTD1-deficiency or treatment with PARPi led to ameliorated or delayed symptoms in several inflammatory disease models[107]. On a molecular level, this is thought to be mainly dependent on the function of ARTD1 as a cofactor of NF-κB[108,109].

Furthermore, ARTD1was shown to be implicated in adipogenesis, as PARPi-treated mice on a high-fat diet accumulated less white adipose tissue and were lighter compared to vehicle-treated mice[110]. Also, during the *in vitro* differentiation of fibroblasts to adipocytes, PAR is formed, and the inhibition or depletion of ARTD1 delays adipogenesis, indicating an important role for ADP-ribosylation in the differentiation of fat cells[111]. This effect has been shown to work likely via the binding of ARTD1 to the peroxisome proliferator-activated receptor 2 (PPARγ2), a key factor in terminal adipocyte differentiation[110]. ARTD1 binds and PARylates PPARγ2, which enhances PPARγ2 binding to ligands, triggers the exchange of co-

factors at PPARγ2 response elements (PPREs), and leads to PPARγ2-target gene expression[111]. These events coincide with a change in DNA methylation and the histone mark landscape, the exact mechanism of which remains unclear[110-112].

One mode of action by which ARTD1 regulates cellular responses is via transcriptional regulation. Firstly, similar to its function as a cofactor of NF-κB in inflammation, ARTD1 was shown to form complexes with transcription factors in processes such as development and differentiation. Oct-1 and Sox2 are only two out of many other transcription factors whose activating or repressing function on transcription is dependent on ARTD1 binding and activity[113,114]. Secondly, ARTD1 can directly act on chromatin itself, and PARylation was shown to open chromatin structure, thereby making the DNA more accessible[115].

1.6 Chromatin organization

DNA packaging

The genetic information of every cell is packaged within the nucleus in the form of chromosomes. The components making up the chromosomes are collectively called chromatin, which itself is a complex structure consisting of proteins, DNA and RNA molecules. Histones are the main protein component, building up the so called nucleosome, which is a histone octamer, each containing two units of H2A, H2B, H3, and H4 with 146 base pairs of DNA wrapped around[116]. Early attempts to visualize chromatin showed that DNA wrapped around histones builds up in the form of a chain, which served as a base for the so called beads-on-a-string model[117]. Higher order structures are built with inclusion of H1 in between nucleosomes, wrapping another 20 bp of DNA around, which yields a 30 nm wide fiber that upon binding to additional scaffold proteins makes up the individual chromosomes[118]. However, the latest developments in electron microscopy revealed that this view might need to be changed, as chromatin seems to rather be made up of flexible and disordered chains of 5-24 nm diameter packed together at different densities[119]. The packaging of DNA into chromatin and chromosomes is required to keep an order and allow for segregation of sister chromosomes during cell divisions. However, this high degree of packaging poses various challenges during repair, replication, or transcription, where DNA needs to be highly accessible for various proteins such as polymerases and transcription factors.

Euchromatin and heterochromatin

Cell cycle, cell type and other internal and external cues influence chromatin structure. Ways to alter chromatin are the recruitment of remodeling complexes capable of loosening or tightening chromatin by displacing nucleosomes or by using PTMs such as acetyl-, methyl-, ADP-ribosyl- and phosphogroups to modify histones[120,121]. Simplified, chromatin comes in two flavors, euchromatin and heterochromatin, both states marked with different PTMs of histone tails protruding from the nucleosome. Open, accessible euchromatin is marked with acetylation of H3 and H4, and promoters of actively transcribed genes are marked with H3K4me3[121]. Promoters of repressed genes are marked by H3K9me3 and H3K27me3[122].

1.7 Chromatin ADP-ribosylation

Histone ADP-ribosylation

Besides the commonly known acetylation and methylation of histones, core histones as well as H1 were found to be ADP-ribosylated already almost 40 years ago[19,123,124]. ADP-ribosylation is mostly detected on the protruding histone tails. *In vitro*, ARTD1 and ARTD10 modify core histones[20,125]. ARTD2 did not show activity on histones, but the nuclear MAR writer ARTD3 modifies the linker histone H1[20,126]. Analysis of histones purified from cells confirmed also *in vivo* ADP-ribosylation of histones[26]. As described above, several ARTDs and erasers are present in the cell nucleus (see Table 1 and 2). However, it is not yet clear which ARTD modifies which histone residue *in vivo*.

Global chromatin ADP-ribosylation

Different approaches have been undertaken to study the effect of ADP-ribosylation on overall chromatin structure aside from histones. *In vitro* PARylation of chromatin in the presence of NAD^+ and ARTD1 led to a reversible decondensation[127,128]. Further studies have shown ADP-ribosylated chromatin to be more susceptible to micrococcal nuclease digest[129]. *In vivo*, studies on the Hsp70 locus in *Drosophila melanogaster* support the aforementioned findings as ARTD1 activity has been shown to loosen up chromatin to ensure gene transcription[115].

Global chromatin ADP-ribosylation *in vivo* has been analyzed so far using two different approaches. In the first protocol, a PAR antibody was used to perform ChIP

upon crosslinking and TCA precipitation[130]. A recently developed ChAP protocol describes the enrichment of PARylated chromatin using the WWE domain of RNF146 and the subsequent sequencing of associated DNA[36,131]. It will be interesting to see how these techniques develop and whether the establishment of specific protocols addressing MARylated chromatin will help understand better the roles of ADP-ribosylation.

DNA ADP-ribosylation

In addition to direct chromatin modification or interference with chromatin remodelers and transcription factors, ARTDs have been implicated in DNA ADP-ribosylation. Pierisin, a protein found in a cabbage butterfly (*Pieris rapae*), modifies guanines, which is cytotoxic[132]. Whether mammalian DNA is naturally ADP-ribosylated or not remains to be elucidated.

Together, all these findings support a view where ADP-ribosylation and removal thereof might greatly influence accessibility, structure and function of chromatin at different loci (Figure 3).

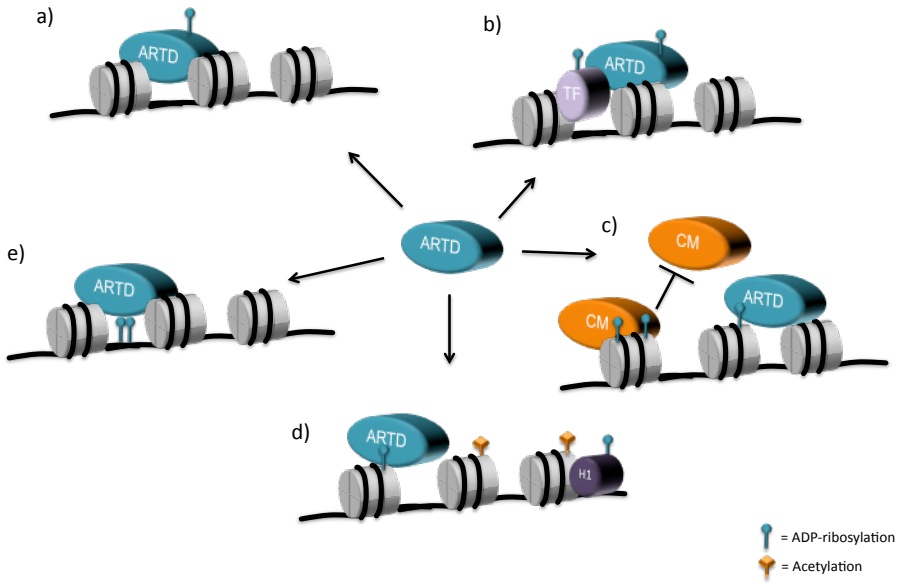

Figure 3: ARTDs in chromatin regulation. ARTDs could influence chromatin on different levels. a) Direct interaction of an ARTD with promoters in order to stimulate or repress transcription; b) ARTDs as cofactors of transcription factors (TF); c) ADP-ribosylation of chromatin might work either as scaffold or might sterically hinder access of chromatin remodeling proteins and complexes (CM); d) ADP-ribosylation of histones might either coincide or be mutually exclusive with other histone marks; e) emerging as a new DNA PTM as well, ADP-ribosylation might serve as an additional level of regulation of DNA stability and accessibility. Modified from[133].

2 Aim of the thesis

Since the discovery of ADP-ribosylation as a PTM, most research was focused on ARTD1-mediated PARylation and its functions. Recently, several studies started investigating the role of mono-ARTDs and the pathways they are regulating, and thus revealing that also MARylation is an important regulatory PTM in cells. The identification of MACROD1, MACROD2 and TARG as erasers for MARylated acidic amino acid residues (i.e. D/E) as well as of ARH1 as eraser for MARylated R's provided strong evidence that ADP-ribosylation is a fully reversible PTM, also implying that erasers for S and K MARylation may exist as well (Figure 4).

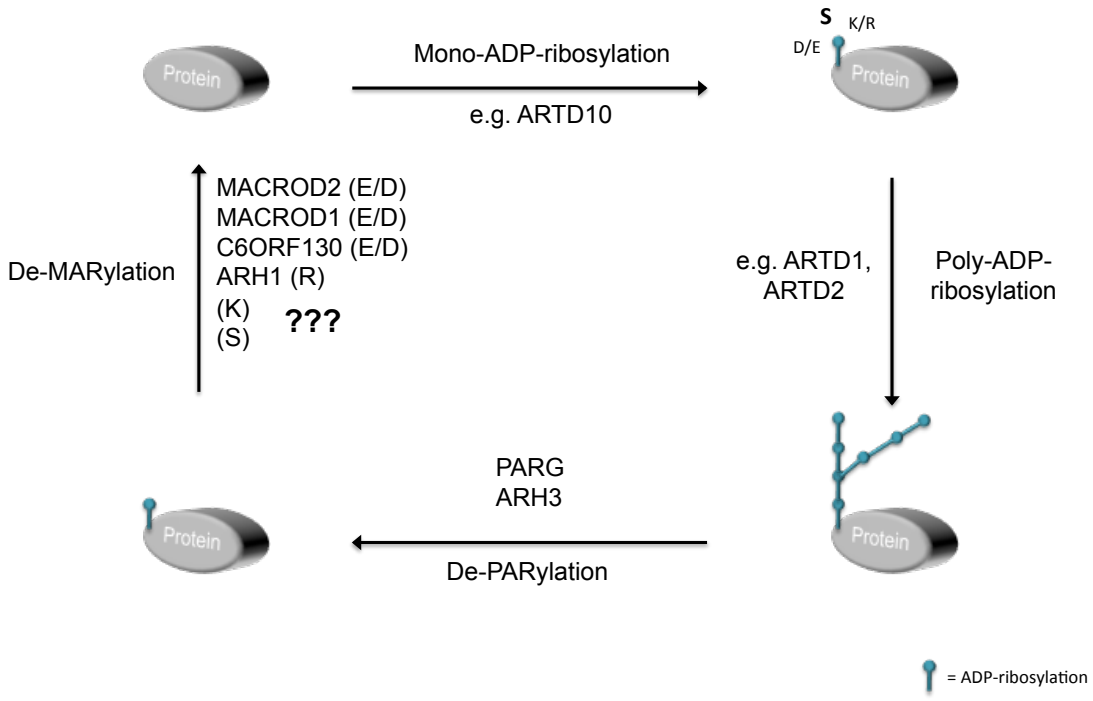

Figure 4: The ADP-ribosylation cycle. ADP-ribosylation of D/E and R is reversible. No known hydrolases for the removal of K and S ADP-ribosylation have been identified yet.

The aim of this thesis was to identify the enzyme(s) able to hydrolyze the linkage of ADP-ribose attached to K and S. Moreover, the enzyme should be further characterized in its physiological context, including the identification of its targets and the investigation of its role in the cellular and organismal context.

3 Results

3.1 Overview of published manuscripts

Cell fate regulation by chromatin ADP-ribosylation

Authors: **Jeannette Abplanalp** and Michael O. Hottiger

Journal: Seminars in Cell & Developmental Biology, 2017; 63, p. 114-122

Contribution J.A.: Writing and drafting of the manuscript and figures.

New Quantitative Mass Spectrometry Approaches Reveal Different ADP-ribosylation Phases Dependent On the Levels of Oxidative Stress

Authors: Vera Bilan, Nathalie Selevsek, Hans A.V. Kistemaker, **Jeannette Abplanalp**, Roxane Feurer, Dmitri V. Filippov and Michael O. Hottiger

Journal: Mol Cell Proteomics, 2017; 5, p.949-958

Contribution J.A.: Performing Western blot analysis of oxidative stress markers in lysates of H_2O_2-treated HeLa cells (Suppl. Figure 3A).

3.2 Overview of submitted manuscripts

Proteomic analyses identify ARH3 as a serine mono-ADP-ribosylhydrolase

Authors: **Jeannette Abplanalp**, Mario Leutert, Emilie Frugier, Roxane Feurer, Jiro Kato, Joel Moss, Amedeo Caflisch and Michael O. Hottiger

Journal: Manuscript submitted

Contribution J.A.: Planning, performing and evaluating of most experiments. Writing of the manuscript.

Mono-ADP-ribosylhydrolase assays

Authors: **Jeannette Abplanalp***, Ann-Katrin Hopp* and Michael O. Hottiger, * equal contribution

Journal: Manuscript submitted

Contribution J.A.: Writing and drafting of the manuscript and figures.

Seminars in Cell & Developmental Biology 63 (2017) 114–122

Contents lists available at ScienceDirect

Seminars in Cell & Developmental Biology

journal homepage: www.elsevier.com/locate/semcdb

Review

Cell fate regulation by chromatin ADP-ribosylation

Jeannette Abplanalp, Michael O. Hottiger (PhD, DVM) (Prof., Head of Department) *

Department of Molecular Mechanisms of Disease, University of Zurich, Winterthurerstr. 190, 8057 Zurich, Switzerland

ARTICLE INFO

Article history:
Received 15 June 2016
Received in revised form 24 August 2016
Accepted 16 September 2016
Available online 28 September 2016

Keywords:
ARTD
PARP
Chromatin
Histone
ADP-ribosylation
Differentiation
Pluripotency

ABSTRACT

ADP-ribosylation is an evolutionarily conserved complex posttranslational modification that alters protein function and/or interaction. Intracellularly, it is mainly catalyzed by diphtheria toxin-like ADP-ribosyltransferases (ARTDs), which attach one or several ADP-ribose residues onto target proteins. Several specific mono- and poly-ADP-ribosylation binding modules exist; hydrolases reverse the modification. The best-characterized ARTD family member, ARTD1, regulates various DNA-associated processes. Here, we focus on the role of ARTD1-mediated chromatin ADP-ribosylation in development, differentiation, and pluripotency, and the recent development of new methodologies that will enable more insight into these processes.

Contents

* Corresponding author.
E-mail address: michael.hottiger@dmmd.uzh.ch (M.O. Hottiger).

http://dx.doi.org/10.1016/j.semcdb.2016.09.010
1084-9521/

1. ADP-ribosylation—a posttranslational protein modification

1.1. NAD^+ and ADP-ribosylation

Nicotinamide adenine dinucleotide (NAD^+) is a main component of cellular redox reactions and thus an important player in energy metabolism. Upon accepting two electrons and a proton, NAD^+ forms the reducing agent NADH, which fuels the mitochondrial electron transport chain [1]. Additional roles of NAD^+, which include ADP-ribosylation, are emerging and are reviewed in [2]. ADP-ribosylation is an evolutionarily conserved posttranslational modification found in all living cells (with the exception of yeast) and involves the covalent attachment of the NAD^+ ADP-ribose moiety onto proteins. Proteins are modified with either a single ADP-ribose molecule (mono-ADP-ribosylation or MARylation), or several ADP-ribose molecules, generating linear or branched poly-ADP-ribose (PAR) chains (PARylation). Recent advances in mass spectrometry and purification techniques have allowed identification of the amino acids modified by ADP-ribosylation. The acidic amino acids aspartate and glutamate, as well as the basic amino acids lysine and arginine, are the major ADP-ribosylation sites targeted [3]. Other amino acids, including cysteine, diphtamide, phosphoserine and asparagine, are also modified, but are quantitatively less abundant [3].

1.2. Writers of mono- and poly-ADP-ribosylation

Three different enzyme families catalyze ADP-ribosylation. Extracellular ADP-ribosylation is mediated by cholera toxin-like ADP-ribosyltransferases (ARTCs) [4]. Diphteria toxin-like ADP-ribosyltransferases (ARTDs; formerly known as PARPs [5]) are the main enzymes that catalyze intracellular ADP-ribosylation. A subset of sirtuins also catalyzes intracellular ADP-ribosylation [6]. As this review focuses on chromatin ADP-ribosylation, we will only discuss ARTDs and more specifically nuclear ARTDs. Based on sequence similarities to ARTD1/PARP1, the first and best-characterized ARTD, a total of 18 human ARTDs have been identified so far with most ARTDs catalyzing MARylation, and ARTD1, ARTD2, ARTD5 and ARTD6 catalyzing PARylation [7]. ARTD9, ARTD13 and ARTD18 have no reported ADP-ribosylation activity.

1.3. Erasers of mono- and poly-ADP-ribosylation

Identification of the PAR-degrading enzyme poly (ADP-ribose) glycohydrolase (PARG) substantiated that ADP-ribosylation is a reversible protein modification [8,9]. The non-homologous ARH3 is another protein that degrades PAR [10,11]. Interestingly, even though both PARG and ARH3 efficiently hydrolyze the linkage between two ADP-ribose moieties, neither of them is able to hydrolyze the amino acid-bound ADP-ribose. The first enzyme identified to remove an amino acid-bound ADP-ribose was ARH1, which is specific for ADP-ribosylated arginine [12]. The identification of the macrodomain-containing proteins MACROD1, MACROD2 and C6orf130 (or TARG), which cleave ADP-ribose from glutamate and aspartate, marked the full reversibility of ADP-ribosylation from these residues [13–15]. MACROD1 and MACROD2 are named after the macrodomain-containing protein first identified, the histone variant macro-H2A, which recognizes MAR- and PARylation, but does not hydrolyze ADP-ribose [16–18]. So far, proteins that reverse lysine ADP-ribosylation are not known.

1.4. Readers—domains that recognize ADP-ribosylation

A growing number of domains that specifically bind ADP-ribosylated proteins are known:

PAR-binding motif (PBM): The PBM was the first PAR-binding motif found and is a stretch of around 20 hydrophobic amino acids interspersed with basic residues. The PBM appears to bind to PAR [19]. Bioinformatic analyses have revealed several hundred proteins in the human genome that might contain one or more PBMs, suggesting an intricate network of proteins, whose function and activity may depend on ADP-ribosylation [20].

PAR-binding zinc finger (PBZ): The PAR-binding zinc finger (PBZ) domain is a 30 amino acid consensus sequence that binds to two consecutive ADP-ribose moieties within PAR [21,22]. So far, only two human proteins, APFL and CHFR, have been shown to possess a PBZ, and their abilities to bind PAR chains is important for their respective roles in the DNA damage response and in cell cycle regulation [23].

Macrodomains: Compared to PBMs and PBZs, macrodomains are longer motifs (130–190 amino acids) that bind to different forms of NAD^+ derivatives, such as OAADP-ribose, MAR and the terminal ADP-ribose moiety of PAR [18]. Macrodomains have been found to be present in eleven proteins, including the different isoforms of the histone variant macroH2A, the macrodomain-containing MAR erasers MACROD1/D2 and C6orf130, and the ARTD family members ARTD7, ARTD8 and ARTD9, which contain two or even three consecutive macrodomains [24].

WWE domain: The WWE domain, which got its name from the conserved three amino acid repeat (tryptophan (W), tryptophan (W) and glutamate (E)), is found in a dozen human proteins. It binds to the *iso*-ADP-ribose moiety generated by two consecutive ADP-ribose units in a PAR chain. To date, WWE domains have been identified exclusively in certain ARTD family members and some E3 ubiquitin ligases, suggesting a functional link between ubiquitylation and ADP-ribosylation [25]. Experimental evidence has demonstrated that PAR-dependent ubiquitylation is indeed a relevant cellular regulatory mechanism [26,27].

Newly emerging PAR readers: In addition to the four aforementioned relatively well-described PAR-binding domains, additional motifs with affinities to MARylated and PARylated targets have recently been identified. Domains like the FHA or BRCT, which bind to phosphorylation, also interact with PAR [28]. Due to the structural similarities between PAR and nucleic acids, several RNA and DNA-binding motifs bind to PAR. These include the RNA recognition motif (RRM), RG/RGG motifs, the DNA-binding oligosaccharide-binding fold (OB-fold) and the PilT protein N-terminus domain (PIN domain) [29]. For a more in depth view on ADP-ribosylation binding motifs, see some recent reviews [29–31].

1.5. Cellular and organismal functions of ADP-ribosylation

Cells are constantly exposed to oxidative, genotoxic, oncogenic, inflammatory and metabolic stress, which leads to the activation of signaling cascades [32]. Genotoxic and oxidative stress

induce ADP-ribosylation via activation of ARTD1 [33,34]. The stimuli and conditions that activate and regulate the remaining ARTD family members have not yet been identified. PAR formation has been described to contribute to chromatin dynamics, genome stability maintenance, transcription, cell metabolism and development [29,35,36]. At the organismal level, ARTD1-mediated ADP-ribosylation regulates various pathological states, including cancer, inflammation, neurodegenerative and vascular diseases [37]. For a more comprehensive review on the different cellular functions of ADP-ribosylation and ARTDs, see other reviews [38,39].

2. Chromatin ADP-ribosylation in development and differentiation

In this chapter, several aspects on how ADP-ribosylation affects development and differentiation are discussed. The current literature and proposed mechanisms and functions of chromatin ADP-ribosylation in development and differentiation are summarized in Table 1.

2.1. ADP-ribosylation in development

2.1.1. ADP-ribosylation in spermatogenesis

During spermatogenesis, changes in global nuclear organization occur, including the repackaging of the genome from histones to protamines [40]. During this process, topoisomerase 2-β (TOP2B) induces DNA breaks, leading to DNA repair as a result of the phosphorylation of the histone variant H2AX (γH2AX) and PARylation at these sites, and ARTD1-mediated PARylation results in protamine inclusion and DNA decondensation [41,42]. Moreover, inhibition of ADP-ribosylation leads to abnormal histone retention in mature sperm [42]. In both humans and rodents, high levels of ARTD1 and PARG mRNA and protein are found in primary spermatocytes, suggesting a role for PAR in germinal cells [43,44]. Indeed, especially during spermatid elongation, PAR is detected concurrently with γH2AX, suggesting that ARTD1 is activated by spermatogenesis-induced DNA breaks [43].

ARTD11 is another important player in spermatogenesis, whose absence leads to abnormally shaped nuclei and chromatin detachment [45]. The mechanism behind this phenotype is not yet clear.

2.1.2. Primordial germ cell development

Primordial germ cells (PGCs), the future gametes important for reproduction, are formed during embryo gastrulation. During this process, epigenetic information, such as DNA methylation, is largely (if not completely) erased in these cells [46,47]. Upon entry into the genital ridges, PGCs undergo various nuclear changes, including heterochromatin decondensation and an increase in nuclear size [46].

During these events, important base excision repair (BER) players are upregulated at both the mRNA and protein level [48]. This coincides with ARTD1 activation and nuclear PAR formation, as well as a loss of 5-methyl-cytosine (5mC) [48]. In addition to this BER-related function, ARTD1 is activated in PGCs before the actual DNA damage response, and inhibiting ARTD1 enzymatic activity impairs methylation removal and leads to a decrease in the amount of TET1, a DNA demethylating enzyme [49]. Taken together, these findings suggest an important role for ADP-ribosylation in genome reprogramming.

2.1.3. Combined ARTD1 and ARTD2 deletion is embryonically lethal

Artd1 knockout mice are viable and fertile, but are susceptible to genomic instability and misregulated gene expression [50]. Disruption of *Artd2* sensitizes mice to ionizing radiation, and mouse embryonic fibroblasts from these mice show increased genomic instability and chromosome missegregation following treatment with alkylating agents [51]. Interestingly, *Artd1* and *Artd2* double knockouts are not viable and die at the gastrulation stage, indicating that ARTD1 and ARTD2 are essential for development in early embryos and mediate non-overlapping functions during embryogenesis, but are also redundant to some extent [51]. The lethality caused by the combined lack of ARTD1 and ARTD2 might be due to their common genome stabilizing function, as knockout of DNA repair factors such as *Xrcc1*, *Ape1*, *Fen1* or *LigIII* has also been shown to cause embryonic lethality, as reviewed in [52].

2.2. ADP-ribosylation in differentiation

ADP-ribosylation, especially mediated by ARTD1, has important effects on chromatin and cellular differentiation (Fig. 1). This review discusses some of the important developmental aspects and how ARTD1 influences them. For the phenotypes observed upon depletion of other ARTD family members, the reader is referred to [53].

2.2.1. Neuronal differentiation

Astrocytes are glial cells in the central nervous system mainly providing a structural scaffold. When growing rat astrocytes in culture, two peaks of high *Artd1* expression and activity are observed [54]. The first one marks the proliferation state, whereas the second peak coincides with differentiation [54]. These peaks are enhanced when astrocyte differentiation is increased by the addition of nerve growth factor or fibroblast growth factor β [54]. In rat neuronal stem cells (NSCs), neuronal differentiation is prevented when the expression of *achaete-scute homolog 1* (*Ascl1*) is repressed by a complex of hairy/enhancer of split (HES1) and groucho/transducin-like enhancer of split (TLE) [55]. ARTD1 is part of the HES1-TLE complex, and upon differentiation, calcium/calmodulin-dependent protein kinase II (CaMK-II) δ activates ARTD1 via phosphorylation (either directly or indirectly) [55]. This, in turn, leads to a cofactor exchange within the complex, phosphorylation of HES1 and transcription of *Ascl1* and subsequent neuronal differentiation [55]. Whether these findings are relevant to situations in vivo has to be further investigated.

2.2.2. Adipocyte differentiation

Commitment and differentiation of fibroblast-like preadipocytes to mature adipocytes require the interplay of several important transcription factors such as CCAAT-enhancer-binding proteins (C/EBPs) and the Krüppel-like family of transcription factors (KLFs) [56]. The peroxisome proliferator-activated receptor γ 2 (PPARγ2) is a key factor in terminal differentiation [56]. ARTD1, which seems to be activated by TOP2B in a manner similar to spermatogenesis, is required for *Pparg* expression, and depletion or inhibition of ARTD1 leads to a delay in adipocyte differentiation and altered histone marks in the *Pparg* promoter region [57]. PARylated ARTD1 binds PPARγ2 and enhances its ligand binding activity, which, in turn, triggers exchange of co-factors at PPARγ2 response elements (PPREs) and induces PPARγ2-dependent gene expression [58] (Fig. 2a). Interestingly, TET1 was found to demethylate PPRE regions in a PAR-dependent manner, demonstrating that ADP-ribosylation can modulate DNA methylation states [59]. Treating high-fat diet fed mice with PARP inhibitors results in lower body weight and reduces subcutaneous white adipose tissue accumulation compared to vehicle-treated mice [58]. This phenotype is also observed at the cellular level, as adipocytes isolated from PARP inhibitor-treated mice are significantly smaller and show a reduced expression of PPARγ2 target genes [58]. ARTD2 is involved in adipogenesis by recruitment to PPREs, where it acts as a cofactor of PPARγ2 [60]. However, whether enzymatic activity is needed for this function is unclear.

Table 1
Current knowledge on chromatin ADP-ribosylation in development and differentiation.

Process	ARTD member involved	Role	Putative mechanism of ARTD involved	References
Spermatogenesis	ARTD1	Enhancing	DNA break repair and chromatin decondensation	[41–43]
	ARTD11	Required	Unknown	[45]
Germ cell development	ARTD1	Enhancing	Base-excision repair	[48,49]
Neuronal differentiation	ARTD1	Repressive	Repression of neuronal differentiation genes	[54,55]
Adipogenesis	ARTD1	Enhancing	Promoting transcription of adipogenic genes	[57–59]
	ARTD2	Enhancing	Promoting transcription of adipogenic genes	[60]
Osteoclastogenesis	ARTD1	Repressive	Repression of osteoclastogenic genes	[61–64]
Cardiomyocyte differentiation	ARTD1	Enhancing	Promoting transcription of cardiomyocyte differentiation genes	[66]
Myofibroblast differentiation	ARTD1	Enhancing	Promoting myofibroblast marker gene expression via methylation	[67]
Hematopoiesis	ARTD2	Required	DNA damage control	[69]
Erythropoiesis	ARTD2	Required	DNA damage control	[71]
Dendritic cell differentiation	ARTD1	Required	Enhancing transcription factor binding to target genes	[72]
T cell differentiation	ARTD1	Enhancing	Unknown	[73,74]
	ARTD8	Enhancing	Enhancing transcription factor binding to target genes	[75]
B cell differentiation	ARTD1	Enhancing	DNA break repair	[77–79]
	ARTD8	Enhancing	Promoting transcription of prosurvival factors	[80]
Induced pluripotency	ARTD1	Enhancing	Promoting transcription of pluripotency genes	[81–87]

2.2.3. Osteoclastogenesis

Osteoclasts are multinucleated cells important for bone remodeling. The first evidence of ARTD1 involvement in osteoclastogenesis came from the identification of ARTD1 as a transcriptional repressor that binds to the promoter of V-type proton ATPase isoform 3 (*Tcirg1*) [61]. *Tcirg1* is induced during RANKL-stimulated osteoclastogenesis following cleavage of the DNA-binding domain of ARTD1 [61]. In follow-up studies, ARTD1 was found to function in a similarly repressive manner, regulating the expression of tartrate-resistant acid phosphatase (*Tracp*), matrix metallopeptidase 9 (*Mmp9*) and brain-type cytoplasmic creatine kinase (*Ckb*), three factors that are also upregulated during osteoclastogenesis [62,63]. Thus, ARTD1 works as a negative regulator of osteoclastogenesis. Indeed, a recent study has found that *Artd1* knockout mice have less bone mass and lower mineral density as a consequence of increased osteoclastogenesis and that ARTD1 acts by regulating NF-κB-induced *IL1B* expression during sustained osteoclastogenesis, which is achieved by altering the chromatin state of the *IL1B* promoter region [64].

ARTD1 seems necessary for reactive oxygen species-dependent osteodifferentiation, as knockdown of *ARTD1* in the osteosarcoma cell line SAOS-2 causes reduced differentiation [65].

2.2.4. Cardiomyocyte differentiation and myofibroblasts

In cardiomyocyte differentiation, ARTD1 modulates expression of the α- and β-myosin heavy chain genes *Myh6* and *Myh7*, respectively [66]. Embryonic cardiac cells are kept in an undifferentiated state when a repressive chromatin-remodeling complex consisting of ARTD1, histone deacetylase (HDAC) and transcription activator BRG1 binds to the *Myh6* promoter, and activating complexes, without HDACs, assemble on *Myh7* promoters [66]. When adult cardiomyocyte differentiation is triggered, loss of BRG1 reverses expression of *Myh6* and *Myh7* [66] (Fig. 2b).

Myofibroblasts have characteristics of both fibroblast and smooth muscle cells. ARTD1 is thought to enhance myofibroblast differentiation, as *Artd1* overexpression leads to enhanced expression of the myofibroblast marker *alpha-actin-2* (*Acta2*), while its knockdown decreases *Acta2* expression through regulating the DNA-methylation state of several CpG sites [67].

Interestingly, inhibition of both ADP-ribosylation and knockdown of *Artd1* have beneficial effects in various ischemia-reperfusion mouse models [68]. The underlying mechanisms leading to this phenotype need further investigations.

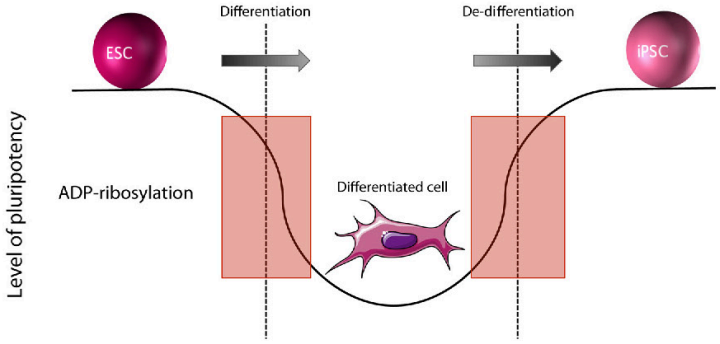

Fig. 1. The role of ADP-ribosylation in cell differentiation and induced pluripotency. During cell differentiation, ADP-ribosylation plays a dual role. On the one hand, ARTD1, by PARylation, keeps chromatin in an open state at some loci. On the other hand, ARTD1 acts as a scaffold, recruiting important players to promoters, thereby regulating expression of genes that lead to differentiation into specific lineages, as shown in neuronal and Adipocyte differentiation, where ARTD1 activates differentiation (see Sections 2.2.1 and 2.2.2, respectively), or by repressing the transcription of genes important for differentiation, as observed in osteoclastogenesis and cardiomyocyte differentiation (see Sections 2.2.3 and 2.2.4, respectively). In induced pluripotency, ARTD1 induces chromatin decompaction and keeps loci in an open state by ADP-ribosylating chromatin, thereby allowing access to transcription factors necessary for inducing and maintaining a pluripotent cell state (see Section 2.2.6).

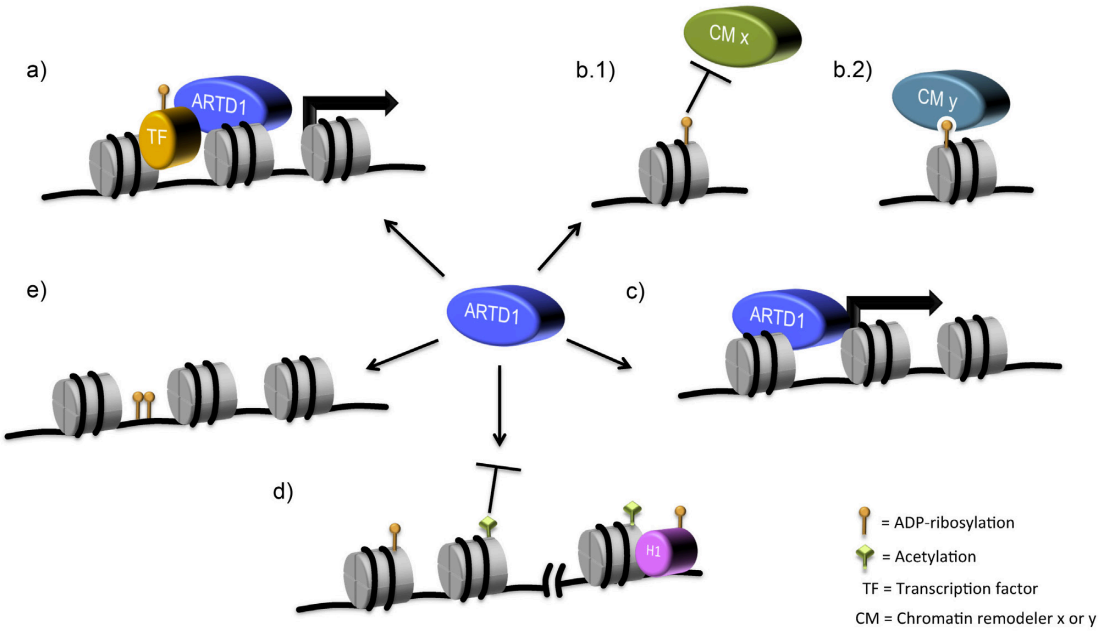

Fig. 2. Potential mechanisms by which ARTD1 might influence chromatin structure/function in differentiation and pluripotency. a) ARTD1 can act as a transcription factor (TF) cofactor, e.g. in adipocyte differentiation, where ARTD1 binds to PPARg2 and thereby modulates PPARg2-dependent gene expression (Section 2.2.2); b.1) ADP-ribosylation, being a rather bulky modification, might either keep chromatin remodelers (CM) such as HDACs and DNMTs away from histones, or b.2) alternatively, PAR could also work as a scaffold recruiting CMs (Section 2.2.4); c) Gene expression can be directly influenced by binding of ARTD1 to promoters, as seen for pluripotency in ESCs, where ARTD1 occupies promoter regions of *Nanog*, *Sox2*, and *Zfp42* (Section 2.3.1); d) As described in Section 3.3, ADP-ribosylation of histones might either co-exist or be exclusive with other marks (e.g. H1 ADP-ribosylation co-exits with H3 and H4 acetylation, but H4K16 acetylation and ADP-ribosylation are mutually exclusive; e) similar to DNA methylation, ADP-ribosylation of DNA might be another way of how ADP-ribosylation regulates DNA-dependent processes. However, this still needs to be confirmed in mammalian cells (Section 3.4).

2.2.5. Hematopoiesis

Upon a sublethal dose of whole body irradiation, bone marrow failure and premature death of mice was observed in *Artd2* but not *Artd1* knockout mice [69]. This effect is most probably associated with the role of Artd2 in the DNA damage response, as the effect was reversed by additionally knocking out p53, a factor known to play a critical role in DNA damage-induced apoptosis in hematopoietic stem cells [69,70].

Artd2 also plays a critical role in erythropoiesis. Thus, erythrocyte differentiation is impaired and mature erythrocyte lifespan is shortened in *Artd2*-deficient compared to wild-type mice, and leads to chronic anemia [71]. Similarly to the effect seen in hematopoietic stem cells, the presence of γ-H2AX foci in erythroblasts from *Artd2*-deficient mice suggests that impaired DNA-damage control is responsible for the anemic phenotype in these mice [71]. Together, these studies reveal an important role of *Artd2* in maintenance and differentiation of hematopoietic stem cells.

2.2.6. Immune cells

Dendritic cells: Monocytes can differentiate into antigen-presenting dendritic cells. This process coincides with increased *ARTD1* mRNA and protein levels [72]. Furthermore, inhibition of ARTD activity was found to reduce NF-κB and AP-1 DNA binding activity, thereby regulating gene transcription of their respective target genes [72].

T cells: A study investigating the differentiation of $CD4^+CD25^+/Foxp3^+$ regulatory T cells (Treg) showed their increase in *Artd1* knockout mice compared to wildtype by a so far unknown mechanism [73]. Differentiation of T cells into T helper 2 (Th2), but not Th1 cells, is promoted by ARTD1 [74]. The same is observed for ARTD8 (a cofactor of STAT6, CoaSt6), which modulates DNA-binding of STAT6 to the *Gata3* promoter region [75]. Interestingly, T cell differentiation is also impaired in *Artd2* knockout mice, which suggests that PAR plays an important general role in T cell development [76].

B cells: ARTD1 also takes part in B cell maturation. When stimulated with antigens, gene conversions introduced by DNA lesions through activation-induced cytidine deaminase (AID) and, subsequent, mutagenic repair, generates immunoglobulin variants [77]. ARTD1 is expressed in germinal centers and its deficiency increases non-mutagenic repair of AID-induced lesions, which ultimately impairs gene conversion [78]. During class switch recombination, which also requires AID, lack or inhibition of ARTD1 leads to an increase in class switches to IgA, IgG1 and IgG2b and a decrease in IgG2a [79]. ARTD8 promotes B lymphocyte IL-4-mediated survival after irradiation or withdrawal from a trophic environment by regulating the expression of apoptotic factors [80].

2.3. ADP-ribosylation in maintenance of pluripotency

2.3.1. ADP-ribsoylation in embryonic stem cells

Pluripotency in embryonic stem cells (ESC) requires ADP-ribosylation. ESCs maintain a metastable state by keeping the expression of key pluripotency factors balanced with the help of reversible histone marks [81]. By occupying the promoter regions of the pluripotency markers *Nanog*, *Sox2* and *Zfp42*, ARTD1 and ARTD14 maintain these genes in an open chromatin state, and, conversely, upon depletion of *Artd1* and *Artd14*, DNA methylation and repressive histone marks (H3K9me3 and H3K27me3) are introduced at these loci [81] (Fig. 2c).

2.3.2. ADP-ribosylation in induced pluripotency

ARTD1 also plays a role in the reprogramming of induced pluripotent stem cells (iPSCs) obtained by adding the four key factors Oct4, Sox2, Klf4 and c-Myc to somatic cells [82] (Fig. 1). Compared to mouse embryonic fibroblasts and differentiated cells, ARTD1 levels and PARylation are upregulated in iPSCs, and ARTD1 was shown to act downstream of c-Myc and PARylate various chromatin-remodeling factors [83]. Moreover, ADP-ribosylation of SOX2 is required for expression of *Fgf4*, an otherwise indispensible repressed factor that initiates "stemness" reprogramming [84–86]. ARTD1 and TET2 have both been found to localize to *Nanog* and *Esrrb* loci, where they establish active histone marks and ARTD1 facilitates Oct4 access to these loci [87]. Taken together, the findings summarized in this chapter underscore the importance of ARTD1 and its activity in reprogramming, establishing and maintaining pluripotency.

3. Function of chromatin ADP-ribosylation in pluripotency, stemness and differentiation

3.1. Chromatin aspects

Even though proposed almost 50 years ago, the simple and elegant Waddington model of cell differentiation still holds true to date [88]. In his model, Waddington proposes a pluripotent cell to be a marble on top of a hill; the marble takes different choices as it rolls down the hill and these choices become rarer, the further downhill the marble rolls. The final destination at the bottom of the hill represents the full differentiation of a cell. This simple model nicely illustrates how a cell undergoes differentiation into a specific lineage. Numerous studies have demonstrated that pluripotent stem cells, which can give rise to all of the different cell types of a body, can be isolated from embryos or induced from adult cells by reprogramming [47]. Recent findings indicate that a particularly 'open' chromatin state contributes to maintenance of pluripotency [89]. Two principles maintaining pluripotency are emerging: First, specific factors maintain a globally open chromatin state accessible for transcriptional activation; second, additional chromatin regulators contribute to the local silencing of lineage-specific genes until differentiation is triggered [89]. The same principles are thought to be active during the open chromatin reacquisition process upon reprogramming to pluripotency, and during de-differentiation of cancer cells (Fig. 1).

Concerning differentiation, there are also two main processes involved. On one hand, differentiation at the DNA level is achieved through transcription factors and "inherited" chromatin modifications, stabilizing specific gene expression patterns, and preventing transcription of genes not appropriate for a specific lineage, and on the other hand, the accessibility to the DNA prevents or enhances access for these differentiation factors [90]. Accessibility is regulated in large by the structure and compaction of chromatin. The degree of chromatin compaction directly impacts DNA-associated processes, like transcription, replication and DNA repair. Local chromatin structure and compaction are affected by several factors, e.g. chromatin structural protein density (i.e. histone proteins) and the chemical modification state. Histone protein acetylation, methylation, and/or phosphorylation, as well as the recruitment of chromatin remodeling complexes that displace nucleosomes influence chromatin compaction in particular [91,92]. For a more comprehensive review on chromatin regulation of differentiation and development, see [93]. In this chapter, we will focus on how the aspects discussed in Chapter 2 might be achieved by ADP-ribosylation at the mechanistic level.

3.2. Structural aspects of chromatin ADP-ribosylation

Chromatin poses a barrier for all DNA-associated processes, like replication and transcription, by hindering transcription factor and DNA-binding protein access to DNA [94]. ARTD1 is an important factor that contributes to the change in chromatin state from condensed to more accessible. Insight into this mechanism of action came when researchers found that addition of ARTD1 to chromatin in the absence of NAD^+ causes chromatin compaction and that subsequent NAD^+ addition stimulates PAR formation and chromatin decondensation [95] (Fig. 1). Importantly, complimentary studies have demonstrated that addition of PARG reverses this process [96] and that chromatin relaxation does not coincide with in vitro histone modification alterations or nucleosomes loss [97]. In vivo studies in fruit flies have provided supporting evidence, demonstrating that active ARTD1 decondenses chromatin to allow gene transcription [98]. ADP-ribosylated nucleosomes reduce chromatin compaction in vitro, making it more susceptible to micrococcal nuclease digestion [99]. Moreover, ADP-ribosylated chromatin from HeLa cells is more prone to degradation by nuclease treatment [100]. Finally, in vivo PARylation increases DNA accessibility without changing the content of ARTD1 and H3, suggesting that ADP-ribosylation alters nucleosome interactions rather than inducing histone eviction [101].

In conclusion, in addition to the functional level at which ADP-ribosylation affects chromatin accessibility, PARylation and MARylation also directly influence chromatin structure, which might be equally important.

3.3. Histone ADP-ribosylation and crosstalk with histone marks

Multiple posttranslational modifications have been described for histones tails. While analyses on histone ADP-ribosylation were initially performed with cell extracts and exogenously radiolabeled NAD^+ as substrate [102–105], a recently developed mass spectrometry (MS)-based method revealed that histones and DNA-associated proteins are also endogenously extensively and dynamically ADP-ribosylated [106].

Histone ADP-ribosylation is thought to mainly be carried out by the nuclear writers ARTD1, ARTD2 and ARTD3 [37]. However, one cannot exclude modification by other members of the ARTD family, which either modify histones in the cytoplasm or shuttle to the nucleus themselves. Indeed, in vitro modification reactions have demonstrated that ARTD1, ARTD3, ARTD10, and ARTD14 can modify the four core histones [107–110]. The close proximity of histones and their tails within the nucleus, together with the limited number of modifiable amino acids support a theory, in which crosstalk between ADP-ribosylation and other histone marks tightly regulate histone functions. As ADP-ribose modifications are rather bulky, they are likely to heavily influence histone accessibility, nucleosome incorporation and other aspects of histone function.

Crosstalk with acetylation: Early studies have suggested that ADP-ribosylation and acetylation coincide at the same nucleosomes with the linker histone H1 being the major target for ADP-ribosylation and histones H3 and H4 being primarily acetylated [111,112]. Interestingly, in vitro ADP-ribosylation of the H4K16 site is inhibited when preacetylated peptides are used as substrate [107]; thus suggesting that acetylation and ADP-ribosylation of a specific lysine residue are mutually exclusive (Fig. 2d). In cardiomyocytes, ARTD1 is found to be associated with HDACs at specific loci, suggesting interplay of ADP-ribosylation and acetylation [66].

Crosstalk with methylation: Histone H1 is methylated at several sites by the histone lysine N-methyltransferase SET7/9 [113]. Interestingly, in vitro ADP-ribosylation of H3 prevents methylation of H3 by SET7/9, but promotes linker histone H1 methylation,

demonstrating that the modification of one histone can either promote or inhibit the modification state of other histones [113]. In vivo, crosstalk of ADP-ribosylation and methylation is observed in cells from *ARTD1* knockout mice, where the myofibroblast marker gene *Acta2* is found to be hypermethylated [67]. Moreover, the demethylase TET1 is regulated by ARTD1 in PGC development and adipogenesis [49,59]

Crosstalk with phosphorylation: Phosphorylated histones can be ADP-ribosylated, but ADP-ribosylation of histones represses their propensity to be phosphorylated [112]. This is likely due to steric hindrance, preventing kinase binding [114]. Thus, it is not clear whether the ADP-ribosylation of histone tails occurs in a mutually exclusive manner with certain histone marks but not with others, or whether the same amino acid can be differentially modified. Further studies are therefore required.

3.4. ADP-ribose as an epigenetic mark?

Epigenetic modifications are defined as modifications that induce structural chromatin adaptations (due to histone or DNA modifications) to register, signal or perpetuate altered activity states. These chromosomal changes are maintained and inherited even when the initial signal is removed. Treatment of mammalian cells with a first generation ADP-ribosylation inhibitor results in hypermethylation of CpG islands [115]. Moreover ARTD1 reportedly affects DNA methylation [116,117] and controls CTCF-dependent insulator function e.g. by connecting active loci enriched in circadian genes to repressed lamina-associated domains (LADs) [118]. However, no developmental defects linked to the functions of CTCF have been observed in the different ARTD knockout mouse models available [119]. Apart from the ability to modify proteins, some ARTs also ADP-ribosylate DNA. First evidence was found in the cabbage butterfly *Pieris rapae*, which expresses a protein homologous to the cholera and diphtheria toxins and is toxic to several cancer cell lines [120]. Pierisin, the *Streptomyces scabies* potato pathogen Scabin and the clam ADP-ribosylating protein CARP-1 found in several clam species, have recently been shown to ADP-ribosylate guanine-containing substrates, including small nucleotides, single or double-stranded oligo DNA strands and genomic DNA [121–124]. It is not clear whether mammalian DNA can also be ADP-ribosylated, whether DNA ADP-ribosylation interferes with DNA methylation and/or histone modification states, or whether ADP-ribosylation acts in a chromatin-independent manner by modifying DNA directly (Fig. 2e). Taking all of the above findings into consideration, it is clear that ADP-ribosylation needs to be added to the histone mark catalogue as an additional important player in chromatin regulation [125].

3.5. Open questions

While many questions concerning ADP-ribosylation and its role in development and differentiation have been answered, especially in the context of chromatin, still many remain open. We are currently lacking the technical tools that can easily distinguish between the different degrees of ADP-ribosylation (i.e., MARylation, oligo (O)ARylation, and PARylation), but are close to their development. Thus, defining the specificities of additional ADP-ribosylation binding domains might help identifying suitable binders for specifically detecting the different modifications. Advances in peptide synthesis using ADP-ribose linked amino acids are required for generating antibodies targeting specific modification sites. It will be interesting to provide more insights as to which extent and how the different ARTDs influence chromatin architecture and gene expression. Knockout mice of the respective ARTDs will shed more light on these issues. Until recently, the enrichment and localization of genome-wide ADP-ribosylated chromatin has proven to be difficult and research has mainly focused on defining the ADP-ribosylation states at specific loci. Petesch and Lis were able to detect spreading of ADP-ribosylation at the promoter of heat shock protein 70 (*Hsp70*) upon heat shock [126]. This methodology made use of an adapted chromatin immunoprecipitation (ChIP) protocol, in which samples were crosslinked and precipitated with trichloroacetic acid before immunoprecipitation with a PAR antibody [126]. However, a recent study improved this methodology by eliminating the requirement for commercially available PAR antibodies, and uses well-characterized ADP-ribosylation reader domains (see Chapter 1.4) to pull down ADP-ribosylated chromatin (ADPr-ChAP) [101]. Using the RNF146 WWE domain, and a corresponding binding-deficient mutant control, oxidative stress-induced ADP-ribosylation was found at heterochromatic regions with high nucleosome density and repressive histone marks, and in a second adipogenesis cellular model, ADP-ribosylation localized to the promoter regions of PPARγ-dependent target genes [101]. Thus, the use of different PAR- and MAR-binding domains might aid in the identification of additional ADP-ribosylated chromatin components and help us to deepen our understanding of the physiological role of chromatin ADP-ribosylation in the cell.

Acknowledgements

The authors would like to thank Stephan Christen and Deena Leslie Pedrioli (both University of Zurich) for editorial assistance and critical input during the writing. We apologize to all the researchers, whose work could not be included in the review due to space restrictions. Work on ADP-ribosyltransferases in the laboratory of M.O.H is supported by the Swiss National Science Foundation (SNF 310030B_138667, 310030_157019).

References

[1] L.A. Sazanov, Nat. Rev. Mol. Cell Biol. 16 (2015) 375–388.
[2] C. Canto, K.J. Menzies, J. Auwerx, Cell Metab. 22 (2015) 31–53.
[3] F. Rosenthal, M.O. Hottiger, Front. Biosci. 19 (2014) 1041–1056.
[4] M. Seman, S. Adriouch, F. Haag, F. Koch-Nolte, Curr. Med. Chem. 11 (2004) 857–872.
[5] M.O. Hottiger, P.O. Hassa, B. Luscher, H. Schuler, F. Koch-Nolte, Trends Biochem. Sci. 35 (2010) 208–219.
[6] R.H. Houtkooper, E. Pirinen, J. Auwerx, Nat. Rev. Mol. Cell Biol. 13 (2012) 225–238.
[7] S. Vyas, I. Matic, L. Uchima, J. Rood, R. Zaja, R.T. Hay, I. Ahel, P. Chang, Nat. Commun. 5 (2014) 4426.
[8] M. Miwa, T. Sugimura, J. Biol. Chem. 246 (1971) 6362–6364.
[9] K. Ueda, J. Oka, S. Naruniya, N. Miyakawa, O. Hayaishi, Biochem. Biophys. Res. Commun. 46 (1972) 516–523.
[10] S. Oka, J. Kato, J. Moss, J. Biol. Chem. 281 (2006) 705–713.
[11] T. Ono, A. Kasamatsu, S. Oka, J. Moss, Proc. Natl. Acad. Sci. U. S. A. 103 (2006) 16687–16691.
[12] J. Moss, M.K. Jacobson, S.J. Stanley, Proc. Natl. Acad. Sci. U. S. A. 82 (1985) 5603–5607.
[13] F. Rosenthal, K.L. Feijs, E. Frugier, M. Bonalli, A.H. Forst, R. Imhof, H.C. Winkler, D. Fischer, A. Caflisch, P.O. Hassa, B. Luscher, M.O. Hottiger, Nat. Struct. Mol. Biol. 20 (2013) 502–507.
[14] G. Jankevicius, M. Hassler, B. Golia, V. Rybin, M. Zacharias, G. Timinszky, A.G. Ladurner, Nat. Struct. Mol. Biol. 20 (2013) 508–514.
[15] R. Sharifi, R. Morra, C. Denise Appel, M. Tallis, B. Chioza, G. Jankevicius, M.A. Simpson, I. Matic, E. Ozkan, B. Golia, M.J. Schellenberg, R. Weston, J.G. Williams, M.N. Rossi, H. Galehdari, J. Krahn, A. Wan, R.C. Trembath, A.H. Crosby, D. Ahel, R. Hay, A.G. Ladurner, G. Timinszky, R.S. Williams, I. Ahel, EMBO J. 32 (2013) 1225–1237.
[16] J. Pehrson, V. Fried, Science 257 (1992) 1398–1400.
[17] G. Kustatscher, M. Hothorn, C. Pugieux, K. Scheffzek, A.G. Ladurner, Nat. Struct. Mol. Biol. 12 (2005) 624–625.
[18] G. Timinszky, S. Till, P.O. Hassa, M. Hothorn, G. Kustatscher, B. Nijmeijer, J. Colombelli, M. Altmeyer, E.H. Stelzer, K. Scheffzek, M.O. Hottiger, A.G. Ladurner, Nat. Struct. Mol. Biol. 16 (2009) 923–929.
[19] J. Pleschke, H. Kleczkowska, M. Strohm, F. Althaus, J. Biol. Chem. 275 (2000) 40974–40980.
[20] J.-P. Gagné, M. Isabelle, K. Lo, S. Bourassa, M. Hendzel, V. Dawson, T. Dawson, G. Poirier, Nucleic Acids Res. 36 (2008) 6959–6976.
[21] S. Eustermann, C. Brockmann, P. Mehrotra, J.-C. Yang, D. Loakes, S. West, I. Ahel, D. Neuhaus, Nat. Struct. Mol. Biol. 17 (2010) 241–243.

[22] G.Y. Li, R.D. McCulloch, A.L. Fenton, M. Cheung, L. Meng, M. Ikura, C.A. Koch, Proc. Natl. Acad. Sci. U. S. A. 107 (2010) 9129–9134.
[23] I. Ahel, D. Ahel, T. Matsusaka, A.J. Clark, J. Pines, S.J. Boulton, S.C. West, Nature 451 (2008) 81–85.
[24] R.C. Aguiar, K. Takeyama, C. He, K. Kreinbrink, M.A. Shipp, J. Biol. Chem. 280 (2005) 33756–33765.
[25] Z. Wang, G.A. Michaud, Z. Cheng, Y. Zhang, T.R. Hinds, E. Fan, F. Cong, W. Xu, Genes Dev. 26 (2012) 235–240.
[26] Y. Zhang, S.M. Liu, C. Mickanin, Y. Feng, O. Charlat, G.A. Michaud, M. Schirle, X.Y. Shi, M. Hild, A. Bauer, V.E. Myer, P.M. Finan, J.A. Porter, S.M.A. Huang, F. Cong, Nat. Cell Biol. 13 (2011) (623-U292).
[27] H.C. Kang, Y.I. Lee, J.H. Shin, S.A. Andrabi, Z. Chi, J.P. Gagne, Y. Lee, H.S. Ko, B.D. Lee, G.G. Poirier, V.L. Dawson, T.M. Dawson, Proc. Natl. Acad. Sci. U. S. A. 108 (2011) 14103–14108.
[28] M. Li, L.Y. Lu, C.Y. Yang, S. Wang, X. Yu, Genes Dev. 27 (2013) 1752–1768.
[29] F. Teloni, M. Altmeyer, Nucleic Acids Res. 44 (2016) 993–1006.
[30] T. Kalisch, J.C. Ame, F. Dantzer, V. Schreiber, Trends Biochem. Sci. 37 (2012) 381–390.
[31] R. Zaja, A. Mikoc, E. Barkauskaite, I. Ahel, Biomolecules 3 (2012) 1–17.
[32] N. Kourtis, N. Tavernarakis, EMBO J. 30 (2011) 2520–2531.
[33] X. Luo, W.L. Kraus, Genes Dev. 26 (2012) 417–432.
[34] C. Hegedus, L. Virag, Redox Biol. 2 (2014) 978–982.
[35] M. Stilmann, M. Hinz, S.C. Arslan, A. Zimmer, V. Schreiber, C. Scheidereit, Mol. Cell 36 (2009) 365–378.
[36] D. Ahel, Z. Horejsi, N. Wiechens, S.E. Polo, E. Garcia-Wilson, I. Ahel, H. Flynn, M. Skehel, S.C. West, S.P. Jackson, T. Owen-Hughes, S.J. Boulton, Science 325 (2009) 1240–1243.
[37] P.O. Hassa, S. Haenni, M. Elser, M.O. Hottiger, Microbiol. Mol. Biol. Rev. 70 (2006) 789–829.
[38] B.A. Gibson, W.L. Kraus, Nat. Rev. Mol. Cell Biol. 13 (2012) 411–424.
[39] K.L. Feijs, P. Verheugd, B. Luscher, FEBS J. 280 (2013) 3519–3529.
[40] C. Rathke, W.M. Baarends, S. Awe, R. Renkawitz-Pohl, Biochim. Biophys. Acta-Gene Regul. Mech. 1839 (2014) 155–168.
[41] L. Marcon, G. Boissonneault, Biol. Reprod. 70 (2004) 910–918.
[42] M.L. Meyer-Ficca, J.D. Lonchar, M. Ihara, M.L. Meistrich, C.A. Austin, R.G. Meyer, Biol. Reprod. 84 (2011) 900–909.
[43] M. Meyer-Ficca, H. Scherthan, A. Bürkle, R. Meyer, Chromosoma 114 (2005) 67–74.
[44] B.B. Maymon, M. Cohen-Armon, H. Yavetz, L. Yogev, B. Lifschitz-Mercer, S.E. Kleiman, A. Botchan, R. Hauser, G. Paz, Fertil. Steril. 86 (2006) 1402–1407.
[45] M.L. Meyer-Ficca, M. Ihara, J.J. Bader, N.A. Leu, S. Beneke, R.G. Meyer, Biol. Reprod. 92 (2015) 80.
[46] P. Hajkova, K. Ancelin, T. Waldmann, N. Lacoste, U.C. Lange, F. Cesari, C. Lee, G. Almouzni, R. Schneider, M.A. Surani, Nature 452 (2008) 877–881.
[47] P. Hajkova, S. Erhardt, N. Lane, T. Haaf, O. El-Maarri, W. Reik, J. Walter, M.A. Surani, Mech. Dev. 117 (2002) 15–23.
[48] P. Hajkova, S. Jeffries, C. Lee, N. Miller, S. Jackson, M. Surani, Science 329 (2010) 78–82.
[49] F. Ciccarone, F.G. Klinger, A. Catizone, R. Calabrese, M. Zampieri, M.G. Bacalini, M. De Felici, P. Caiafa, PLoS One 7 (2012) e46927.
[50] C.M. Simbulan-Rosenthal, D.H. Ly, D.S. Rosenthal, G. Konopka, R. Luo, Z.Q. Wang, P.G. Schultz, M.E. Smulson, Proc. Natl. Acad. Sci. U. S. A. 97 (2000) 11274–11279.
[51] J. Menissier de Murcia, M. Ricoul, L. Tartier, C. Niedergang, A. Huber, F. Dantzer, V. Schreiber, J.C. Ame, A. Dierich, M. LeMeur, L. Sabatier, P. Chambon, G. de Murcia, EMBO J. 22 (2003) 2255–2263.
[52] R. Hakem, EMBO J. 27 (2008) 589–605.
[53] M.O. Hottiger, Annu. Rev. Biochem. 84 (2015) 227–263.
[54] M. Chabert, C. Niedergang, F. Hog, M. Partisani, P. Mandel, Biochim. Biophys. Acta 1136 (1992) 196–202.
[55] B.-G. Ju, D. Solum, E. Song, K.-J. Lee, D. Rose, C. Glass, M. Rosenfeld, Cell 119 (2004) 815–829.
[56] E.D. Rosen, O.A. MacDougald, Nat. Rev. Mol. Cell Biol. 7 (2006) 885–896.
[57] S. Erener, M. Hesse, R. Kostadinova, M.O. Hottiger, Mol. Endocrinol. 26 (2012) 79–86.
[58] M. Lehmann, E. Pirinen, A. Mirsaidi, F.A. Kunze, P.J. Richards, J. Auwerx, M.O. Hottiger, Nucleic Acids Res. 43 (2015) 129–142.
[59] K. Fujiki, A. Shinoda, F. Kano, R. Sato, K. Shirahige, M. Murata, Nat. Commun. 4 (2013) 2262.
[60] P. Bai, S.M. Houten, A. Huber, V. Schreiber, M. Watanabe, B. Kiss, G. de Murcia, J. Auwerx, J. Menissier-de Murcia, J. Biol. Chem. 282 (2007) 37738–37746.
[61] G.E. Beranger, D. Momier, N. Rochet, D. Quincey, J.M. Guigonis, M. Samson, G.F. Carle, J.C. Scimeca, J. Bone Miner. Res. 21 (2006) 1757–1769.
[62] G.E. Beranger, D. Momier, N. Rochet, G.F. Carle, J.C. Scimeca, J. Bone Miner. Res. 23 (2008) 564–571.
[63] J. Chen, Y. Sun, X. Mao, Q. Liu, H. Wu, Y. Chen, J. Biol. Chem. 285 (2010) 36315–36321.
[64] A. Robaszkiewicz, C. Qu, E. Wisnik, T. Ploszaj, A. Mirsaidi, F.A. Kunze, P.J. Richards, P. Cinelli, G. Mbalaviele, M.O. Hottiger, Sci. Rep. 6 (2016) 21131.
[65] A. Robaszkiewicz, K. Erdelyi, K. Kovacs, I. Kovacs, P. Bai, E. Rajnavolgyi, L. Virag, Free Radic. Biol. Med. 53 (2012) 1552–1564.
[66] C.T. Hang, J. Yang, P. Han, H.L. Cheng, C. Shang, E. Ashley, B. Zhou, C.P. Chang, Nature 466 (2010) 62–67.
[67] B. Hu, Z. Wu, P. Hergert, C.A. Henke, P.B. Bitterman, S.H. Phan, Am. J. Pathol. 182 (2013) 71–83.
[68] P. Pacher, C. Szabo, Cardiovasc. Drug Rev. 25 (2007) 235–260.
[69] J. Farres, J. Martin-Caballero, C. Martinez, J.J. Lozano, L. Llacuna, C. Ampurdanes, C. Ruiz-Herguido, F. Dantzer, V. Schreiber, A. Villunger, A. Bigas, J. Yelamos, Blood 122 (2013) 44–54.
[70] A. Villunger, E.M. Michalak, L. Coultas, F. Mullauer, G. Bock, M.J. Ausserlechner, J.M. Adams, A. Strasser, Science 302 (2003) 1036–1038.
[71] J. Farres, L. Llacuna, J. Martin-Caballero, C. Martinez, J.J. Lozano, C. Ampurdanes, A.J. Lopez-Contreras, L. Florensa, J. Navarro, E. Ottina, F. Dantzer, V. Schreiber, A. Villunger, O. Fernandez-Capetillo, J. Yelamos, Cell Death Differ. 22 (2015) 1144–1157.
[72] A. Aldinucci, G. Gerlini, S. Fossati, G. Cipriani, C. Ballerini, T. Biagioli, N. Pimpinelli, L. Borgognoni, L. Massacesi, F. Moroni, A. Chiarugi, J. Immunol. 179 (2007) 305–312.
[73] F. Nasta, F. Laudisi, M. Sambucci, M. Rosado, C. Pioli, J. Immunol. 184 (2010) 3470–3477.
[74] M. Sambucci, F. Laudisi, F. Novelli, E. Bennici, M.M. Rosado, C. Pioli, Sci. World J. 2013 (2013) 375024.
[75] P. Mehrotra, A. Hollenbeck, J.P. Riley, F. Li, R.J. Patel, N. Akhtar, S. Goenka, J. Allergy Clin. Immunol. 131 (521–531) (2013) e512.
[76] J. Yelamos, Y. Monreal, L. Saenz, E. Aguado, V. Schreiber, R. Mota, T. Fuente, A. Minguela, P. Parrilla, G. de Murcia, E. Almarza, P. Aparicio, J. Menissier-de Murcia, EMBO J. 25 (2006) 4350–4360.
[77] H. Arakawa, J. Hauschild, J.M. Buerstedde, Science 295 (2002) 1301–1306.
[78] M.N. Paddock, B.D. Buelow, S. Takeda, A.M. Scharenberg, PLoS Biol. (2010) 8.
[79] P. Shockett, J. Stavnezer, J. Immunol. 151 (1993) 6962–6976.
[80] S.H. Cho, S. Goenka, T. Henttinen, P. Gudapati, A. Reinikainen, C.M. Eischen, R. Lahesmaa, M. Boothby, Blood 113 (2009) 2416–2425.
[81] S.J. Roper, S. Chrysanthou, C.E. Senner, A. Sienerth, S. Gnan, A. Murray, M. Masutani, P. Latos, M. Hemberger, Nucleic Acids Res. 42 (2014) 8914–8927.
[82] K. Takahashi, S. Yamanaka, Cell 126 (2006) 663–676.
[83] S.H. Chiou, B.H. Jiang, Y.L. Yu, S.J. Chou, P.H. Tsai, W.C. Chang, L.K. Chen, L.H. Chen, Y. Chien, G.Y. Chiou, J. Exp. Med. 210 (2013) 85–98.
[84] F. Gao, S.W. Kwon, Y. Zhao, Y. Jin, J. Biol. Chem. 284 (2009) 22263–22273.
[85] F.A. Weber, G. Bartolomei, M.O. Hottiger, P. Cinelli, Stem Cells 31 (2013) 2364–2373.
[86] Y.S. Lai, C.W. Chang, K.M. Pawlik, D. Zhou, M.B. Renfrow, T.M. Townes, Proc. Natl. Acad. Sci. U. S. A. 109 (2012) 3772–3777.
[87] C.A. Doege, K. Inoue, T. Yamashita, D.B. Rhee, S. Travis, R. Fujita, P. Guarnieri, G. Bhagat, W.B. Vanti, A. Shih, R.L. Levine, S. Nik, E.I. Chen, A. Abeliovich, Nature 488 (2012) 652–655.
[88] C.H. Waddington, The Strategy of the Genes; A Discussion of Some Aspects of Theoretical Biology, Allen & Unwin, London, 1957.
[89] A. Gaspar-Maia, A. Alajem, E. Meshorer, M. Ramalho-Santos, Nat. Rev. Mol. Cell Biol. 12 (2011) 36–47.
[90] T. Graf, T. Enver, Nature 462 (2009) 587–594.
[91] A.J. Bannister, T. Kouzarides, Cell Res. 21 (2011) 381–395.
[92] C.R. Clapier, B.R. Cairns, Annu. Rev. Biochem. 78 (2009) 273–304.
[93] A. Wutz, Adv. Exp. Med. Biol. 786 (2013) 307–328.
[94] L. Bintu, T. Ishibashi, M. Dangkulwanich, Y.Y. Wu, L. Lubkowska, M. Kashlev, C. Bustamante, Cell 151 (2012) 738–749.
[95] G. Poirier, G. de Murcia, J. Jongstra-Bilen, C. Niedergang, P. Mandel, Proc. Natl. Acad. Sci. U. S. A. 79 (1982) 3423–3427.
[96] G. de Murcia, A. Huletsky, D. Lamarre, A. Gaudreau, J. Pouyet, M. Daune, G. Poirier, J. Biol. Chem. 261 (1986) 7011–7017.
[97] C. Realini, F. Althaus, J. Biol. Chem. 267 (1992) 18858–18865.
[98] A. Tulin, A. Spradling, Science 299 (2003) 560–562.
[99] C. Hough, M. Smulson, Biochemistry 23 (1984) 5016–5023.
[100] M.A. Perez-Lamigueiro, R. Alvarez-Gonzalez, Ann. N. Y. Acad. Sci. 1030 (2004) 593–598.
[101] G. Bartolomei, M. Leutert, M. Manzo, T. Baubec, M.O. Hottiger, Mol. Cell 61 (2016) 474–485.
[102] P. Adamietz, R. Bredehorst, H. Hilz, Eur. J. Biochem. 91 (1978) 317–326.
[103] L. Burzio, P. Riquelme, S. Koide, J. Biol. Chem. 254 (1979) 3029–3037.
[104] N. Ogata, K. Ueda, O. Hayaishi, J. Biol. Chem. 255 (1980) 7610–7615.
[105] N. Ogata, K. Ueda, H. Kagamiyama, O. Hayaishi, J. Biol. Chem. 255 (1980) 7616–7620.
[106] R. Martello, M. Leutert, S. Jungmichel, V. Bilan, S.C. Larsen, C. Young, M.O. Hottiger, M.L. Nielsen, Nat. Commun. (2016) (in press).
[107] S. Messner, M. Altmeyer, H. Zhao, A. Pozivil, B. Roschitzki, P. Gehrig, D. Rutishauser, D. Huang, A. Caflisch, M.O. Hottiger, Nucleic Acids Res. 38 (2010) 6350–6362.
[108] S.L. Rulten, A.E. Fisher, I. Robert, M.C. Zuma, M. Rouleau, L. Ju, G. Poirier, B. Reina-San-Martin, K.W. Caldecott, Mol. Cell 41 (2011) 33–45.
[109] H. Kleine, E. Poreba, K. Lesniewicz, P.O. Hassa, M.O. Hottiger, D.W. Litchfield, B.H. Shilton, B. Lüscher, Mol. Cell 32 (2008) 57–69.
[110] L. MacPherson, L. Tamblyn, S. Rajendra, F. Bralha, J.P. McPherson, J. Matthews, Nucleic Acids Res. 41 (2013) 1604–1621.
[111] N. Malik, M. Smulson, Biochemistry 23 (1984) 3721–3725.
[112] M. Wong, M. Miwa, T. Sugimura, M. Smulson, Biochemistry 22 (1983) 2384–2389.
[113] I. Kassner, M. Barandun, M. Fey, F. Rosenthal, M.O. Hottiger, Epigenet. Chromatin 6 (2013) 1.
[114] Y. Tanigawa, M. Tsuchiya, Y. Imai, M. Shimoyama, Biochem. Biophys. Res. Commun. 113 (1983) 135–141.
[115] A. de Capoa, F. Febbo, F. Giovannelli, A. Niveleau, G. Zardo, S. Marenzi, P. Caiafa, FASEB J. 13 (1999) 89–93.

[116] T. Guastafierro, B. Cecchinelli, M. Zampieri, A. Reale, G. Riggio, O. Sthandier, G. Zupi, L. Calabrese, P. Caiafa, J. Biol. Chem. 283 (2008) 21873–21880.
[117] T. Osada, A.M. Ryden, M. Masutani, Biochem. Biophys. Res. Commun. 434 (15–21) (2013) 1.
[118] T. Landseer, Keats-Shelley Rev. 27 (2013) 23–24.
[119] A. Sparago, F. Cerrato, M. Vernucci, G.B. Ferrero, M.C. Silengo, A. Riccio, Nat. Genet. 36 (2004) 958–960.
[120] T. Kono, M. Watanabe, K. Koyama, T. Kishimoto, S. Fukushima, T. Sugimura, K. Wakabayashi, Cancer Lett. 137 (1999) 75–81.
[121] M. Watanabe, T. Kono, Y. M.Atsushima-Hibiya, T. Kanazawa, N. Nishisaka, T. Kishimoto, K. Koyama, T. Sugimura, K. Wakabayashi, Proc. Natl. Acad. Sci. U. S. A. 96 (1999) 10608–10613.
[122] T. Takamura-Enya, M. Watanabe, Y. Totsuka, T. Kanazawa, Y. Matsushima-Hibiya, K. Koyama, T. Sugimura, K. Wakabayashi, Proc. Natl. Acad. Sci. U. S. A. 98 (2001) 12414–12419.
[123] B. Lyons, R. Ravulapalli, J. Lanoue, M.R. Lugo, D. Dutta, S. Carlin, A.R. Merrill, J. Biol. Chem. 291 (2016) 11198–11215.
[124] T. Nakano, Y. Matsushima-Hibiya, M. Yamamoto, S. Enomoto, Y. Matsumoto, Y. Totsuka, M. Watanabe, T. Sugimura, K. Wakabayashi, Proc. Natl. Acad. Sci. U. S. A. 103 (2006) 13652–13657.
[125] M.O. Hottiger, FEBS Lett. 585 (2011) 1595–1599.
[126] S.J. Petesch, J.T. Lis, Mol. Cell 45 (2012) 64–74.

MCP MOLECULAR & CELLULAR PROTEOMICS ASBMB

Technological Innovation and Resources

New Quantitative Mass Spectrometry Approaches Reveal Different ADP-ribosylation Phases Dependent On the Levels of Oxidative Stress*[S]

Vera Bilan‡§, Nathalie Selevsek¶, Hans A. V. Kistemaker‖, Jeannette Abplanalp‡§, Roxane Feurer‡, Dmitri V. Filippov‖, and Michael O. Hottiger‡**

Oxidative stress is a potent inducer of protein ADP-ribosylation. Although individual oxidative stress-induced ADP-ribosylated proteins have been identified, it is so far not clear to which extent different degrees of stress severity quantitatively and qualitatively alter ADP-ribosylation. Here, we investigated both quantitative and qualitative changes of the hydrogen peroxide (H_2O_2)-induced ADP-ribosylome using a label-free shotgun quantification and a parallel reaction monitoring (PRM) mass spectrometry approach for a selected number of identified ADP-ribosylated peptides. Although the major part of the basal HeLa ADP-ribosylome remained unchanged upon all tested H_2O_2 concentrations, some selected peptides change the extent of ADP-ribosylation depending on the degree of the applied oxidative stress. Low oxidative stress (*i.e.* 4 μM and 16 μM H_2O_2) caused a reduction in ADP-ribosylation of modified proteins detected under untreated conditions. In contrast, mid to strong oxidative stress (62 μM to 1 mM H_2O_2) induced a significant increase in ADP-ribosylation of oxidative stress-targeted proteins. The application of the PRM approach to SKOV3 and A2780, ovarian cancer cells displaying different sensitivities to PARP inhibitors, revealed that the basal and the H_2O_2-induced ADP-ribosylomes of SKOV3 and A2780 differed significantly and that the sensitivity to PARP inhibitors correlated with the level of ARTD1 expression in these cells. Overall, this new PRM-MS approach has proven to be sensitive in monitoring alterations of the ADP-ribosylome and has revealed unexpected alterations in proteins ADP-ribosylation depending on the degree of oxidative stress. ***Molecular & Cellular Proteomics 16: 10.1074/mcp.O116.065623, 949–958, 2017.***

ADP-ribosylation of proteins is a reversible post-translational modification (PTM)[1] in which the ADP-ribose moiety of NAD^+ is transferred onto a specific amino acid of the acceptor protein. Intracellular ADP-ribosylation is catalyzed by diphtheria toxin-like ADP-ribosyltransferases consisting of 17 members in humans (ARTDs, also known as PARPs) (1). Whereas many ARTDs catalyze mono-ADP-ribosylation (MARylation), only ARTD1, ARTD2, ARTD5, and ARTD6 can extend MAR by attaching additional ADP-ribose units and producing poly-ADP-ribosylation (PAR) chains (2). Under steady state conditions, PAR levels are low and hardly detectable (3). The induction of PAR synthesis occurs in response to different stress stimuli such as oxidative stress, DNA damage, and ionizing radiation and is mainly ARTD1 dependent (3). Treatment of cells with hydrogen peroxide (H_2O_2), which mimics oxidative stress in cells, induces the PLC/IP3R/Ca^{2+}/PKCα signaling cascade to subsequently activate nuclear ARTDs (mainly ARTD1) and to induce within a few minutes PAR formation in the nucleus (4, 5). The half-life of PARylation is short, and the polymers are quickly degraded by poly (ADP-ribose) glycohydrolase (PARG).

Cellular ADP-ribosylation has been linked to the development of neurodegenerative (6, 7) and metabolic diseases,

From the ‡Department of Molecular Mechanisms of Disease, University of Zurich, Winterthurerstrasse 190, CH-8057 Zurich, Switzerland; §Molecular Life Science (MLS) program of the Life Science Zurich Graduate School, University of Zurich, Winterthurerstrasse 190, CH-8057 Zurich, Switzerland; ¶Functional Genomics Center Zurich, University of Zurich/ETH Zurich, Winterthurerstrasse 190, CH-8057 Zurich, Switzerland; ‖Leiden Institute of Chemistry, Department of Bio-organic Synthesis, Leiden University, Einsteinweg 55, 2333 CC, Leiden, The Netherlands

Received November 16, 2016, and in revised form, March 20, 2017
Published, MCP Papers in Press, March 21, 2017, DOI 10.1074/mcp.O116.065623

Author contributions: V.B. and N.S. planned the experiments. V.B. performed the experiments, analyzed and interpreted the results and wrote the manuscript. H.A.V.K. and D.V.F. performed synthesis of the peptides. R.F. performed pull-down experiments with the peptides, J.A. performed the detection of oxidative stress markers by Western Blot. M.O.H. supervised the experiments and provided overall guidance.

[1] The abbreviations used are: PTM, post-translational modification; PRM-MS, parallel reaction monitoring mass spectrometry; ARTD, ADP-ribosyltransferase diphtheria toxin-like; PAR, poly-ADP-ribose; MAR, mono-ADP-ribose; AUC, area under the curve; ER, endoplasmic reticulum; PARPi, ADP-ribosylation inhibitor; LFQ, label free quantification; PARylation, reaction of PAR synthesis; MARylation, reaction of attachment of MAR to the target protein; AGC, automated gain control; PARG, poly (ADP-ribose) glycohydrolase.

Proteomic analyses identify ARH3 as a serine mono-ADP-ribosylhydrolase

Jeannette Abplanalp[1,2], Mario Leutert[1,2], Emilie Frugier[3], Roxane Feurer[1], Jiro Kato[4], Joel Moss[4], Amedeo Caflisch[3], Michael O. Hottiger[1,*]

[1] Department of Molecular Mechanisms of Disease, University of Zurich, Winterthurerstrasse 190, 8057 Zurich, Switzerland

[2] Molecular Life Science PhD Program of the Life Science Zurich Graduate School, Winterthurerstrasse 190, 8057 Zurich, Switzerland

[3] Department of Biochemistry, University of Zurich, Winterthurerstrasse 190, 8057 Zurich, Switzerland

[4] Laboratory of Translational Research, National Heart, Lung, and Blood Institute, NIH, Bethesda, MD 20892-1590, USA

[*] corresponding author: michael.hottiger@dmmd.uzh.ch

Abstract

ADP-ribosylation is a posttranslational modification that exists in monomeric and polymeric forms. Whereas the writers (e.g. ARTD1/PARP1) and erasers (e.g. PARG, ARH3) of poly-ADP-ribosylation (PARylation) are relatively well described, the enzymes involved in mono-ADP-ribosylation (MARylation) have been less well investigated. While erasers for the MARylation of glutamate/aspartate and arginine have been identified, the respective enzymes with specificity for serine are still missing. Here, we report that *in vitro*, ARH3 specifically binds and demodifies proteins and peptides that are MARylated. Structural modelling and site-directed mutagenesis of ARH3 revealed that numerous residues are critical for both the mono- and the poly-ADP-ribosylhydrolase activity of ARH3. Notably, a mass spectrometry approach showed that ARH3-deficient MEFs are characterized by a specific increase in serine-ADP-ribosylation *in vivo* under untreated conditions as well as following hydrogen-peroxide stress. Together, our results establish ARH3 as a mono-ADP-ribosylhydrolase with specificity for serine-MARylation and as an important regulator of the basal and stress induced ADP-ribosylome.

Keywords: Mono-ADP-ribosyl(-acceptor) hydrolases, serine, post-translation modification, PARG, ARH3, PARP, proteomics

Introduction

ADP-ribosylation is an evolutionarily conserved covalent posttranslational modification (PTM) mainly catalyzed by ADP-ribosyltransferases (ARTs)[1,2]. These enzymes use nicotinamide adenine dinucleotide (NAD^+) as a substrate to transfer ADP-ribose (ADPr) moieties onto specific amino acid residues of target proteins[3], leading to mono-ADP-ribosylation (MARylation), or to extend ADP-ribosylated sites to linear and branched chains of poly-ADP-ribose (PAR) also called poly-ADP-ribosylation (PARylation)[2]. To date, at least 16 different enzymes catalyze MARylation in mammals. The cholera toxin-like ARTs (ARTCs) ARTC1, 2 and 5 have been shown to specifically mono-ADP-ribosylate their target proteins[4]. Moreover, the majority of diphtheria toxin-like ARTs (ARTDs), as well as two Sirtuins, namely Sirt4 and 6, have been shown to possess MARylation activity[5,6]. Only ARTD1/2, and Tankyrase 5/6 were described to extend the protein-bound ADP-ribose unit to poly-ADP-ribose chains[2].

While the role of PARylation is well established and has been extensively studied within the last decades, especially in the context of DNA-damage and cell death[1,7], the specific roles of MARylation are less well established. It is currently unknown whether the nuclear MARylation state has a physiological role or whether it simply reflects a metabolic intermediate step that allows the building up of PAR chains. Nonetheless, an increasing number of studies suggest MARylation to be implicated in various cellular processes, including immunomodulation, ER stress, cytoskeleton rearrangement, cell metabolism and host-pathogen interactions[8]. Studying the enzymes that form (mono-ART) and remove or demodify MARylation (mono-ADP-ribosyl(-acceptor) hydrolase, mono-ARH) is most instructive for understanding the physiological role of MARylation. While the ARTCs have been shown to specifically MARylate arginine sites, the target amino acids modified by specific ARTDs are currently unknown. However, the following amino acid residues are known to be ADP-ribosylated by mammalian ARTDs: glutamate, aspartate, lysine, arginine and serine with serine having been recently identified as the major nuclear ADPr acceptor site[9,10]. A focus of current investigations lies on the ADPr acceptor site specificity of the different ARTDs and on the question whether additional amino acids can be ADP-ribosylated.

ADP-ribosylation of proteins is reversible. In mammals, two enzymes, PARG and ARH3, are known to degrade PAR chains[11,12]. The two PAR hydrolases are structurally very distinct though they both hydrolyze PAR chains[13]. Whereas several cytosolic, mitochondrial and nuclear isoforms of PARG have been described[14], ARH3 seems to exist in only one isoform, which, however, was reported to be likewise present in the cytosol, mitochondria and nucleus[15]. PARG has both endo- and exo-glycosidase activities that hydrolyze the glycosidic linkage between ADP-ribose moieties of PAR chains[16-19]. On the other hand, according to the three-dimensional structure of ARH3, the cavity of ARH3 only docks to the terminal ADP-ribose moiety of the PAR chain[13], suggesting that ARH3 has exoglycosidase activity, and thus is unable to substitute for PARG.

ARH3 was initially identified as an ARH1-like protein with PAR hydrolase activity, generating ADP-ribose from PAR[12]. ARH3 seems to be ubiquitously expressed in mouse and human tissues[12]. The 39-kDa ARH3 shares amino acid sequence similarity with both ARH1 and ARH2. ARH3 activity, like that of ARH1, needs Mg^{2+}. Critical vicinal acidic amino acids in ARH3, identified by mutagenesis (i.e. Asp77and Asp78), are located in a region similar to that required for activity in ARH1[12].

ARH3 also participates in nuclear and cytoplasmic PAR degradation under oxidative stress conditions induced by hydrogen peroxide[15]. ARH3 deficient (KO) mouse embryonic fibroblasts (MEFs) were more susceptible to hydrogen peroxide-induced cytotoxicity than WT MEFs[15]. Cell death in ARH3 KO MEFs occurred in a caspase-independent manner, accompanied by nuclear shrinkage, chromatin condensation, and exposure of phosphatidylserine on the cell surface. Cytoplasmic PAR seen in ARH3 KO MEFs appeared to enhance Apoptosis Inducing Factor-release from mitochondria and translocation to the nucleus, leading to large-scale DNA fragmentation and chromatin condensation. Thus, despite the fact that ARH3 has lower PAR-degrading activity than PARG[12], the different substrates for PAR degradation and the cellular localization may contribute to their unique roles in the regulation of parthanatos, the PARP-dependent form of programmed cell death[20].

The first enzyme described to hydrolyze MARylation was ADP-ribosylarginine hydrolase 1 (ARH1), which releases ADPr from arginine residues[21]. ARH1-deficient mice show spontaneous development of various tumors, suggesting a role for MARylation in tumorigenesis[22]. In contrast, ARH3 does not hydrolyze mono-ADP-ribose-arginine, -cysteine, -diphthamide, or -asparagine bonds[12,13,23], but ARH3 was found to hydrolyze *O*-acetyl-ADP-ribose (*O*AADPR)[23,24], a product of the Sir2-catalyzed NAD-dependent histone deacetylation reaction[25-28] to produce ADP-ribose in a time- and Mg^{2+} dependent reaction and thus could participate in two signaling pathways[23]. There is so far no evidence for PARG having any mono-ARH activity. Recently, we and others identified the mammalian proteins MACROD1, MACROD2 and TARG (the latter is also referred to as OARD1 or C6ORF130) as novel glutamate- and aspartate-specific mono-ADP-ribosylhydrolases[29-31]. The physiological role of each of these three hydrolases as well as their precise site specificity, however, remains poorly understood. Mutations within the gene encoding for TARG have been linked to the development of severe neurological dysfunction in humans[31]. MACROD1 and MACROD2 were previously described to be mutated or differentially expressed in the context of different cancers[32,33]. MACROD1 has also been proposed to be a regulator of adipogenesis and insulin secretion[34]. Whether the reported phenotypes are dependent on the ability of these three enzymes to hydrolyze MAR has yet to be elucidated. No hydrolases capable of releasing ADPr from other ADP-ribose acceptor sites (e.g. serine or lysine residues) have yet been published. This is in part due to the fact that the identification of MAR hydrolases substrates has so far been difficult to assess owing to technical limitations in identifying ADP-ribosylated proteins and the respective acceptor amino acids.

However, recent advances in enrichment protocols and the adaptation of specialized peptide fragmentation techniques in mass spectrometry allowed identification of the cellular ADP-ribosylome in untreated and hydrogen-peroxide treated cells as well as in mouse organs[10,35].

We report here, when comparing ARH3 and PARG activity, that ARH3 was found, in addition to its PAR hydrolase activity, to preferentially catalyze demodification of MARylated serines, as shown by *in vitro* demodification of MARylated proteins and mass spectrometry (MS) analysis of enriched ADP-ribosylated peptides. Structural modeling revealed amino acids in the catalytic cleft of ARH3 that proved important for both binding and hydrolysis of MARylated and PARylated peptides. A comprehensive cellular proteomics approach demonstrated the *in vivo* relevance of ARH3's serine-mono-ARH activity by a specific increase in unique serine-ADPr sites in MEFs from ARH3-deficient ($ARH3^{-/-}$) animals as compared to wildtype controls. Finally, we provide a rich dataset of ARH3 targeted proteins and their corresponding ADP-ribosylation sites.

Materials and Methods

All chemicals were purchased from Sigma unless otherwise stated.

Cloning and protein purification

Human ARTD1 was cloned, expressed and purified as previously described[36]. GST-histone tail fusion proteins (GST-H3 and GST-H2B tail) were cloned and purified as previously described[37]. Wildtype human ARH1 and ARH3 were cloned using primers (Microsynth) to amplify the sequence from a purchased cDNA clone (BioCat) by PCR and cloned into pGEX6P-3 using restriction enzymes BamHI and XhoI (NEB). ARH3 mutants were cloned by site-directed mutagenesis with fragment and overlap PCRs. The catalytic domain of mouse ARTD8 (residues 1216-1817) was cloned into pGEX6P-3 using restriction enzymes BamHI and SalI (NEB). Sequencing of plasmids was performed at Microsynth.

Plasmids were transformed into BL21 *E. coli*, and protein expression induced by adding 1 mM IPTG at OD_{600} 0.4-0.6 for 3 h at 30 °C. Batch purification of GST-tagged proteins was performed using glutathione sepharose 4B beads (GE Healthcare) according to the manufacturer's manual. Expression and purification of all recombinant proteins was analyzed by SDS–PAGE followed by Coomassie staining.

***In vitro* ADP-ribosylation assay with recombinant proteins**

To obtain ADP-ribosylated ARTD1, H3 and H2B tails, and HMGB1, recombinant proteins were incubated in reaction buffer RB (50 mM Tris-HCl pH 7.4, 4 mM $MgCl_2$ and 250 µM dithiothreitol (DTT)) at a ratio 1:3 (ARTD1 to histone tail) with 100 nM [^{32}P]NAD^+ (Perkin Elmer) and 200 nM of double-stranded annealed 40 bp long oligomer (5'-3' TGCGACAACGATGAGATTGCCACTACTTGAACCAGTGCGG) for 15' at 37°C. ADP-ribosylation was stopped by adding 10 µM PJ34.

Automodification of ARTD8 was carried out in RB with 150 nM [^{32}P]NAD^+ and 10 µM cold NAD^+ for 1h at 37°C. The reaction was stopped by filtering through an Illustra MicroSpin G-50 column (GE Healthcare) according to the manufacturer's manual.

ADP-ribosylation of actin was performed as described earlier[38]. Briefly, 2 µg β/γ actin (Cytoskeleton Inc.) was incubated with 50 ng CDTa in the presence of 100 nM [^{32}P]NAD^+, 150 µM cold NAD^+ and reaction buffer (5 mM HEPES, pH 7.5, 0.1 mM CaCl2, 0.5 mM NaAc, 0.1 mM ATP) at 37 °C. The reaction was stopped by filtering through a G50 column.

***In vitro* de-ADP-ribosylation assay with recombinant proteins**

Demodification reactions were performed in RB. Unless otherwise stated, 10 pmol automodified ARTD1 and 30 pmol transmodified histone tail were incubated with 10 pmol PARG or ARH3 for 15' at 37 °C. For demodification of ARTD8, 30 pmol automodified recombinant protein were incubated

with 30 pmol PARG or ARH3 for 1 h at 37 °C. Chemical demodification of ADP-ribosylated actin was performed by addition of 0.5 M hydroxylamine and incubation for 15 min at 37°C or overnight incubation at 37°C with the respective hydrolases. Reactions were stopped by adding SDS-loading buffer, with subsequent boiling at 95 °C for 5 min. Samples were run on an SDS-PAGE gel, stained with Coomassie blue, photographed, destained, and exposed on phosphorscreens overnight or up to one day. Images were taken with a Typhoon FLA 9400 phosphorimager (GE Healthcare). Signal intensities were analyzed and quantified using ImageJ. For quantification of the MAR hydrolase activity, the signal intensity (radioactivity and Coomassie) for every stained band was determined using ImageJ. The radioactivity signal R normalized to the respective Coomassie signal C results in the specific modification signal S.

$$S = \frac{R}{C}$$

The specific activity A of the demodifying enzyme is given by

$$A = 1 - \frac{S_X}{S_i}$$

where S_X is the specific modification signal of a given condition (enzyme X) and S_i is the specific modification signal of the input sample.

Pulldown using biotinylated ADP-ribosylated H2B peptide

To test binding of ARH3 and PARG to biotinylated ADP-ribosylated or non-modified H2B peptide (synthesis as described in[39]), peptides were bound to streptavidin sepharose high performance beads (GE Healthcare). For each pull-down, 5 µl of beads were primed by washing three times in binding buffer (50 mM NaCl, 50 mM Tris-HCl pH 8, 0.05% NP-40) and incubated overnight at 4°C in 1 ml binding buffer with 5 µg of the modified or unmodified peptide. Beads were washed with 1 ml incubation buffer (0.1% NP-40, 1x protease inhibitor cocktail (Roche), 50 mM Tris-HCl pH 8, 1 mM DTT, 50 mM NaCl). Two µg of recombinant protein were incubated with the beads and 1 ml incubation buffer for 3h at 4°C. Subsequently, the beads were washed 3 times with incubation buffer and once with 1 ml cold PBS before addition of SDS-loading buffer, sample boiling and western blotting.

Cells

MEFs from $Arh3^{+/+}$ and $Arh3^{-/-}$ mice were cultured as previously described[15]. HeLa, HEK and U2OS cells were cultured in DMEM supplemented with 5% penicillin/streptomycin (P/S) and 10% fetal calf serum (FCS).

Enrichment of ADP-ribosylated Peptides from Cell Lysate

For the PARG/ARH3 peptide demodification assay, HeLa cells were treated with 1 mM H_2O_2 in PBS

containing 1 mM $MgCl_2$ and further processed as described previously[40] with the following alterations: Tannic acid (75 µM) was added to the lysis buffer and PARG treatment was omitted after tryptic digestion. For every condition, the macrodomain enrichment was performed in triplicates on 7 mg peptides. The eluted MARylated and PARylated peptides were reconstituted in 50 mM Tris–HCl, pH 8, 10 mM $MgCl_2$, 250 mM DTT and 50 mM NaCl. 45 pmol ARH3 or PARG were added to the peptide mixture and the demodification reactions were performed at 37°C for 1h. Subsequently, the mixture was filtered through a Microcon-30 cut off centrifugal filter (Merck Millipore), acidified with TFA and desalted on reverse phase C18 StageTips.

The MEF wildtype and Arh3 knockout cells were either left in DMEM for 1 h or treated with 500 uM H_2O_2 for 1 h in DMEM. After one wash with PBS, cells were scraped and lysed by adding 6 M guanidine-hydrochloride (Gnd-HCL), 5 mM tris(2-carboxyethyl)phosphine (TCEP), 100 mM Tris pH 8, 95°C[41]. The samples were diluted with 25 mM Tris, pH 8, and digested with trypsin (Promega). The peptide mixture was treated with PARG to obtain only MARylated peptides, and the peptides were enriched using a macrodomain affinity pulldown as described previously[40].

Liquid Chromatography and MS Analysis

MS analysis for the recombinant PARG/ARH3 peptide demodification assay was performed on an Orbitrap Q Exactive mass spectrometer (Thermo Fisher Scientific) coupled to a nano EasyLC 1000 (Thermo Fisher Scientific). The peptides were loaded onto a self-made column (75 mm x 150 mm), which was packed with reverse-phase C18 material (ReproSil-Pur 120 C18-AQ, 1.9 µm, Dr. Maisch GmbH). Solvent compositions in channels A and B were 0.1% formic acid in H_2O and 0.1% formic acid in acetonitrile, respectively. The peptides were separated at a flow rate of 300 nL/min by a 130 min elution gradient protocol from 2% to 25% B in 100 min, 25% to 35% B in 10 min, 35% to 95% in 10 min and 95% B for 10 min.

The mass spectrometer was set to acquire full-scan MS spectra (300–1700 m/z) at a resolution of 70'000 after accumulation to an automated gain control (AGC) target value of $3x10^6$. Charge state screening was enabled, and unassigned charge states, and single charged precursors were excluded. Ions were isolated using a quadrupole mass filter with a 2 m/z isolation window. A maximum injection time of 250 ms was set. HCD fragmentation was performed at a normalized collision energy (NCE) of 25%. Selected ions were dynamically excluded for 30 s.

The identification of ADP-ribosylated peptides from MEF cells was performed on an Orbitrap Fusion Tribrid mass spectrometer (Thermo Fisher Scientific), coupled to a nano EasyLC 1000 liquid chromatograph (Thermo Fisher Scientific). We applied an ADP-ribose product-dependent method called HCD-PP-EThcD as described in[42]. Briefly, the method includes high-energy data-dependent HCD, followed by high-quality HCD and EThcD MS/MS when more than two ADP-ribose fragment peaks (136.0623, 250.0940, 348.07091, and 428.0372) were observed in the HCD scan. A detailed description of the MS parameters can be found in[42]. Solvent compositions in channels A and B were

0.1% formic acid in H2O and 0.1% formic acid in acetonitrile, respectively.

Peptides were loaded onto an Acclaim PepMap 100 (Thermo Scientific) trap column, 75 µm x 2 cm, packed with C18 material, 3 µm, 100 A, and separated on an analytical EASY-Spray column (Thermo Scientific, 75 µm × 500 mm) packed with reverse-phase C18 material (PepMap RSLC, 2 µm, 100 A). Peptides were eluted over 110 min at a flow rate of 300 nL/min. An elution gradient protocol from 2% to 25% B, followed by two steps, 35% B for 5 min and 95% B for 5 min, was used.

MS Data Analysis

MS and MS/MS spectra were converted to Mascot generic format (MGF) by use of Proteome Discoverer, v2.1 (Thermo Fisher Scientific, Bremen, Germany). When multiple fragmentation techniques (HCD and EThcD) were utilized, separate MGF files were created from the raw file for each type of fragmentation. MGF files were further processed as described in[42]. The MGFs resulting from measurement following the peptide demodification assay were searched against the UniProtKB human database (taxonomy 9606, version 20140422), which included 35'787 Swiss-Prot entries, 37'802 TrEMBL entries, 73'589 decoy hits, and 260 common contaminants. The MGFs resulting from the MEF cell measurements were searched against the UniProtKB mouse database (taxonomy 10090, version 20160902), which included 24'905 Swiss-Prot, 34'616 TrEMBL entries, 59'783 decoy hits, and 262 common contaminants.

Mascot 2.5.1.3 (Matrix Science) was used for peptide sequence identification with previously described search settings[43] and some modification for the EThcD searches[42]. Enzyme specificity was set to trypsin, allowing up to 4 missed cleavages. The ADP-ribose variable modification was set to a mass shift of 541.0611, with scoring of the neutral losses equal to 347.0631 and 249.0862. The marker ions at m/z 428.0372, 348.0709, 250.0940, 136.0623 were ignored for scoring. S, R, K, D and E residues were set as variable ADP-ribose acceptor sites. Carbamidomethylation was set as a fixed modification on C and oxidation as a variable modification on M. Peptides are considered correctly identified when a Mascot score >20 and an expectation value <0.05 are obtained. For the ADP-riboslyation site analyses, peptides identified with EThcD fragmentation, having a mascot localization score > 95% were used if not stated otherwise.

To perform a label-free quantification based on the MS1 precursor peak area of the identified peptides in the peptide demodification assay, Progenesis QI software (v. 3.0.6039.34628, Nonlinear Dynamics, Purham, NC) was applied. Raw data was imported into Progenesis and aligned based on the MS1 peak retention time. All samples were normalized based on the total signal intensity to account for sample loading variations. The obtained results were exported as MGF and searched with Mascot as indicated above. The Mascot search results were imported into Scaffold software (v.4.7.2) and filtered for protein and peptide FDR values of 0.01. When multiple precursors were observed for the same peptide, the values were summed up to obtain the total level of the peptide. In order to ensure the correct assignment of the ADP-ribose localization on the peptide, we compared the

identified ADP-ribosylated peptides here to our high quality EThcD dataset published in[42]. The so-called demodified peptides were obtained by matching the ADP-riboslyated peptides identified in this experiment to their non-modified counterparts.

For the ADP-riboslyation site motif analysis, we used Weblogo[44], including ADP-ribosylated peptides identified with a mascot localization score > 80%, and a sequence window of 6 amino acids around the modified site. Volcano plot analysis of the quantified ADP-riboslyated peptides and their non-modified counterparts was performed using two-sample testing in Perseus, with a permutation-based FDR of 5% and an S0 value of 2[45]. Gene ontology analysis was performed using the PANTHER data base[46].

Gene expression

MEF cells were washed with PBS before performing RNA extraction with the NucleoSpin RNA II kit (Macherey-Nagel). RNA was quantified with a NanoDrop (Thermo Fisher Scientific) and reverse transcribed according to the supplier's protocol (High Capacity cDNA Reverse Transcription Kit, Applied Biosystems). Quantitative real-time polymerase chain reactions (qPCR) were performed with KAPA SYBR fast (Kapa Biosystems) and a Rotor-Gene Q 2plex HRM System (Qiagen).

Chromatin extraction

Cells were washed with 1 ml ice-cold PBS, collected, centrifuged at 1'000 g for 5 min at 4 °C and washed twice more with PBS. The pellet was resuspended is 3 volumes chromatin extraction buffer (200 mM NaCl, 10 mM HEPES pH 8, 3 mM $MgCl_2$, 0.5 % Triton X-100, 1x protein inhibitor cocktail (Roche)) and incubated rolling for 30 min at room temperature. Centrifugation at 10'000 g for 10 min at 4°C gave rise to the soluble fraction (supernatant). The pellet was resuspended with an equal amount of chromatin extraction buffer. The soluble fraction was sonicated once for 30 s, the chromatin fraction three times for 30 s. Protein concentration was measured using a Bradford assay (Biorad) and samples were subjected to SDS-PAGE and Western blotting.

Western blotting

For western blot analysis, proteins were separated by sodium dodecyl sulphate-polyacrylamide gel electrophoresis and bands visualized by using IR-Dye-conjugated antibodies (1:15'000, LI-COR) and detection by the Odyssey infrared imaging system (LI-COR). Antibodies used for Western blotting were anti-tetra-HIS (1:1'000, Qiagen), anti-GST-Z5 (1:1'000, Santa Cruz), anti-Tubulin (1:10'000, Sigma), anti-H3 (1:5'000 abcam), anti-ARH3 (custommade, Genosphere Biotech).

Modeling

Sequence alignments of human ARH3 and *R. rubrum* DRAG (Uniprot identifiers Q9NX46 and P14300, respectively) were performed using the Clustal Omega program on the Uniprot

webserver[47,48]. The WITNOTP program (molecular modeling software developed by A. Widmer at Novartis AG, Basel) was used to protonate all protein and ligand structures, and water molecules. In particular, His182 of ARH3 was positively charged for all minimizations. WITNOTP further served to align protein structures based on their Cα atoms (using the option STRUCTAL -3), to modify selected atom coordinates and to modify the ADP ribose ligand by addition of heavy atoms. All minimizations were performed with CHARMM[49] using the CHARMM36 forcefield for the protein atoms, water molecules and magnesium atoms, and the CHARMM general forcefield for each of the ligands[50]. Electrostatic potential surfaces, following application of pdb2pqr software[51,52], were calculated with the Adaptive Poisson-Boltzmann Solver (APBS) software package[53]. Figures were created with Pymol (The PyMOL Molecular Graphics System, Version 1.8 Schrödinger, LLC).

Results

ARH3 has mono-ADP-ribosyl-acceptor hydrolase activity

When comparing the efficiency of PARG and ARH3 in PAR degradation, we observed that ARH3 removed radioactive-labelled ADPr from auto-modified ARTD1 to an extent comparable to PARG, but demodified trans-modified recombinant H3 and H2B histone tails almost completely (**Figure 1a, left panel, Suppl Figure 1a**). The quantification of the assay revealed that ARH3 removes 80% of the PAR modification from the H3 tail whereas PARG hydrolyzed only approximately 30% (**Figure 1a, right panel**). To biochemically characterize the enzymatic reaction catalyzed by ARH3 and PARG, we performed concentration- and time-dependent experiments. ARH3, but not PARG, efficiently demodified ARTD1-transmodified H3 histone tails, suggesting that ARH3 might be a mono-ADP-ribosylhydrolase (**Suppl Figure 1b and c**). To corroborate this observation, we chose a radioactive *in vitro* MARylation/de-MARylation assay using the auto-modification ability of ARTD8 known to be a mono-ART. Intriguingly, in the demodification step using either PARG or ARH3, the radioactive signal was substantially reduced only in the presence of ARH3, but not by PARG, indicating that indeed ARH3 has *in vitro* mono-ARH activity (**Figure 1b**).

Numerous residues of the catalytic site contribute to both poly- and mono-ARH activity of ARH3

Having established that ARH3 has mono-ARH activity, we set out to study which amino acids of the catalytic cleft of ARH3 are involved in MAR binding and/or MAR hydrolase activity. To identify the crucial amino acids, we performed an automatic overlap of the 3D structures of ARH3 and the structurally-related bacterial mono-glycohydrolase DraG (PDB code 2WOE) (**Figure 1c, left panel**). The structural similarity was striking with an average deviation of only 1.4 Å for more than 200 pairs of corresponding Cα atoms (located mainly in the α-helices and close to the binding site of ADPr) despite the sequence identity of only 25%. Most importantly, upon structural overlap of the DraG/ADPr complex (PDB code 2WOE), the pose of ADPr fitted in the structure of ARH3 (PDB code 2FP0) with the linear ribose close to the two Mg ions, and without any steric conflict except for the slight re-orientation of Tyr149 during energy minimization (**Figure 1c, right panel**). Thus, we used the structural overlap to identify one potentially catalytically important water molecule and seven conserved amino acid residues with the following potential functions: holding water molecules in place (E41, D77), holding Mg^{2+} ion in place (D314, T317, E41), and binding of substrate (i.e. adenine and phosphate) (S148, H182, Y149) (**Figure 1c, right panel, and Suppl Figure 1d**). To strengthen these findings, the binding of ARH3 to MARylated peptides was further studied by mutational analysis and by comparison with results of previously described ARH3 mutants[12,23]. To test the binding to a MARylated peptide, we applied a recently developed pull-down assay using biotinylated synthetic ADP-ribosylated peptides with sequences derived from histone H2B tails (**Suppl Figure 1e**)[10,54]. These peptides were bound to streptavidin-beads and incubated with either glutathione-S-transferase (GST), wild type (WT) GST-tagged ARH3, or His-tagged PARG. After

pull-down and Western blotting with an anti-GST and anti-His antibody, respectively, a single 55 kDa band representing GST-ARH3 was detected only when ADPr-modified peptides were used for the pull-down, while PARG apparently neither bound the unmodified nor the modified peptide under the tested conditions (**Figure 1d and Suppl Figure 1f**). The data thus strongly suggest that ARH3, but not PARG, binds MARylated peptides. To substantiate that the above identified residues indeed play a role for either MAR-binding or MAR-hydrolase activity of ARH3, we generated amino acid point mutants (e.g. E41A, E41Q, D77N, G115D, S148A, Y149A, H182A, D314A and T317A) plus a double alanine replacement for D77 and D78. MAR-binding assays using the above described pull-down approach with chemically modified H2B peptides revealed six residues to be crucial for binding of ARH3 to MARylated peptides (or overall ARH3 structure) (E41, D77, G115, S148, Y149 and H182) (**Suppl Figure 2a**). However, the E41A, the D77/78A as well as the D314A and T317A mutants retained their binding capacity. With respect to enzymatic activity, demodification assays using ARTD1 auto-modified with radioactively labelled NAD^+ showed that all identified residues that retained binding capacity after mutation (i.e. E41A, D77/78A and D314A) are still crucial for the PAR hydrolase activity of ARH3 (**Figure 1e**), in line with previously published data[13]. Similar results were obtained when analyzing H3 tails modified by ARTD1 (**Suppl Figure 2b**). However, since the data with ARTD1-modified targets does not allow a conclusion about the MAR hydrolase activity per se but only about the combined PAR/MAR hydrolase activity of ARH3, the same ARH3 mutants were tested with automodified ARTD8, which acts as mono-ART and therefore solely catalyzes MARylation (**Figure 1f**). These experiments revealed that most of the tested ARH3 mutants also lost their activity to demodify MARylated ARTD8. Only E41A retained weak activity, although not to the same extent compared to WT ARH3. In contrast, the E41Q mutant completely lost the mono-ADP-ribosyl-hydrolase activity, which is most likely due to its loss of ADP-ribose binding capacity.

In summary, while the D77, D78, G115, S148, Y149, H182, D314 and T317 ARH3 mutants lost the ability to demodify both PARylated and MARylated target proteins, we identified the amino acid residue E41 to be slightly less important for the demodification of MARylated target proteins.

ARH3 hydrolyzes serine ADP-ribosylation in vitro

To address which ADPr acceptor sites can be demodified by ARH3, we applied a label-free quantification (LFQ) mass spectrometry (MS) approach, which was previously applied by our group[55]. We used hydrogen-peroxide stressed HeLa cells as a model system to generate a broad array of ADP-ribosylated proteins[35]. To prevent ADP-ribosylation and de-ADP-ribosylation of proteins during lysis, tannic acid, which inhibits both PARG and ARH3 (**Suppl Figure 2c**) as well as PJ34 (a PARP inhibitor) were added to the lysis buffer. Tryptic digest and subsequent Af1521 enrichment[35,56] resulted in an enriched pool of PARylated and MARylated peptides which was subjected to demodification by either recombinant ARH3 or PARG (**Suppl Figure 2d**). Subsequent shotgun LC-MS/MS analysis revealed that PARG treatment resulted in the identification of many spectra with

MARylated peptides, while ARH3 treatment significantly reduced the quantity of spectra with MARylated peptides (**Figure 2a**). Vice versa, the frequency of completely demodified peptides, i.e. the non-modified version of identified ADP-ribosylated peptides, increased upon ARH3 treatment (**Figure 2a**). ARH3 could de-modify most of the MARylated peptides detected after PARG treatment, suggesting that ARH3 is indeed able to completely demodify peptides and that most of the identified ADP-ribosylated proteins after H_2O_2 treatment in HeLa cells were modified with a comparable and ARH3 resolvable linkage (**Figure 2b**). This data was acquired using HCD peptide fragmentation. In principle, this approach allows the identification of ADP-ribosylated peptides and the determination of the ADP-ribosylation sites, although we have recently reported that the accuracy of ADPr acceptor assignment is difficult when potential acceptor amino acids are located beside each other due to extensive fragmentation of the ADP-ribose moiety[10,35]. In contrast, ETD based fragmentation and especially EThcD fragmentation is advantageous for this task and provides much higher accuracy and confidence for the localization of the ADPr acceptor site on the identified peptide. Therefore, to accurately annotate the modification sites for a part of the modified peptides, we matched the identified ADP-ribosylated peptides from this MS measurement to a high-quality dataset recently generated on the same biological setting using a combined HCD and EThcD approach[10,35], (**Suppl Table 1**). We performed LFQ of the ADP-ribosylated peptides and their non-modified counterparts, based on the MS1 precursor peak area. This quantitative analysis confirmed that the MARylated peptides detected after PARG treatment were lost when the peptides were treated with ARH3 instead, which resulted in a gain of the corresponding unmodified peptides (**Suppl Figure 2e**). To address which peptides and more precisely which amino acid acceptor sites are specifically de-modified by ARH3, we performed a volcano plot analysis of the quantitative data combined with our previously published high accuracy EThcD ADPr-site localization data[10] (**Figure 2c**). ARH3 demodified the majority of PARylated/MARylated peptides, while only a small set of MARylated peptides could not be demodified by ARH3. Almost all monitored peptides with annotated serine-ADPr were significantly demodified by ARH3, while some of the non-demodified MARylated peptides contained arginine as ADPr acceptor site (**Figure 2c**), providing strong evidence that ARH3 specifically demodifies peptides with ADP-ribosylated serine residues. Since the mapped ADP-ribosylated peptides with an accurately assigned ADPr acceptor sites using the EThcD setting were still low in numbers, we also matched our data to high scoring HCD fragmentation spectra and repeated the volcano plot analysis (**Suppl Fig. 2f**). Although the site localization is more promiscuous with the HCD data, the analysis strengthened our conclusion that ARH3 is completely demodifying MAR/PARylated serine, but no MARylated arginine.

One of the most prevalent protein groups found to be demodified by ARH3 among these spectra consisted of nuclear proteins including histones. To verify that ARH3 specifically demodifies serine ADPr acceptor sites *in vivo*, we carefully monitored, among the above described enriched peptide pools, two peptides with serine ADPr acceptor sites (i.e. H3 and HMGA1) that were recently

published to be modified at these serine residues[57] and two peptides with known arginine-acceptor sites[35] (i.e. P4HB and PDIA3). Detailed analysis confirmed that the serine sites were significantly demodified by ARH3 whereas the modified arginine ADPr acceptor sites remained equally abundant whether the peptides were treated with PARG or with ARH3 (**Figure 2d**). Thus, our data strongly indicates that ARH3 is a serine specific mono-ARH *in vitro*. It remains to be determined which residue(s) regulate the specificity of DRAG and ARH1 (both arginine specific) and ARH3 (serine specific). The structural overlap of DRAG with ARH3 revealed that G115 could be a possible candidate (**Suppl Figure 2g**). However, mutating residue G115 of AHR3 to aspartate did not confer arginine-MAR-hydrolase activity, when tested on CDTa-mediated ADP-ribosylated actin (**Suppl Figure 2h**).

ARH3 regulates basal and hydrogen peroxide-induced serine ADP-ribosylation in vivo

With the above experiments, we showed that human ARH3 is a serine-specific mono-ARH *in vitro*. To address whether ARH3 contributes to the demodification of MARylated proteins *in vivo*, we mapped all ADP-ribosylated peptides (i.e. the ADP-ribosylomes) of wildtype (WT) and ARH3-deficient (KO) MEFs which both expressed *PARG* comparably (**Suppl Figure 3a**). Notably, human and mouse ARH3 share a high amino acid sequence identity. Analyses of ADP-ribosylated peptides were performed according to a LC-MS/MS measurement tailored for the analysis of ADP-ribosylated peptides [10,35]. Importantly, samples were all treated with PARG before enrichment and during the MS measurement ADP-ribose fragment ions were used for the selection of modified peptides to produce high quality HCD as well as EThcD spectra for the accurate localization of the ADP-ribose modification on the peptide sequence. Notably, the total quantity of ADP-ribosylated peptides derived from KO MEFs tremendously increased compared to WT MEFs already under basal (i.e. untreated) conditions (**Suppl Figure 3b**). In addition, we found a roughly 5-fold increase in the number of different ADP-ribosylated peptides, indicating that ARH3 strongly contributes to the ADP-ribosylation state of many proteins (**Figure 3a**). Most of the identified proteins were modified at only one site, while few where modified at several sites (**Suppl Figure 3c**). KO MEFs were earlier described to form PAR with different kinetics compared to their WT counterparts[15]. When analyzing the cellular ADP-ribosylome of ARH3 WT versus KO cells treated with 500 µM H_2O_2 for 60 minutes, we found an increased number of ADP-ribosylated peptides in both cell types as expected and described before for HeLa cells[55], but to a much larger extent in ARH3 KO cells (**Figure 3a and Suppl Figure 3b**). Interestingly, the overlapping fraction of modified peptides comparing WT versus KO remained significant after H_2O_2 treatment, and many more ADP-ribosylation sites could be observed in the KO cells (**Figure 3a**). Measurement of biological replicates confirmed the reproducibility of the biological finding and analysis pipeline (**Suppl Figure 3d**).

Utilizing the EThcD generated ADP-ribosylated peptide spectra, we found that there is a significant and specific increase in the number of unique serine-ADP-ribosylated sites both in

untreated and in H_2O_2 treated conditions comparing KO to WT cells (**Figure 3b**). Using EThcD spectra with a localization score of >95%, only peptides with modified serines could be identified. The inclusion of also HCD spectra, which are not ideal for ADPr site localization, led to the identification of more and but also different sites (e.g. lysine residues), (**Suppl Figure 3e**). Gene ontology analysis revealed that most of the proteins whose ADP-ribosylation increased in KO cells regulate DNA-associated processes in the chromatin context, although to a different extent dependent on the treatment and the cell type analyzed (**Figure 3c**). This is in agreement with the observation that a large part of ARH3 is associated with chromatin (**Suppl Figure 3f**). To confirm that the identified proteins are direct ARH3 targets, we biochemically validated the demodification of one candidate target, HMGB1. After *in vitro* ARTD1-dependent ADP-ribosylation, ARH3, but not PARG, almost completely demodified HMGB1 (**Figure 3d**).

Since it was reported that the amino acids surrounding an ADP-ribosylation site influence the binding of certain macrodomains (Kistemaker, H.A., et al. 2016), we analyzed the amino acid sequence of ARH3-targeted ADP-ribosylation sites. For this, we created sequence logos within a 13 amino acid window with the identified ADP-ribosylation site in the center. As previously observed by us and others[10,35], we could confirm a primitive KS motif for a significant portion of serine-ADPr sites in untreated ARH KO cells and upon H_2O_2 treatment of ARH3 WT and KO cells (**Figure 3e**), indicating that ARH3 is targeting the same ADP-ribosylation sites under basal and after H_2O_2 treatment. A list of all identified ADP-ribosylated proteins and peptides can be found in the supplementary materials **(Suppl Table 2).**

Finally, based on the modeling of ADPr in the putative ARH3 binding site, we added the tripeptide GSK by restraining it during energy minimization by a covalent bond between the serine side chain and the ADPr ribose close to E41 (**Figure 3f**). Interestingly the lysine next to the modified serine residue strongly associated with an acidic patch close to the postulated active site, indicating that the neighboring amino acids of an ADPr acceptor sites might contribute to the binding and subsequent demodification by ARH3. Moreover, in this model, the modified serine side chain occupies a cavity lined by G115; mutation of this residue to aspartate might accordingly prevent binding (**Suppl Figure 2a**).

In summary, our results provide strong evidence that ARH3 is responsible for the demodification of MARylated as well as PARylated peptides modified at a serine residue *in vivo* with potentially important consequences on DNA-associated processes both in physiological and pathological conditions. This data puts ARH3 in line with PARG as the direct antagonist of nuclear ARTD mediated ADP-ribosylation, with ARH3 having the potential to completely reverse serine protein ADP-ribosylation.

Discussion

We report here that ARH3, in addition to its PAR-degrading activity, exhibits a serine specific mono-ARH activity. This is reflected by the fact that ARH3 demodifies ARTD1-modified target proteins to a greater extent than PARG and, more convincingly, even demodifies MARylated ARTD8. Furthermore, we showed that ARH3 binds to MARylated peptides and we identified crucial amino acid residues responsible for binding and demodification of MARylated targets (**Figure 1**). Using mass spectrometry approaches, we showed that ARH3 preferentially demodifies serine acceptor sites (**Figure 2**). Finally, we provided *in vivo* evidence for an important regulatory role of ARH3 in chromatin organization and gene expression both under physiological and pathological conditions (**Figure 3**).

ARH3 was earlier described to bind free ADP-ribose with micromolar affinity and efficiently demodify PAR but not mono-ADP-ribose-arginine, -cysteine, -diphthamide, or -asparagine bonds[12,13]. In addition to confirming that ARH3 does not demodify arginine, we identified ARH3 as serine-specific mono-ARH due to our unbiased MS approach. The finding of increased frequency of fully demodified peptides using the *in vitro* approach (**Figure 2**) demonstrates, on the molecular level, that the chemical specificity of the mono-ARH activity of ARH3 is indeed that of a glycohydrolase (and not for instance, of a phosphodiesterase), since we found no left-over traces of the ADPr modification by MS. It still remains to show how the specificity of DRAG, ARH1 and ARH3 is controlled. Initial attempts failed to render ARH3 an arginine-specific ARH by mutating G115 to aspartate, suggesting that mutation of G115 is not sufficient and that other amino acids contribute the specificity.

Interestingly, different viral macrodomains (e.g. Chikungunya virus, O'nyong'nyong virus, Sindbis virus or Venezuelan Equine Encephalitis virus) have recently been reported to demodify ARTD8 *in vitro*[58], suggesting that potentially viral macrodomains might share the target specificity with ARH3. ARH3 did not completely demodify several MARylated target proteins (e.g. ARTD8 or HMGB1; **Figure 1b**, remaining modification of 30%), indicating that either the tested *in vitro* conditions were sub-optimal, that the amino acid sequence might contribute to the ability of the modified serine to be demodified or that additional amino acids are MARylated *in vitro,* which cannot be demodified by ARH3. Comparably, PARG and ARH3 were both not able to reduce the auto-modification of ARTD1 to an undetectable level (**Figure 1a**), raising the question as to what renders ARTD1 resistant to full demodification. This finding is however in agreement with our earlier observation that ARTD1 is found to be modified already under basal conditions in different cell types ([55] and data not shown). The inability to demodify ARTD1 could be due to steric hindrance since the detected acceptor sites span a rather short domain of ARTD1 and might inhibit full demodification, or the acceptor-site linkage might not be cleaved (e.g. lysine modification) due to promiscuous enzymatic activity *in vitro*.

The molecular architecture of ARH3 constitutes the archetype of an all-α-helical protein fold and provides insights into the reversibility of protein ADP-ribosylation[13]. Two Mg^{2+} flanked by highly

conserved amino acids pinpoint the active-site crevice. The structural overlay of DraG and ARH3 provided insights into a conserved catalytic cleft containing two potentially catalytically important water molecules. The known D77/78A mutants have been described before to be important for the binding of the water molecule. Interestingly, neither the water nor the Mg^{2+} ion seem to be important for the binding of the ADP-ribose to ARH3. Notably, the mutation analysis also provide evidence that the PAR- and MAR-hydrolase activity are dependent on a large set of common residues. Interestingly, only the mutation of E41 to Q but not A affected the demodification of MARylated ARTD8. Based on preliminary modeling of a lysine-containing ADP-ribosylated serine tripeptide, it is suggested that E41 interacts not only with the magnesium cations (via binding site water molecules), but possibly further with the tripeptide backbone. Mutation of E41 to alanine is anticipated to disturb the water structure surrounding the magnesium cations, with resulting loss of catalytic activity. By contrast, mutation of E41 to glutamine may be hypothesized to interfere with the binding of the ADP-ribosylated serine backbone and its flaking amino acid residues.

ARH3 was localized to mitochondria but is also present in the nucleus and the cytosol[12,59]. Our own data provide evidence that a substantial amount of ARH3 is associated with chromatin (**Suppl Fig. 3f**). Interestingly, most of the identified potential ARH3 targets under basal conditions were nuclear protein previously assigned to DNA-associated processes (**Figure 3c**), indicating that ARH3 is predominantly functionally relevant in the nucleus under the tested conditions. The detection of ADP-ribosylated peptides in ARH3 KO MEFs already under basal conditions strongly suggest that ARH3 contributes to the demodification of proteins under basal conditions, although we can not exclude that other enzymes might contribute to the observed increase of the ADP-ribosylome as well (**Figure 3a**). Moreover, due to the lack of MS-based methods that discriminate between MARylated and PARylated proteins, we can currently not exclude that the identified ADP-ribosylated peptides in ARH3 KO cells are only MARylated. However, given that we are not able to detect any signal by neither immunofluorescence nor Western blotting using the available antibodies against PAR strongly indicates that the majority of these peptides are MARylated (data not shown). This conclusion is further supported by the observation that the knockdown of PARG leads to PAR formation under basal conditions that can be observed by immunofluorescence using an anti-PAR antibody (data not shown). The *in vivo* experiment also revealed that at least two types of acceptor sites (i.e. serine and arginine) are modified *in vivo*. Interestingly, proteins ADPr-modified at arginines were described to localize to the ER[55], while the proteins modified at serines rather localize to the nucleus. It is tempting to speculate that different ARTs are responsible for the identified ADPr acceptor sites.

Besides PARG, ARH3 also participates in nuclear and cytoplasmic PAR degradation under oxidative stress conditions, thus providing a reason why ARH3 deficient (KO) MEFs were more susceptible to hydrogen peroxide-induced cytotoxicity compared to WT MEFs[15]. In view of our findings, ARH3 might, under oxidative stress conditions, not only protect cells by degrading PAR, but also by demodifying MARylated proteins. ARH3 thus possess both PAR and MAR hydrolase

activity. It remains to be investigated under which cellular conditions ARH3 would preferably demodify MARylated versus PARylated target proteins. This certainly also depends on the binding affinity of ARH3 to PAR- and MARylated targets. Along this line, the identified lysine residue located next to the modified serine residue (**Figure 3e**) might significantly contribute to the binding of modified peptides to ARH3 and thus favor this type of activity.

It is currently not known which cellular ARTD is responsible for ADP-ribosylation under basal conditions. Since many of the identified nuclear proteins were modified at serines upon treatment with H_2O_2, and H_2O_2 is known to mainly induce ARTD1[60], it is tempting to speculate that the proteins identified in ARH3 KO cells under unstressed conditions are modified by ARTD1 as well. In the presence of ARH3, these proteins might be immediately demodified and thus not detectable. It remains to be defined which mechanisms activate the nuclear ARTD family members to modify the detected ADP-ribosylome under basal conditions. Whether the same known molecular mechanisms (e.g. spontaneous DNA lesions, DNA replication stress) induce ARTD1/2 activation under unstressed conditions needs to be further clarified. The functional relevance of the newly identified protein ADP-ribosylation sites and the potential cross talk with other modifications (e.g. serine phosphorylation) need to be further investigated. Considering the structural and potentially functional differences between PARG and ARH3, ARH3 might be an interesting therapeutical target. Specific inhibitors for ARH3 activity might help resolving its biological function in cells, both under physiological and pathophysiological conditions.

In summary, we show that the PAR hydrolase ARH3 also has serine-specific mono-ARH activity and that ARH3 activity very likely contributes to chromatin organization and DNA associated processes, both in physiological and pathological conditions.

Author contributions

JA and MOH planned the experiments. JA performed the experiments and analyzed the results. ML performed mass spectrometry analysis and EF and AC structural analysis. KJ and JM provided WT and ARH3 KO MEFs. RF performed H2B-peptide pulldowns. MOH supervised the experiments and provided overall guidance; MOH, JA and ML wrote the manuscript.

Acknowledgment

We thank Monika Fey (University of Zurich) for the expression and purification of recombinant human ARTD1 as well as PARG and Tobias Suter (University of Zurich) for helpful discussion and providing editorial assistance. CDTa was kindly provided by Klaus Aktories (University of Freiburg). We thank Hans A.V. Kistemaker and Dmitri V. Filippov (University of Leiden) for providing chemically ADP-ribosylated peptides. We thank Paolo Nanni and Peter Gehrig (FGCZ, University of Zurich) for technical support for the MS measurements. JM and JK were supported by the Intramural Research Program, NIH, NHLBI. Research in the group of AC is funded by the Swiss National Science Foundation (SNF 315230_149897). ADP-ribosylation research in the laboratory of MOH is funded by the Canton of Zurich and the Swiss National Science Foundation Grants (SNF 310030B_138667) as well as the Forschungskredit from the Universität Zürich (to ML).

Conflict of interest

The authors declare no conflict of interest.

Figure 1

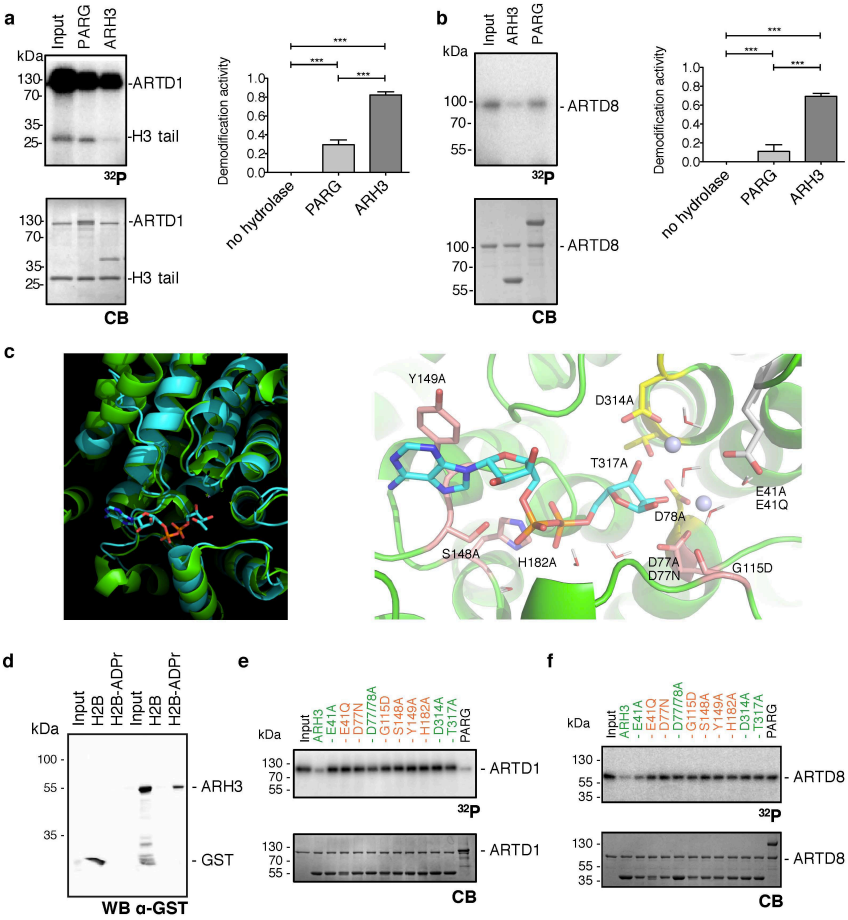

Figure 1: ARH3 has mono-ARH activity. (**a**) left panel: Recombinant H3 histone tail was *in vitro* ADP-ribosylated using recombinant ARTD1 in the presence of ^{32}P-labelled NAD^{+}. Equal fractions were left untreated (Input) or were treated with PARG or ARH3. Above: radioactivity exposure, below: Coomassie Blue-stained poly-acrylamide gel. Right panel: Quantification of (**a**) expressed as demodification activity (= reduction of the radioactive signal, normalized to amount of protein, n = 3). (**b**) left panel: Auto-modification of recombinant ARTD8 in the presence of ^{32}P-labelled NAD results in MAR-labelled ARTD8 (Input) that was subsequently treated with recombinant PARG or ARH3. Above: radioactivity exposure, below: Coomassie Blue-stained poly-acrylamide gel. Right panel: Quantification of (**b**) expressed as demodification activity (= reduction of the radioactive signal, normalized to amount of protein, n = 3). (**c**) Left panel: Structural overlap of human ARH3 (green)

and the DraG/ADPr complex (cyan). Right panel: Zoom in the active site of ARH3 with side chains of key residues which were mutated (labels). The binding mode of ADPr (carbon atoms in cyan) was obtained by energy minimization starting from the pose obtained by the structural overlap. (**d**) Western blot of pull-downs of GST alone (left) or GST-ARH3 using the biotinylated peptides with (H2B-ADPr) and without (H2B) modification. (**e**) ARTD1 auto-modified in the presence of ^{32}P-labelled NAD was subjected to demodification using WT and different ARH3 mutants. Red labels: mutants deficient in binding to H2B-ADPr, green labels: mutants retaining binding to H2B-ADPr. (**f**) ARTD8 auto-modified in the presence of ^{32}P-labelled NAD^+ was subjected to demodification using WT and different ARH3 mutants. Red labels: mutants deficient in binding to H2B-ADPr, green labels: mutants retaining binding to H2B-ADPr.

Figure 2

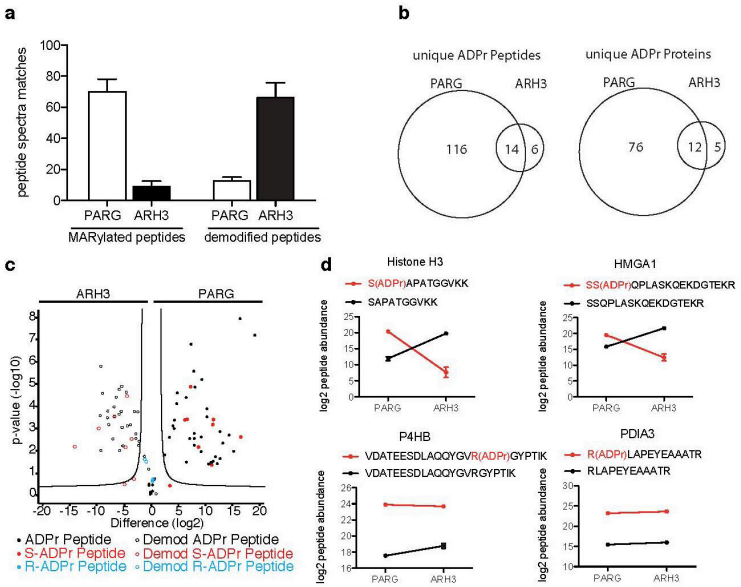

Figure 2: **ARH3 mainly hydrolyzes ADP-ribosylated serines *in vitro.*** (**a**) Number of ADP-ribosylated peptide spectra matches (PSMs) or demodified peptide spectra matches after PARG or ARH3 treatment. (**b**) Venn diagrams of unique ADPr peptides and proteins. (**c**) Volcano plot of ARH3 treated and PARG treated samples. 'Unmodified peptides' are shown as a circle and 'ADP-ribosylated peptides' as a filled circle. ADP-ribosylation sites confirmed by EThcD spectra are annotated and color coded in red as S-ADPr, and in blue as R-ADPr sites. ADP-ribosylated peptides with uncertain ADP-ribosylation site localization are shown in black. The black line represents a permutation-based FDR of 5% and a S0 value of 2. (**d**) Normalized abundance of individual Ser- and Arg-ADPr peptides after PARG or ARH3 treatment.

Figure 3

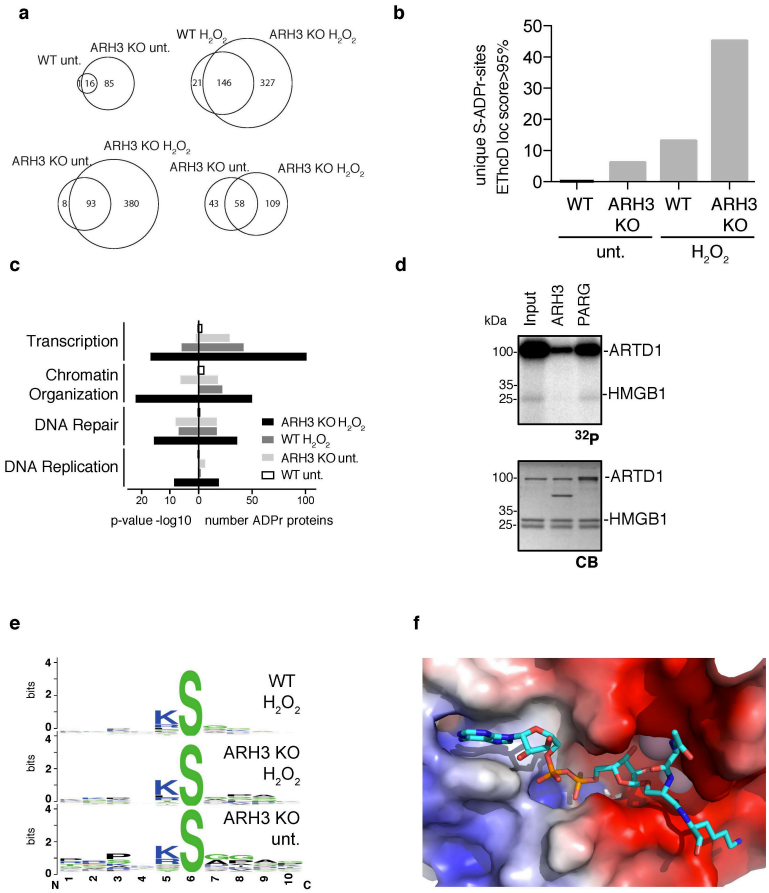

Figure 3: **ARH3 regulates basal and hydrogen peroxide-induced serine ADP-ribosylation *in vivo***. (**a**) Venn diagrams of unique ADP-riboslyated peptides of WT and ARH3-KO (KO) cells under basal and hydrogen peroxide-treated conditions. (**b**) Unique ADP-ribosylation sites detected by EThcD fragmentation in the different samples. (**c**) Gene ontology analysis using the PANTHER database of the identified ADPr-modified proteins. Shown on the left are the p-values and on the right number of identified and annotated ADP-ribosylated proteins. (**d**) Validation of mono-ARH activity of ARH3 on the nuclear protein HMGB1. Recombinant HMGB1 was *in vitro* ADP-ribosylated using recombinant ARTD1 in the presence of ^{32}P-labelled NAD^{+}. Equal fractions were left untreated (Input) or were treated with PARG or ARH3. Above: radioactivity exposure, below: Coomassie Blue-stained poly-acrylamide gel. (**e**) Motif searches for ADP-ribosylated peptides in MEF cells using Weblogo.

(**f**) Energy minimized binding mode of the acetyl-GSK peptide with ADPr-Ser modified. The surface of ARH3 is colored according to electrostatic potential. The positively charged amino group of the K side chain and two of the three backbone amide groups point towards the region of the surface with negative potential.

5. References

1. Luo, X. & Kraus, W.L. On PAR with PARP: cellular stress signaling through poly(ADP-ribose) and PARP-1. *Genes Dev* **26**, 417-432 (2012).

2. Hottiger, M.O. Nuclear ADP-Ribosylation and Its Role in Chromatin Plasticity, Cell Differentiation, and Epigenetics. *Annu Rev Biochem* **84**, 227-63 (2015).

3. Barkauskaite, E., Jankevicius, G. & Ahel, I. Structures and Mechanisms of Enzymes Employed in the Synthesis and Degradation of PARP-Dependent Protein ADP-Ribosylation. *Mol Cell* **58**, 935-46 (2015).

4. Laing, S., Unger, M., Koch-Nolte, F. & Haag, F. ADP-ribosylation of arginine. *Amino acids* **41**, 257-69 (2011).

5. Du, J., Jiang, H. & Lin, H. Investigating the ADP-ribosyltransferase activity of sirtuins with NAD analogs and 32P-NAD. *Biochemistry* **48**, 2878-2890 (2009).

6. Pan, P.W. et al. Structure and Biochemical Functions of SIRT6. *J Biol Chem* **286**, 14575-87 (2011).

7. Caldecott, K.W. Protein ADP-ribosylation and the cellular response to DNA strand breaks. *DNA Repair (Amst)* **19**, 108-13 (2014).

8. Butepage, M., Eckei, L., Verheugd, P. & Luscher, B. Intracellular Mono-ADP-Ribosylation in Signaling and Disease. *Cells* **4**, 569-95 (2015).

9. Leidecker, O. et al. Serine is a new target residue for endogenous ADP-ribosylation on histones. *Nat Chem Biol* **12**, 998-1000 (2016).

10. Bilan, V., Leutert, M., Nanni, P., Panse, C. & Hottiger, M.O. Combining HCD and EThcD fragmentation in a product dependent-manner confidently assigns proteome-wide ADP-ribose acceptor sites. *Anal Chem* **89**, 1523-1530 (2017).

11. Ueda, K., Oka, J., Naruniya, S., Miyakawa, N. & Hayaishi, O. Poly ADP-ribose glycohydrolase from rat liver nuclei, a novel enzyme degrading the polymer. *Biochem Biophys Res Commun* **46**, 516-23 (1972).

12. Oka, S., Kato, J. & Moss, J. Identification and characterization of a mammalian 39-kDa poly(ADP-ribose) glycohydrolase. *J Biol Chem* **281**, 705-13 (2006).

13. Mueller-Dieckmann, C. et al. The structure of human ADP-ribosylhydrolase 3 (ARH3) provides insights into the reversibility of protein ADP-ribosylation. *Proc Natl Acad Sci USA* **103**, 15026-31 (2006).

14. Bonicalzi, M.E., Haince, J.F., Droit, A. & Poirier, G.G. Regulation of poly(ADP-ribose) metabolism by poly(ADP-ribose) glycohydrolase: where and when? *Cell Mol Life Sci* **62**, 739-50 (2005).

15. Mashimo, M., Kato, J. & Moss, J. ADP-ribosyl-acceptor hydrolase 3 regulates poly (ADP-ribose) degradation and cell death during oxidative stress. *Proc Natl Acad Sci U S A* **110**, 18964-9 (2013).

16. Barkauskaite, E. et al. Visualization of poly(ADP-ribose) bound to PARG reveals inherent balance between exo- and endo-glycohydrolase activities. *Nat Commun* **4**, 2164 (2013).

17. Braun, S.A., Panzeter, P.L., Collinge, M.A. & Althaus, F.R. Endoglycosidic cleavage of branched polymers by poly(ADP-ribose) glycohydrolase. *Eur J Biochem* **220**, 369-375 (1994).

18. Brochu, G. et al. Mode of action of poly(ADP-ribose) glycohydrolase. *Biochim Biophys Acta* **1219**, 342-50 (1994).

19. Miwa, M., Tanaka, M., Matsushima, T. & Sugimura, T. Purification and properties of glycohydrolase from calf thymus splitting ribose-ribose linkages of poly(adenosine diphosphate ribose). *J Biol Chem* **249**, 3475-82 (1974).

20. Wang, Y. et al. Poly(ADP-ribose) (PAR) binding to apoptosis-inducing factor is critical for PAR polymerase-1-dependent cell death (Parthanatos). *Sci Signal* **4**, ra20 (2011).

21. Moss, J., Jacobson, M.K. & Stanley, S.J. Reversibility of arginine-specific mono(ADP-ribosyl)ation: identification in erythrocytes of an ADP-ribose-L-arginine cleavage enzyme. *Proc Natl Acad Sci USA* **82**, 5603-7 (1985).

22. Kato, J. et al. ADP-ribosylarginine hydrolase regulates cell proliferation and tumorigenesis. *Cancer Res* **71**, 5327-35 (2011).

23. Ono, T., Kasamatsu, A., Oka, S. & Moss, J. The 39-kDa poly(ADP-ribose) glycohydrolase ARH3 hydrolyzes O-acetyl-ADP-ribose, a product of the Sir2 family of acetyl-histone deacetylases. *Proc Natl Acad Sci U S A* **103**, 16687-91 (2006).

24. Kasamatsu, A. et al. Hydrolysis of O-acetyl-ADP-ribose isomers by ADP-ribosylhydrolase 3. *J Biol Chem* **286**, 21110-7 (2011).

25. Tanner, K.G., Landry, J., Sternglanz, R. & Denu, J.M. Silent information regulator 2 family of NAD- dependent histone/protein deacetylases generates a unique product, 1-O-acetyl-ADP-ribose. *Proc Natl Acad Sci U S A* **97**, 14178-82 (2000).

26. Borra, M.T. et al. Conserved enzymatic production and biological effect of O-acetyl-ADP-ribose by silent information regulator 2-like NAD+-dependent deacetylases. *J Biol Chem* **277**, 12632-41 (2002).

27. Jackson, M.D. & Denu, J.M. Structural identification of 2'- and 3'-O-acetyl-ADP-ribose as novel metabolites derived from the Sir2 family of beta -NAD+-dependent histone/protein deacetylases. *J Biol Chem* **277**, 18535-18544 (2002).

28. Imai, S. & Guarente, L. Ten years of NAD-dependent SIR2 family deacetylases: implications for metabolic diseases. *Trends Pharmacol Sci* **31**, 212-20 (2010).

29. Rosenthal, F. et al. Macrodomain-containing proteins are new mono-ADP-ribosylhydrolases. *Nat Struct Mol Biol* **20**, 502-7 (2013).

30. Jankevicius, G. et al. A family of macrodomain proteins reverses cellular mono-ADP-ribosylation. *Nat Struct Mol Biol* **20**, 508-514 (2013).

31. Sharifi, R. et al. Deficiency of terminal ADP-ribose protein glycohydrolase TARG1/C6orf130 in neurodegenerative disease. *EMBO J* **32**, 1225-1237 (2013).

32. Xi, H.Q., Zhao, P. & Han, W.D. Clinicopathological significance and prognostic value of LRP16 expression in colorectal carcinoma. *World J Gastroenterol* **16**, 1644-8 (2010).

33. Mohseni, M. et al. MACROD2 overexpression mediates estrogen independent growth and tamoxifen resistance in breast cancers. *Proc Natl Acad Sci U S A* **111**, 17606-11 (2014).

34. Zang, L. et al. Identification of LRP16 as a negative regulator of insulin action and adipogenesis in 3T3-L1 adipocytes. *Horm Metab Res* **45**, 349-58 (2013).

35. Martello, R. et al. Proteome-wide identification of the endogenous ADP-ribosylome of mammalian cells and tissue. *Nat Commun* **7**, 12917 (2016).

36. Altmeyer, M., Messner, S., Hassa, P.O., Fey, M. & Hottiger, M.O. Molecular mechanism of poly(ADP-ribosyl)ation by PARP1 and identification of lysine residues as ADP-ribose acceptor sites. *Nucleic Acids Research* **37**, 3723-3738 (2009).

37. Messner, S. et al. PARP1 ADP-ribosylates lysine residues of the core histone tails. *Nucleic Acids Research* **38**, 6350-6362 (2010).

38. Gulke, I. et al. Characterization of the enzymatic component of the ADP-ribosyltransferase toxin CDTa from Clostridium difficile. *Infection and Immunity* **69**, 6004-6011 (2001).

39. Kistemaker, H.A.V. et al. Synthesis and Macrodomain Binding of Mono-ADP-Ribosylated Peptides. *Angewandte Chemie-International Edition* **55**, 10634-10638 (2016).

40. Martello, R. et al. Proteome-wide identification of the endogenous ADP-ribosylome of mammalian cells and tissue. *Nature Communications* **7**(2016).

41. Poulsen, J.W., Madsen, C.T., Young, C., Poulsen, F.M. & Nielsen, M.L. Using Guanidine-Hydrochloride for Fast and Efficient Protein Digestion and Single-step Affinity-purification Mass Spectrometry. *Journal of Proteome Research* **12**, 1020-1030 (2013).

42. Bilan, V., Leutert, M., Nanni, P., Panse, C. & Hottiger, M.O. Combining Higher-Energy Collision Dissociation and Electron-Transfer/Higher-Energy Collision Dissociation Fragmentation in a Product-Dependent Manner Confidently Assigns Proteomewide ADP-Ribose Acceptor Sites. *Analytical chemistry* **89**, 1523-1530 (2017).

43. Rosenthal, F., Nanni, P., Barkow-Oesterreicher, S. & Hottiger, M.O. Optimization of LTQ-Orbitrap Mass Spectrometer Parameters for the Identification of ADP-Ribosylation Sites. *Journal of Proteome Research* **14**, 4072-4079 (2015).

44. Crooks, G.E., Hon, G., Chandonia, J.M. & Brenner, S.E. WebLogo: A sequence logo generator. *Genome Research* **14**, 1188-1190 (2004).

45. Tyanova, S. et al. The Perseus computational platform for comprehensive analysis of (prote)omics data. *Nature methods* **13**, 731-40 (2016).

46. Thomas, P.D. et al. PANTHER: a library of protein families and subfamilies indexed by function. *Genome Res* **13**, 2129-41 (2003).

47. Sievers, F. et al. Fast, scalable generation of high-quality protein multiple sequence alignments using Clustal Omega. *Mol Syst Biol* **7**, 539 (2011).

48. The UniProt, C. UniProt: the universal protein knowledgebase. *Nucleic Acids Res* **45**, D158-D169 (2017).

49. Brooks, B. et al. CHARMM: the biomolecular simulation program. *J Comput Chem* **30**, 1545-614 (2009).

50. Yu, W., He, X., Vanommeslaeghe, K. & MacKerell, A.D., Jr. Extension of the CHARMM General Force Field to sulfonyl-containing compounds and its utility in biomolecular simulations. *J Comput Chem* **33**, 2451-68 (2012).

51. Dolinsky, T.J., Nielsen, J.E., McCammon, J.A. & Baker, N.A. PDB2PQR: an automated pipeline for the setup of Poisson-Boltzmann electrostatics calculations. *Nucleic Acids Res* **32**, W665-7 (2004).

52. Dolinsky, T.J. et al. PDB2PQR: expanding and upgrading automated preparation of biomolecular structures for molecular simulations. *Nucleic Acids Res* **35**, W522-5 (2007).

53. Baker, N.A., Sept, D., Joseph, S., Holst, M.J. & McCammon, J.A. Electrostatics of nanosystems: application to microtubules and the ribosome. *Proc Natl Acad Sci U S A* **98**, 10037-41 (2001).

54. Kistemaker, H.A. et al. Synthesis and Macrodomain Binding of Mono-ADP-Ribosylated Peptides. *Angew Chem Int Ed Engl* (2016).

55. Bilan, V. et al. New quantitative mass spectrometry approaches reveal different ADP-ribosylation phases dependent on the levels of oxidative stress. *Molecular and Cellular Proteomics* (2017).

56. Jungmichel, S. et al. Proteome-wide identification of poly(ADP-Ribosyl)ation targets in different genotoxic stress responses. *Mol Cell* **52**, 272-85 (2013).

57. Bonfiglio, J.J. et al. Serine ADP-Ribosylation Depends on HPF1. *Mol Cell* **65**, 932-940 e6 (2017).

58. Eckei, L. et al. The conserved macrodomains of the non-structural proteins of Chikungunya virus and other pathogenic positive strand RNA viruses function as mono-ADP-ribosylhydrolases. *Sci Rep* **7**, 41746 (2017).

59. Niere, M. et al. ADP-ribosylhydrolase 3 (ARH3), not poly(ADP-ribose) glycohydrolase (PARG) isoforms, is responsible for degradation of mitochondrial matrix-associated poly(ADP-ribose). *J Biol Chem* **287**, 16088-16102 (2012).

60. Andersson, A. et al. PKCalpha and HMGB1 antagonistically control hydrogen peroxide-induced poly-ADP-ribose formation. *Nucleic Acids Res* **44**, 7630-45 (2016).

Supplementary Figures and Legends
ARH3 is a serine-specific mono-ADP-ribosylhydrolase

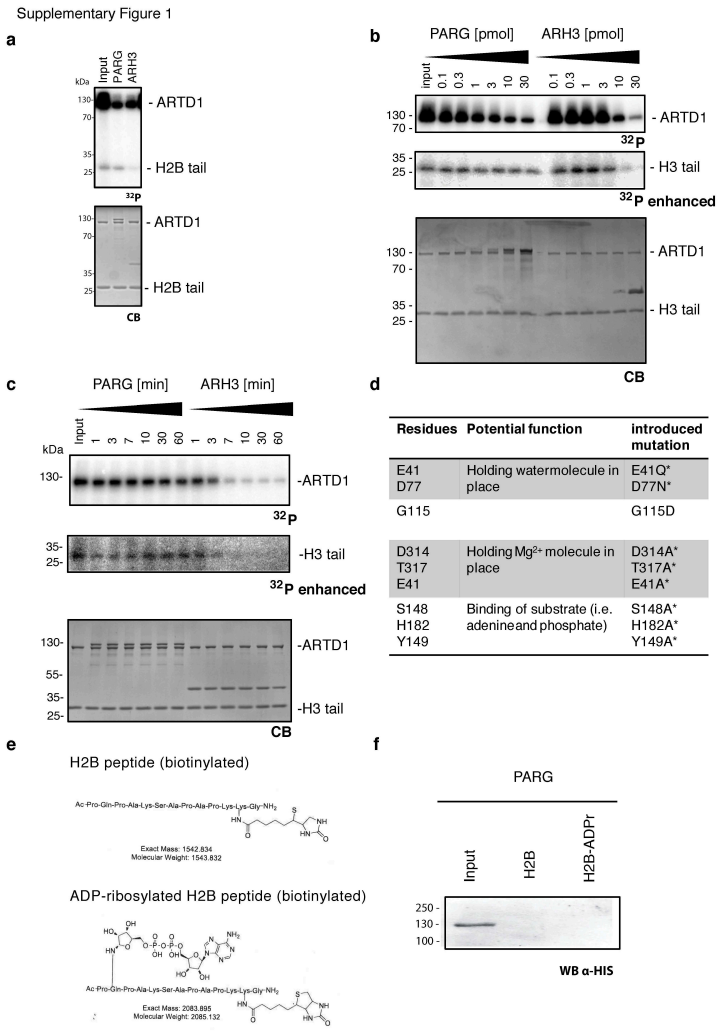

Supplementary Figure 1: (**a**) Recombinant H2B histone tail was *in vitro* ADP-ribosylated using recombinant ARTD1 in the presence of ^{32}P-labelled NAD^{+}. Equal fractions were left untreated (Input) or were treated with PARG or ARH3. Above: radioactivity exposure, below: Coomassie Blue-stained poly-acrylamide gel. (**b**) Dose response of ARH3 and PARG on auto-modified ARTD1 and transmodified H3 histone tail (numbers indicate pmol of PARG and ARH3 used for demodification). (**c**) Time course of PARG and ARH3 activity on auto-modified ARTD1 and transmodified H3 histone tail (numbers indicate duration of the PARG

and ARH3 demodification reaction in min). (**d**) Scheme representing the cloned and purified ARH3 mutants that were used for binding and demodification assays. (**e**) Schematic structure of the biotinylated H2B peptides with and without ADPr-modification. (**f**) Western blot of pull-downs of His-PARG using the biotinylated peptides with (H2B-ADPr) and without (H2B) modification.

Supplementary Figures and Legends
ARH3 is a serine-specific mono-ADP-ribosylhydrolase

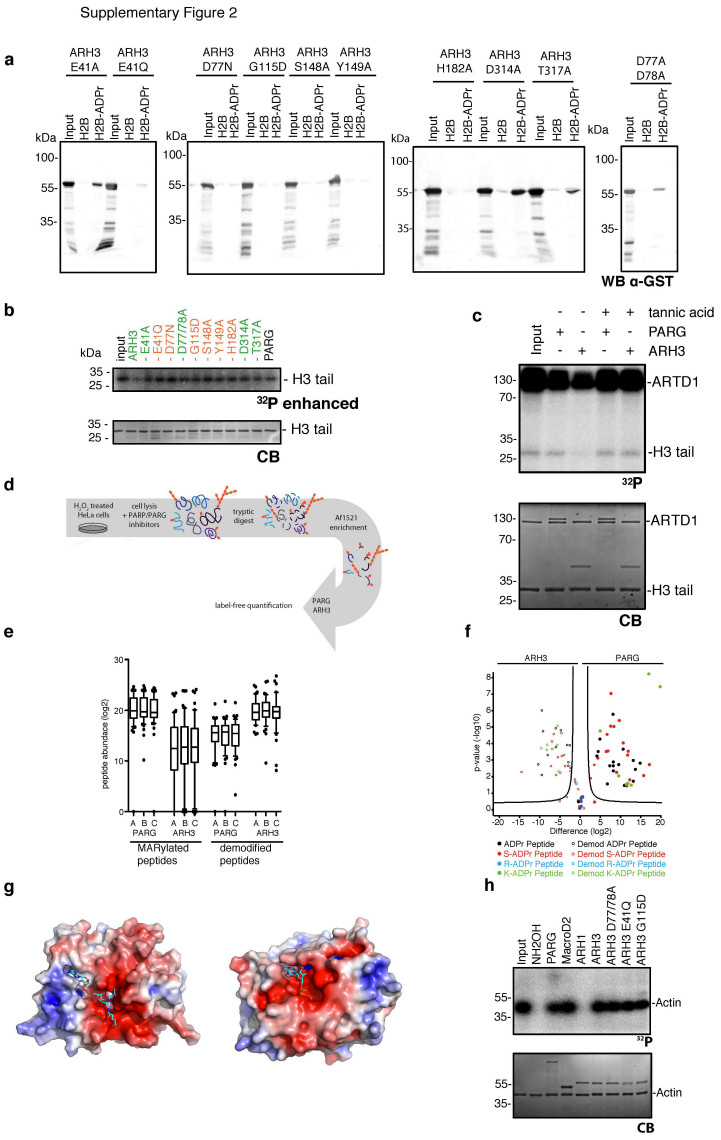

Supplementary Figure 2: (**a**) Western blot of pull-downs of GST-ARH3 mutants using the biotinylated peptides with (H2B-ADPr) and without (H2B) modification for assessment of binding capacity of ARH3 mutants to MARylated peptides. (**b**) Recombinant H3 histone tail was *in vitro* ADP-ribosylated using recombinant ARTD1 in the presence of ^{32}P-labelled NAD^{+}. Equal fractions were left untreated (Input) or were treated with PARG, wildtype and mutant ARH3. Above: radioactivity exposure, below: Coomassie Blue-stained poly-acrylamide gel. (**c**) Recombinant H3 histone tail was *in vitro* ADP-ribosylated using recombinant ARTD1 in the presence of ^{32}P-labelled NAD^{+}. Equal fractions were left

untreated (Input) or were treated with PARG and ARH3 without or in presence of tannic acid. Above: radioactivity exposure, below: Coomassie Blue-stained poly-acrylamide gel. (**d**) Schematic representation of the sample preparation for the LFQ MS experiment. For details see Materials and Methods. (**e**) Normalized abundance of individual ADP-ribosylated or demodified peptide species from three peptide preparations (A, B, C) that were treated with either ARH3 or PARG. (**f**) Volcano plot as in Figure 2c using high scoring EThcD and HCD fragmentation spectra. (**g**) Comparison of ARH3 (PDB code: 2FP0, with a modeled ADP-ribosylated serine within an acetyl glycine-serine-lysine tripeptide in the binding site) and ARH1 (PDB code: 3HFW, with adenosine diphosphate). Protein surfaces are colored according to electrostatic potential (on a scale of -5 to 5 kT/e). (**h**) Actin was *in vitro* ADP-ribosylated with the bacterial toxin CDTa in the presence of ^{32}P-labelled NAD^+. Equal fractions were left untreated (Input) or were treated with hydroxylamine, PARG, MACROD2, ARH1, wildtype and mutant ARH3. Above: radioactivity exposure, below: Coomassie Blue-stained poly-acrylamide gel.

Supplementary Figures and Legends
ARH3 is a serine-specific mono-ADP-ribosylhydrolase

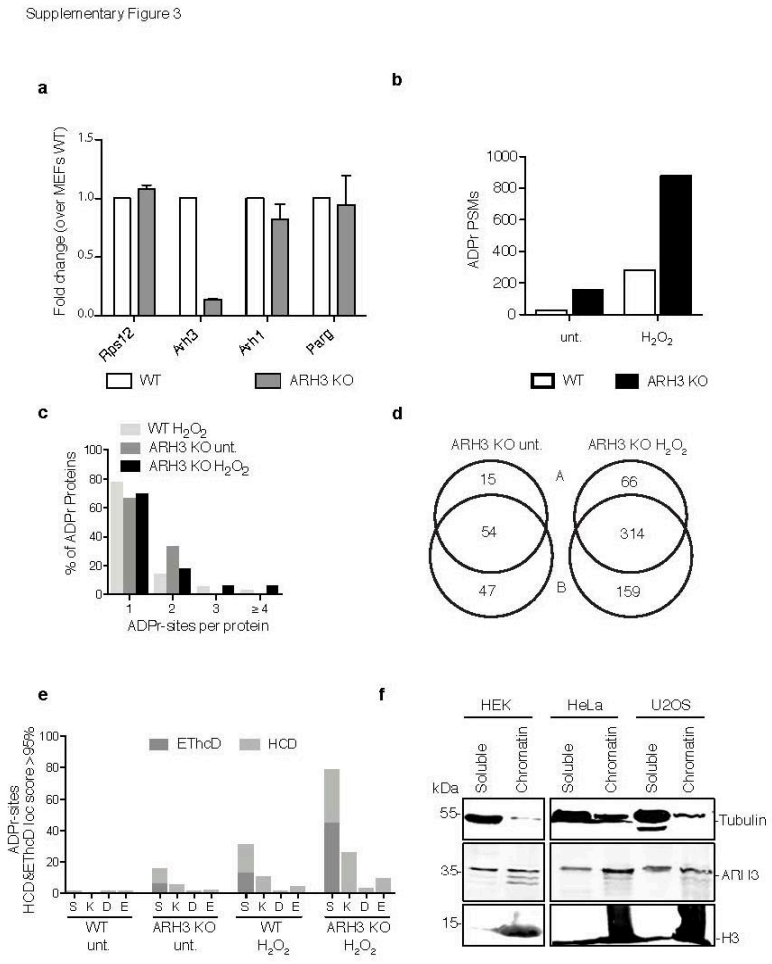

Supplementary Figure 3: (**a**) mRNA levels of *Rps12* (house keeping gene), *Arh3*, *Arh1* and *Parg* in ARH3 WT and KO MEF cells assessed by qRT-PCR. (**b**) ADP-ribosylated peptide spectra matches of WT and ARH3 KO cells in untreated and hydrogen peroxide-treated conditions. (**c**) Number of ADPr sites per protein. (**d**) Venn diagrams of unique ADP-ribosylated peptides identified in biological replicates. (**e**) Number of unique ADP-ribose acceptor amino acids localized with EThcD and HCD. (**f**) Chromatin extraction of HEK, HeLa and U2OS cells followed by western blot analysis with α-tubulin (predominantly found in the soluble fraction), α-H3 (marking the chromatin-bound fraction) and α-ARH3 (detected in both fractions).

Mono-ADP-ribosylhydrolase assays

Jeannette Abplanalp[1,2*], Ann-Katrin Hopp[1,2*], Michael O. Hottiger[1]

[1] Department of Molecular Mechanisms of Disease,
[2] Molecular Life Science PhD Program of the Life Science Zurich Graduate School,
Winterthurerstrasse 190, 8057 Zurich, Switzerland
[*] equally contributing authors

Keywords

Mono-ADP-ribosylhydrolases, Macrodomain, De-ADP-ribosylation assay, PARG, MACROD2, MACROD1, ARH1, ARH3, TARG, OARD1, C6ORF130

Abstract

Despite substantial progress in ADP-ribosylation research in recent years, the identification of ADP-ribosylated proteins, their ADP-ribose acceptors sites and the respective writers and erasers remains challenging. The use of recently developed mass spectrometric methods helps to further characterize the ADP-ribosylome and its regulatory enzymes under different conditions and in different cell types. Validation of these findings may be achieved by *in vitro* assays for the respective enzymes. In the below method, we describe how recombinant ADP-ribosylated proteins are demodified *in vitro* with mono-ADP-ribosylhydrolases of choice to elucidate substrate and potentially also site specificity of these enzymes.

1. Introduction

ADP-ribosylation is an evolutionary conserved covalent posttranslational modification (PTM) mainly catalyzed by ADP-ribosyltransferases (ARTs)(Luo and Kraus 2012; Hottiger 2015). These enzymes use nicotinamide adenine dinucleotide (NAD^+) as a substrate to transfer ADP-ribose moieties onto specific amino acid residues of target proteins (Barkauskaite, Jankevicius et al. 2015), leading to mono-ADP-ribosylation (MARylation), or to extend ADP-ribosylated sites to linear and branched poly-ADP-ribose chains (PARylation)(Hottiger 2015). While the role of PARylation is well established and has extensively been studied within the last decades, especially in the context of DNA-damage and cell death (Luo and Kraus 2012; Caldecott 2014), the physiological relevance of

MARylation remains poorly understood. Nonetheless, an increasing number of studies suggests MARylation to be implicated in various cellular processes, including immunomodulation, ER stress, cytoskeleton rearrangement, cell metabolism and host-pathogen interactions (Butepage, Eckei et al. 2015). To date, at least 16 different enzymes are described to catalyze MARylation in mammals. The cholera toxin-like ARTs (ARTCs) ARTC1, 2 and 5 have been shown to specifically mono-ADP-ribosylate their target proteins (Laing, Unger et al. 2011). Moreover, the majority of diphtheria toxin-like ARTs (ARTDs), as well as two Sirtuins, namely Sirt4 and 6, have been identified to possess MARylation activity (Du, Jiang et al. 2009; Pan, Feldman et al. 2011). The target amino acids modified by specific mono-ARTDs remain unknown.

ADP-ribosylation of proteins is reversed by enzymes capable of hydrolyzing both MAR- and PARylation. In mammals, two enzymes, PARG and ARH3, are known to degrade PAR chains (Ueda, Oka et al. 1972; Oka, Kato et al. 2006). The first enzyme described to hydrolyze MARylation was ADP-ribosylarginine hydrolase 1 (ARH1)(Moss, Jacobson et al. 1985), which releases ADP-ribose from arginine residues. ARH1 deficient mice show spontaneous development of various tumors, suggesting a role for MARylation in cancer development (Kato, Zhu et al. 2011). Recently, three studies identified the mammalian proteins MACROD1, MACROD2 and TARG (also referred to as OARD1 or C6ORF130) as novel glutamate- and aspartate-specific MAR hydrolases, respectively (Jankevicius, Hassler et al. 2013; Rosenthal, Feijs et al. 2013; Sharifi, Morra et al. 2013). The physiological role of each of these three hydrolases as well as their precise site specificity, however, is still poorly understood. Mutations within the gene encoding for TARG have been linked to the development of severe neurological dysfunction in humans (Sharifi, Morra et al. 2013). MACROD1 and MACROD2 were previously described to be mutated or differentially expressed in the context of different cancers (Xi, Zhao et al. 2010; Mohseni, Cidado et al. 2014). MACROD1 has also been proposed to be a regulator of adipogenesis and insulin secretion (Zang, Xue et al. 2013) as well as a transcriptional co-factor for estrogen and androgen receptor signaling (Han, Zhao et al. 2007; Yang, Zhao et al. 2009). Recent studies suggest an implication of MACROD1 in NFκB-mediated gene expression (Wu, Li et al. 2011). Whether the

reported phenotypes are dependent on the ability of the three enzymes to hydrolyze MAR has yet to be elucidated. No hydrolases capable of releasing ADP-ribose from lysine and serine are published to date.

Substrate specificities of MAR hydrolases are thus far difficult to assess due to technical limitations in identifying ADP-ribosylated proteins and the respective acceptor amino acids. Recent advances in the field of proteomics helped to resolve this important question. Improved enrichment protocols and the adaptation of new fragmentation techniques allowed the identification of the cellular ADP-ribosylome in untreated and hydrogen peroxide treated cells as well as in mouse organs (Martello, Leutert et al. 2016; Bilan, Leutert et al. 2017). Serine was recently identified as the major ADP-ribose acceptor site besides glutamate, aspartate, lysine and arginine (Leidecker, Bonfiglio et al. 2016). Whether additional sites are modified is currently still under investigation. Despite the technical progresses described above, mass spectrometry alone is not always sensitive enough to investigate the contribution of a specific enzyme, e.g. a specific MAR hydrolase, to the ADP-ribosylation status of a given protein. Low abundant proteins might be below the detection limit. In addition to this limitation, different hydrolases might exhibit partially redundant functions *in vivo*. Thus, the knockout phenotype of one hydrolase might be masked due to another hydrolase with the same catalytic specificity. *In vitro* hydrolase activity assays on targets premodified with radioactively labeled NAD^+ allow circumventing the problems discussed above. Currently, these hydrolase activity assays represent one of the best possibilities to assess substrate-specificity of a hydrolase. Furthermore, they allow the validation of hits identified by either ADP-ribosylome or interactome analyses performed by mass spectrometry.

2. Materials

Chemicals were purchased from Sigma-Aldrich, unless otherwise stated.

2.1. *In vitro* MARylation

1. GST- or HIS-tagged recombinant mono-ARTD of interest (e.g. N-terminally GST-tagged hARTD10 (residues 818-1025), expressed and purified from *E.coli).*

For long-term storage, recombinant proteins should be stored in liquid nitrogen. Once thawed, proteins can be stored at -20°C for several weeks.

2. GST- or HIS-tagged substrate proteins that are subsequently modified (see 3.2) and serve as MARylated substrate for the de-MARylation experiments in section 3.3 (e.g. GST-tagged histone tails purified from bacteria). Alternatively the de-MARylation of the mono-ARTD can be tested in section 3.3 (omit step 2 of section 3.2).

3. [^{32}P]NAD$^+$ (800Ci/mmol, 5mCi/ml). For non-radioactive detection, alternatively biotin-NAD$^+$ or etheno-NAD$^+$ can be used in combination with streptavidin and the corresponding antibody, respectively.

4. 6.25 µM NAD$^+$ (β-nicotinamide adenine dinucleotide hydrate, ≥99%); the 6.25 µM stock needs to be stored at -80°C.

5. 5x ADP-ribosylation reaction buffer (RB) always prepare freshly: 250 mM Tris–HCl pH 7.4, 20 mM $MgCl_2$, 1.25 mM DTT.

6. 10 mM PARP inhibitor PJ-34 (>98%, hydrochloride hydrate); the 10 mM stock solution has to be stored at -20°C.

7. Illustra MicroSpin G-50 Columns (GE Healthcare).

2.2. *In vitro* de-MARylation

1. GST- or HIS-tagged recombinant hydrolase of interest (e.g. N-terminally GST-tagged MACROD1 and MACROD2, expressed and purified in *E. coli*). Recombinant protein(s) without MAR hydrolase activity as negative control (e.g. C-terminally HIS-tagged PARG purified from insect cells or enzymatically inactive MAR hydrolase mutants purified from *E. coli*).

2. MARylated substrates (e.g. auto-modified ARTDs or pre-modified targets proteins).

3. 6x SDS loading buffer (300 mM Tris-HCl pH 6.8, 30% glycerol (87%), 0.05% bromophenol blue, 12% sodium dodecyl sulfate (SDS, >97%, Calbiochem), 12% β-mercaptoethanol (≥99.0%)).

2.3. SDS-PAGE and autoradiography

1. SDS-PAGE gel consisting of a separating gel (375 mM Tris-HCl pH 8.8, 0.1 % SDS, 7.5 – 15% acrylamide (Serva Electrophoresis GmbH), 0.1% ammonium persulfate (≥99.99%), 0.1% *N,N,N′,N′*-tetramethylethylenediamine (TEMED, ~99%); choose a low percentage separating gel for large proteins (> 100 kDa) or a high percentage separating gel for small proteins) and a stacking gel (125 mM Tris-HCl pH 6.8, 0.1% SDS, 0.05% bromophenol blue, 4.8% acrylamide, 0.1% ammonium persulfate, 0.1% TEMED).

2. Coomassie blue staining solution (45% Methanol (technical grade), 10% acetic acid (80%, both Thommen-Furler AG), 0.25% Coomassie Brilliant Blue R250)).

3. Destaining solution (45% Methanol (technical grade), 10% acetic acid (80%, both Thommen-Furler AG)).

4. Storage Phosphor Screen BAS-IP MS 2040 E Multipurpose Standard, 20 × 40 cm (or similar, GE Healthcare).

5. Phosphor-imager Typhoon FLA 7000 (or similar, GE Healthcare).

6. Alternatively, radioactive signals can be also visualized using exposure on film.

3. Methods

3.1. Overview of the protocol

The ADP-ribosylhydrolase assay presented in this chapter allows addressing the substrate- as well as ADP-ribose acceptor site preference of a given MAR hydrolase *in vitro*. In brief, first, a potential target protein is recombinantly expressed, purified and modified with the help of a MARylating enzyme. Depending on the enzymes used, reaction times and temperatures as well as

NAD^+ concentrations might need optimization and will deviate from the presented protocol. For simplification, the catalytic domain of human ARTD10 (residues 818-1025) is used as an example in this protocol. After either auto- or trans-modification of the enzyme and/or target substrate, the reaction is stopped by addition of either 10 µM PJ34 (or another PARP inhibitor) or by removing residual NAD^+ using a G50 column. The ADP-ribosylated protein is subsequently incubated with the MAR hydrolase of choice. The reaction is terminated by adding SDS loading buffer. The products are analyzed by SDS-PAGE, staining and destaining of the gel, exposure on a phosphor-screen and subsequent visualization using a phosphorimaging system. The quantification of the demodification allows determining the activity of the tested MAR hydrolases.

3.2. *In vitro* MARylation

1. For *in vitro* auto-ADP-ribosylation of hARTD10, 17 pmol of the recombinant catalytic domain of hARTD10 are used. This is important to reach a final amount of 10 pmol per demodification reaction. hARTD1 (818-1025) is incubated in 1x RB with 100 nM radioactively labeled [^{32}P]NAD^+ (0.3 µCi/µl end concentration reached by adding cold 6.25 µM NAD^+) in a final volume of 25 µl for 15 min at 37°C (pipet reaction on ice, NAD^+ added last). Depending on the number of planned demodification reactions (3.3), the reaction might need to be scaled up.

2. For the generation of MARylated target proteins *in trans*, 30-50 pmol of the according protein are added to the reaction mix described above (i.e. point 1). Of note, the concentration of the protein of interest, as well as the incubation time might have to be adjusted.

3. After incubation, the MARylation reaction is stopped by either:

a) adding 10 µM PJ34 or by
b) filtering the reaction using a prepacked G50 column. To this end, vortex the column briefly, remove the cap, and centrifuge for 2 min at 700 g at room temperature, place the column in a new microcentrifuge tube, immediately add the reaction mix (i.e. point 1) and centrifuge again. The eluate is further used for de-modification reactions (see 3.3).

3.3. *In vitro* de-MARylation

1. For each de-modification sample, 15 µl of the MARylation reaction mix (from section 3.2) are incubated with 10 pmol of the hydrolase of interest in 1x RB in a total volume of 25 µl for 15 min at 37°C. Depending on the hydrolase, reaction time as well as temperature might need to be adjusted. As a control, always use one reaction where no hydrolase is added, and one reaction using e.g. recombinant PARG, or an enzymatically inactive mutant of a hydrolase which should not lead to a decrease in signal intensity (see Figure 1A).

2. The reaction is stopped by addition of SDS-loading buffer and subsequent boiling at 95°C for 5 min. Samples can be either stored at -20 °C or directly analyzed by SDS-PAGE.

3.4. SDS-PAGE and autoradiography

1. Samples are loaded on an SDS-PAGE gel and run at 120V for 1-2h.

2. Due to potential interference with the ADP-ribosylation signal of the modified protein, the running front containing free [^{32}P] NAD^+ as well as the stacking gel is cut away.

3. The gel is stained with Coomassie blue for 30 min and subsequently destained with destain solution for 30 min-2 h until sharp protein bands are visible. The Coomassie stained gel is photographed and the bands are quantified using ImageJ for subsequent normalization of the radioactive signals (see 3.5).

4. To protect the sensitive phosphor-screen, the gel can be either dried or is directly packed in a sealable plastic bag or with plastic wrap, before exposure for 1 h or up to several days (might need optimization depending on the used enzymes and signal strength).

5. Using a phosphor-imager, the radioactivity signals are visualized and can be further analyzed and quantified using ImageJ (see Figure 1B).

3.5 Analysis

For the quantification of the MAR hydrolase activity, the signal intensity (radioactivity and Coomassie) for every stained band is measured using e.g. ImageJ. Normalization of the radioactive signal intensity with the Coomassie protein signal intensity for every tested target protein provides a measure of the MARylation status. The MARylation status of each sample is correlated to the input sample (modified, but not demodified), which is arbitrarily set to 1, to allow cross comparison among different samples and to obtain a measure of MAR hydrolase activity.

For the quantification of the MAR hydrolase activity, the signal intensity (radioactivity and Coomassie) for every stained band is measured using e.g. ImageJ. The radioactivity signal R normalized to the respective Coomassie signal C results in the specific modification signal S.

$$S = \frac{R}{C}$$

The specific activity A of the demodifying enzyme is given by

$$A = 1 - \frac{S_X}{S_i}$$

where S_X is the specific modification signal of a given condition (enzyme X) and S_i is the specific modification signal of the input sample (modified, but not demodified) (see Figure 1C).

4. Acknowledgements

The authors would like to thank Tobias Suter (University of Zurich) for providing editorial assistance and critical input during the writing. Work on ADP-ribosyltransferases and hydrolases in the laboratory of M.O.H is supported by the Kanton of Zurich and the Swiss National Science Foundation (SNF 310030_157019).

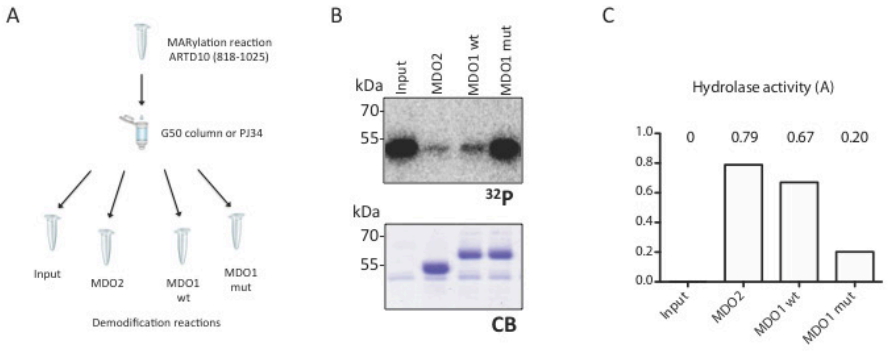

Figure 1: A Scheme of a typical hydrolase assay setup. **B** Radiography and Coomassie pictures of examplary reactions. **C** Quantification of hydrolase activities. The radioactivity signal (^{32}P) normalized by Coomassie Blue (CB) signal is espressed as a fraction of the input. MDO, macrodomain; wt, wildtype; mut, enzymatically inactive mutant.

5. References

Barkauskaite, E., G. Jankevicius, et al. (2015). "Structures and Mechanisms of Enzymes Employed in the Synthesis and Degradation of PARP-Dependent Protein ADP-Ribosylation." Molecular cell **58**(6): 935-946.

Bilan, V., M. Leutert, et al. (2017). "Combining Higher-Energy Collision Dissociation and Electron-Transfer/Higher-Energy Collision Dissociation Fragmentation in a Product-Dependent Manner Confidently Assigns Proteomewide ADP-Ribose Acceptor Sites." Analytical Chemistry **89**(3): 1523-1530.

Butepage, M., L. Eckei, et al. (2015). "Intracellular Mono-ADP-Ribosylation in Signaling and Disease." Cells **4**(4): 569-595.

Caldecott, K. W. (2014). "Protein ADP-ribosylation and the cellular response to DNA strand breaks." DNA repair **19**: 108-113.

Du, J., H. Jiang, et al. (2009). "Investigating the ADP-ribosyltransferase activity of sirtuins with NAD analogues and 32P-NAD." Biochemistry **48**(13): 2878-2890.

Han, W. D., Y. L. Zhao, et al. (2007). "Estrogenically regulated LRP16 interacts with estrogen receptor alpha and enhances the receptor's transcriptional activity." Endocrine-related cancer **14**(3): 741-753.

Hottiger, M. O. (2015). "Nuclear ADP-Ribosylation and Its Role in Chromatin Plasticity, Cell Differentiation, and Epigenetics." Annual review of biochemistry **84**: 227-263.

Hottiger, M. O. (2015). "Nuclear ADP-Ribosylation and Its Role in Chromatin Plasticity, Cell Differentiation, and Epigenetics." Annu Rev Biochem **84**: 227-263.

Jankevicius, G., M. Hassler, et al. (2013). "A family of macrodomain proteins reverses cellular mono-ADP-ribosylation." Nature structural & molecular biology **20**(4): 508-514.

Kato, J., J. Zhu, et al. (2011). "ADP-ribosylarginine hydrolase regulates cell proliferation and tumorigenesis." Cancer research **71**(15): 5327-5335.

Laing, S., M. Unger, et al. (2011). "ADP-ribosylation of arginine." Amino acids **41**(2): 257-269.

Leidecker, O., J. J. Bonfiglio, et al. (2016). "Serine is a new target residue for endogenous ADP-ribosylation on histones." Nature Chemical Biology **12**(12): 998-+.

Luo, X. and W. L. Kraus (2012). "On PAR with PARP: cellular stress signaling through poly(ADP-ribose) and PARP-1." Genes & development **26**(5): 417-432.

Martello, R., M. Leutert, et al. (2016). "Proteome-wide identification of the endogenous ADP-ribosylome of mammalian cells and tissue." Nature Communications **7**.

Mohseni, M., J. Cidado, et al. (2014). "MACROD2 overexpression mediates estrogen independent growth and tamoxifen resistance in breast cancers." Proceedings of the National Academy of Sciences of the United States of America **111**(49): 17606-17611.

Moss, J., M. K. Jacobson, et al. (1985). "Reversibility of arginine-specific mono(ADP-ribosyl)ation: identification in erythrocytes of an ADP-ribose-L-arginine cleavage enzyme." Proceedings of the National Academy of Sciences of the United States of America **82**(17): 5603-5607.

Oka, S., J. Kato, et al. (2006). "Identification and characterization of a mammalian 39-kDa poly(ADP-ribose) glycohydrolase." The Journal of biological chemistry **281**(2): 705-713.
Pan, P. W., J. L. Feldman, et al. (2011). "Structure and biochemical functions of SIRT6." The Journal of biological chemistry **286**(16): 14575-14587.
Rosenthal, F., K. L. Feijs, et al. (2013). "Macrodomain-containing proteins are new mono-ADP-ribosylhydrolases." Nature structural & molecular biology **20**(4): 502-507.
Sharifi, R., R. Morra, et al. (2013). "Deficiency of terminal ADP-ribose protein glycohydrolase TARG1/C6orf130 in neurodegenerative disease." The EMBO journal **32**(9): 1225-1237.
Ueda, K., J. Oka, et al. (1972). "Poly ADP-ribose glycohydrolase from rat liver nuclei, a novel enzyme degrading the polymer." Biochemical and biophysical research communications **46**(2): 516-523.
Wu, Z., Y. Li, et al. (2011). "LRP16 integrates into NF-kappaB transcriptional complex and is required for its functional activation." PloS one **6**(3): e18157.
Xi, H. Q., P. Zhao, et al. (2010). "Clinicopathological significance and prognostic value of LRP16 expression in colorectal carcinoma." World journal of gastroenterology **16**(13): 1644-1648.
Yang, J., Y. L. Zhao, et al. (2009). "The single-macro domain protein LRP16 is an essential cofactor of androgen receptor." Endocrine-related cancer **16**(1): 139-153.
Zang, L., B. Xue, et al. (2013). "Identification of LRP16 as a Negative Regulator of Insulin Action and Adipogenesis in 3T3-L1 Adipocytes." Hormone and Metabolic Research **45**(5): 349-358.

3.3 Unpublished results

ARH3 is dispensable for the embryonic development in mice

Nothing is so far known about the physiological role of ARH3 is unknown and characterization of the *ARH3* knockout (KO) mouse is still missing. We purchased mice with a CRISPR/Cas9-mediated exon deletion in the *Adprhl2* gene (encoding for ARH3) from Genome Research Limited, Wellcome Trust Sanger Institute (Cambridge, UK) and characterized them in more detail. Since the obtained mice were heterozygous (HET), we tested whether the full KO mice would be viable. Mice were bred and all pups from these breedings continuously genotyped. All genotypes, including KO mice, of these breeds were viable. In male mice, 56% more wildtype (WT) than *ARH3* KO pups were born (Figure 5A), but equal numbers of WT and *ARH3* KO females were born (Figure 5B). Considering all mice, the inheritance of the *ARH3* WT and KO allele approximately followed the expected Mendelian ratio (Figure 5C).

A Males

Genotype	Number of animals	%
WT	7	43
HET	6	38
KO	3	19
total	16	100

B Females

Genotype	Number of animals	%
WT	4	19
HET	13	62
KO	4	19
total	21	100

C Males and females

Genotype	Number of animals	%	Expected %
WT	11	30	25
HET	19	51	50
KO	7	19	25
total	16	100	100

Figure 5: Genotyping analysis of pups from heterozygous breeding pairs reveals inheritance of the WT and *ARH3* KO allele according to Mendelian ratios. DNA of all pups from HET breeding pairs was genotyped and the number of WT, *ARH3* KO and HET A) males, B) females, and C) all mice used to calculate the %.

To investigate whether *ARH3* KO mice are fertile, homozygous breeding pairs were set up and the number and sex of the born pups monitored. No differences in litter sizes or altered ratio of females to males was observed comparing WT and *ARH3* KO breeding pairs (data not shown), suggesting that ARH3 is dispensable for embryonic development, for overall survival and fertility of the mice.

ARH3 KO mice show a weight gain during development

To further characterize the phenotype of *ARH3* KO mice, full necropsies of 6-week-old female mice (n = 3 each genotype) were carried out by Giovanni Pellegrini (Laboratory for Animal Model Pathology (LAMP), University of Zurich). No histopathological abnormalities were observed in the *ARH3* KO mice (data not shown). The brains as well as other organs were weighed. The brains weighed 0.425 ± 0.009 g for WT and 0.440 ± 0.005 g for *ARH3* KO mice, respectively (Figure 6A).

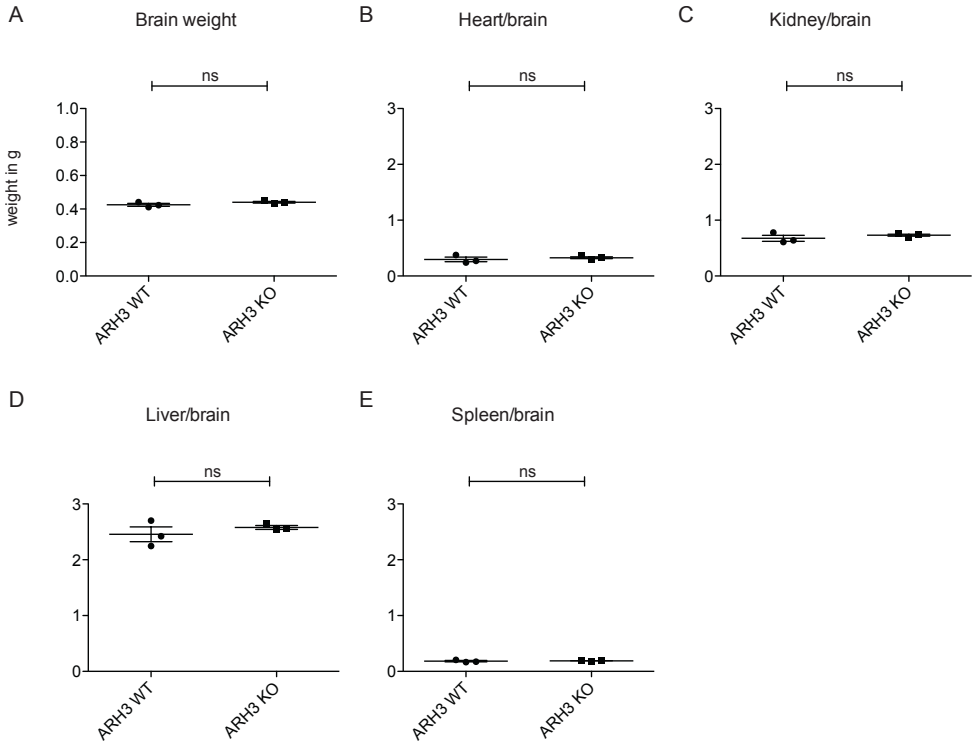

Figure 6: Organ weights of female 6-week-old *ARH3* WT and KO mice are comparable. A) Brain weight in grams of each n = 3 WT and *ARH3* KO mice. Ratio of the B) heart, C) kidney, D) liver, and E) spleen weights divided by the brain weight. Mean ± SEM, ns = not significant, two-tailed Student's t-test.

Heart, kidney, liver and spleen were also weighed and the results normalized to the brain weight (Figure 6B-6E). No significant differences were observed, suggesting that ARH3 is indeed not essential for early mouse development or functionally compensated by another ARH.

During handling and organ isolation of older mice, we discovered that *ARH3* KO animals were bigger and heavier than the WT counterparts, and accumulated

more white adipose tissue upon aging. To quantify this difference, we weighed mice at two different time points, i.e. 8 and 16 weeks of age, in order to observe a potential effect of aging. Male mice at both 8 and 16 weeks of age showed a tendency to be heavier (8 weeks: WT = 23.20 ± 0.37 g and *ARH3* KO = 24.60 ± 0.81; 16 weeks: WT = 29.17 ± 0.67 g and *ARH3* KO = 35.33 ± 2.31 g), however, this difference was not statistically significant, potentially due to the low number of analyzed animals (Figure 7A and 7B). Interestingly, *ARH3* KO female mice (only measured after 16 weeks) were significantly heavier than WT mice (WT = 23.83 ± 0.63 g and *ARH3* KO = 32.12 ± 1.92 g, respectively (Figure 7C).

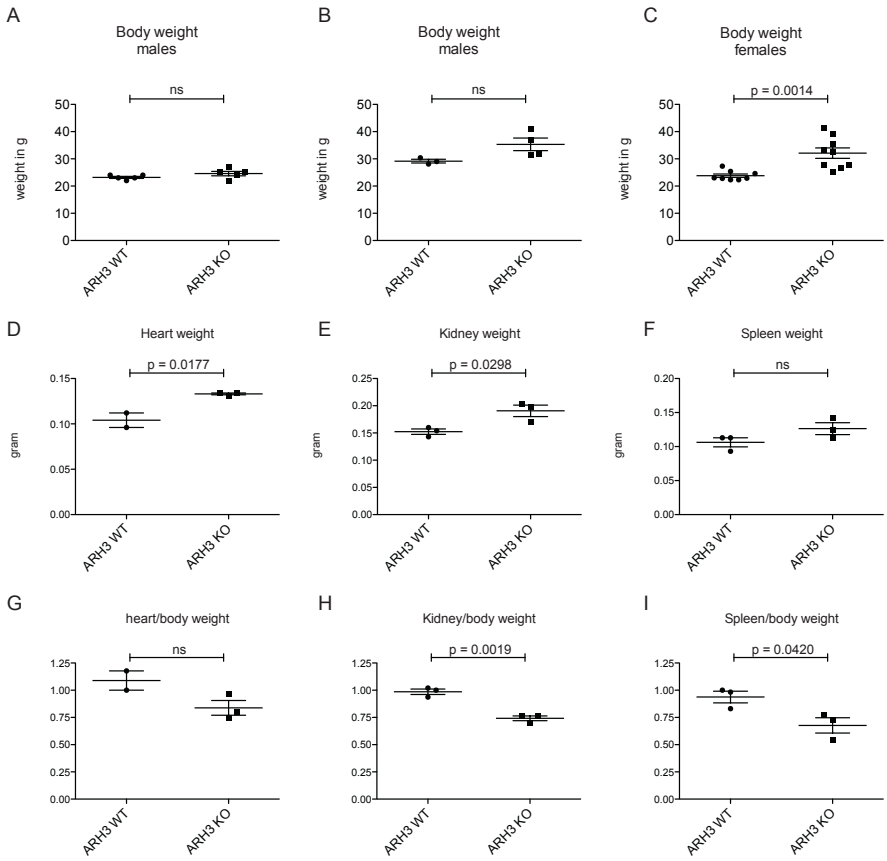

Figure 7: Different aged *ARH3* KO mice are heavier than age-matched WT mice. Body weight in g of A) 8-week-old males (n = 5), B) 16-week-old males (n = 3 WT and 4 *ARH3* KO and C) 16-week-old females (n = 8 WT and 9 *ARH3* KO). Absolute weights of D) heart, E) kidney and F) spleen. Relative G) heart, H) kidney, and I) spleen weights normalized over body weight. (n = 3, one WT heart was not weighed by mistake). Mean ± SEM, ns = not significant, p = p-value, two-tailed Student's t-test.

To investigate whether this gain in total weight is caused by organ weights, we isolated organs from 3 female 16-week-old mice of each genotype. When weighing the heart, kidney and spleen, we observed that the organs, similar to the body weight,

were heavier in *ARH3* KO mice compared to WT (Figure 7D-7F). However, when normalizing the organ weight to the total body weight, the organs of *ARH3* KO animals were rather lighter when compared to WT (Figure 7G-7I), suggesting that *ARH3* KO animals mainly gained weight due to obesity (i.e. increase in white adipose tissue). Although *ARH3* KO mice initially showed no obvious phenotype, we conclude that ARH3 plays an important metabolic role in aging mice and the deficiency of ARH3 leads to a gain in body weight and potentially fat content.

Spleens from *ARH3* KO mice show enhanced MARylation

In this thesis, as well as reported by others during the course of this thesis, we described ARH3 as a mono-ARH capable of fully reversing serine-ADP-ribosylation (Abplanalp *et al*., submitted manuscript, and [134]). We observed that *ARH3* KO mouse embryonic fibroblasts (MEF) expressed an enhanced basal, i.e. untreated, ADP-ribosylome as measured by mass spectrometry.

To confirm this finding in tissue, we isolated kidneys, livers, hearts, lymph nodes, and spleens from 6-week-old male WT, *ARH3* KO, or HET mice, and lysed the tissue in ice-cold RIPA using a Tissue Lyser II. KO of ARH3 was confirmed by Western blot using an antibody against ARH3. MARylation was analyzed with a MAR antibody raised against a chemically MARylated H2B peptide and tubulin served as loading control (Figure 8, next page). ARH3 was not detected in the kidney, liver and heart (Figure 8A-8C). In lymph nodes and the spleen, a distinct band at 39 kDa representing ARH3 was detected only in the WT and to a lower extent in the HET, and completely absent in the tissues of *ARH3* KO (Figure 8D and 8E). Specific bands marking MARylated proteins were identified in the kidney and the liver (Figure 8A and 8B). Heart lysates showed extensive MARylation levels (Figure 8C), presumably due to the activity of the highly abundant ADP-ribosyltransferase ARTC1 (see chapter 1.1.1). In lymph nodes we did not detect any MARylation under the tested conditions (Figure 8D) but in the spleen various MARylated proteins in the lysates of *ARH3* KO and HET animals were detected, with some defined bands around 75 kDa (Figure 8E). We conclude that while ARH3 was not detectable in the kidney, liver, spleen and hearts of 6-week-old mice, ARH3 was present in the lymph nodes and the spleen, suggesting a functional role of ARH3 in these two organs. Considering MARylation, the kidney and liver showed some specific bands not

dependent on ARH3, and enhanced MARylation upon *ARH3* KO was only observed in the spleen.

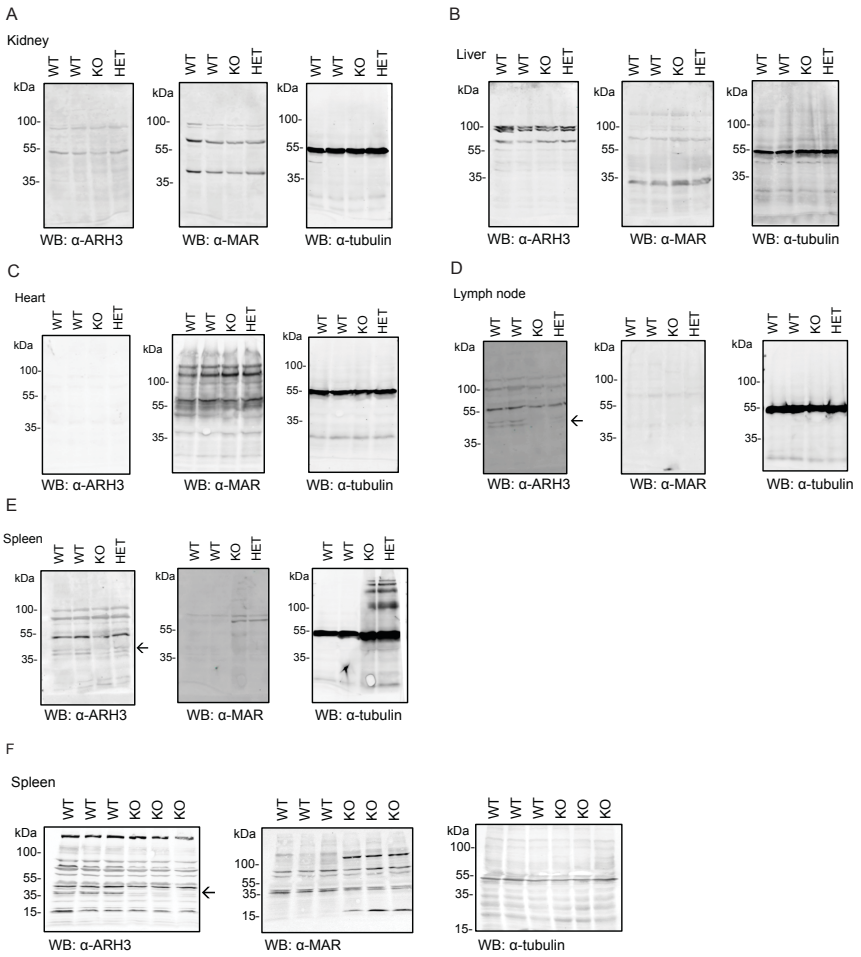

Figure 8: Spleen lysates of *ARH3* KO mice show enhanced basal MARylation compared to other tissues. 200 µg of A) kidney, B) liver, C) heart, D) lymph node or E) spleen of 6-week-old male mice or 200 µg of F) spleen of 16-week-old female mice were blotted against MAR, ARH3 (marked with an arrow), and tubulin. WT = wildtype, KO = knockout, HET = heterozygous.

To confirm that MARylation is indeed enhanced in *ARH3* KO spleens, we additionally isolated organs from 16-week-old female mice (n = 3 WT and *ARH3* KO, each) and repeated the same Western blot analysis as above. Overall, spleen lysates showed enhanced MARylation signals compared to the younger mouse spleens, and *ARH3* KO mice showed two additional MARylated bands with molecular weights of 15 and 100 kDa (Figure 8F). Together, the absence of ARH3 caused enhanced MARylation in spleen tissue of both 6-week and 16-week-old mice and as mice develop, MARylation accumulated in the spleen, indicating that ARH3 seems to

become even more important over time as the enzyme responsible for keeping the basal ADP-ribosylation in the spleen low.

ARH3 reduces the basal spleen ADP-ribosylome

Since the *ARH3* KO showed various MARylated proteins in contrast to WT spleens already at 6 weeks of age (Figure 8E), we aimed to investigate and characterize the ADP-ribosylome in this tissue. The spleens of two WT and KO animals were isolated and lysed as described section 3.4. Tissue lysates were digested with trypsin, treated with PARG and enriched with Af1521 before measured by shotgun mass spectrometry. The spectra were generated using a combination of two different fragmentation techniques, higher-energy collision dissociation (HCD) and electron-transfer/higher-energy collision dissociation fragmentation (EThCD)[25]. Compared to data obtained using *ARH3* KO MEFs (Abplanalp *et al.*, submitted manuscript), where searches included five different possible ADP-ribose acceptor sites (i.e. D, E, K, R and S), we here included also Y, since recent efforts from our laboratory provide evidence that Y can also serve as an ADP-ribose acceptor site (data not shown). We filtered the data with a localization score > 95%, to only obtain ADP-ribose acceptor sites with very high confidence. Spleens from *ARH3* KO mice compared to WT mice showed an overall 3-fold increased number of spectra with ADP-ribosylated peptides (peptide-spectrum matches (PSMs) (Figure 9A).

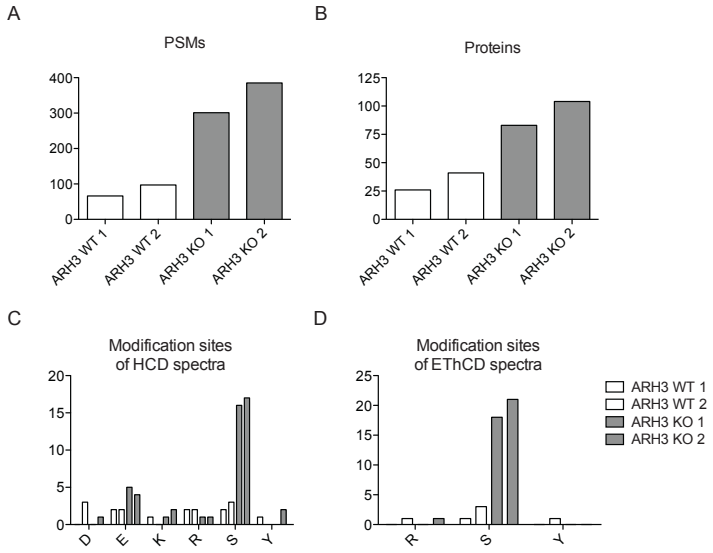

Figure 9: *ARH3* KO spleens show an extensive serine ADP-ribosylome. 10 mg of spleen lysate of 6-week-old mice was digested with trypsin and the ADP-ribosylome enriched before subjecting the samples for mass spectrometric analysis. A) Peptide-sprectrum matches (PSMs) in WT and *ARH3* KO spleens. B) Total ADP-ribosylated proteins. C) Numbers of identified HCD spectra per amino acid. D) Numbers of identified EThCD spectra per amino acid. For C) and D), a modification confidence threshold of > 95% was set.

The same trend was observed when analyzing the data at the protein level, where *ARH3* KO spleens showed a 2.5-fold higher number of ADP-ribosylated targets (Figure 9B). Both HCD and EThCD spectra (Figure 9C and 9D, respectively) revealed that serine is the main ADP-ribose acceptor site in the spleen of *ARH3* KO mice. Taken together, spleens from *ARH3* KO animals harbor an extensive basal ADP-ribosylome, even under unstimulated conditions. We therefore hypothesize that ARH3 is constitutively active in unstressed cells and de-ADP-ribosylates its targets under basal conditions, maintaining a low amount of ADP-ribosylation.

ARH3 mainly demodifies nuclear proteins

Based on the observation that the absence of ARH3 lead to an enhanced ADP-ribosylome, the acquired MS data set was further analyzed. By plotting the proteins into a Venn diagram, a very high overlap between the duplicates was observed (2 spleens from WT and 2 spleens from *ARH3* KO mice), with 18 common proteins between the two WT samples (37%) and 68 common proteins between both *ARH3* KO samples (around 57% overlap) (Figure 10A and 10B, next page).

A total of 17 proteins were modified in all analyzed samples (common to WT and *ARH3* KO), representing the basal ARH3-independent spleen ADP-ribosylome (Figure 10C). For the histone variants H2ax, H1.4, and H2b type 1-b, we observed a considerably higher amount of PSMs measured in the *ARH3* KO spleens compared to WT spleens (Figure 10D), suggesting that they are likely ARH3 target proteins. Another highly modified protein found mainly in the spleen of *ARH3* KO mice was ARTD1 (PARP1), suggesting that ARH3 regulates the ADP-ribosylation state also of ARTD1 and possibly its enzymatic activity. Since the analysis was not quantitative, the level of ARH3 dependency requires additional experiments. Another group of 40 proteins was however exclusively ADP-ribosylated in the *ARH3* KO spleens, and therefore considered to be confirmed targets of ARH3 (Figure 10E). Chromobox protein homolog 5 (Cbx5), lamin-B receptor (Lbr), lamin A/C (Lmna) and nucleophosmin (Npm1) were quite extensively modified in the absence of ARH3. The molecular mass of Lbr and Lmna are 71 kDa and 74 kDa, respectively, which might potentially correspond to the prominent bands detected on the Western blot using the MAR antibody (Figure 8E).

A

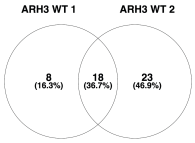

B

C

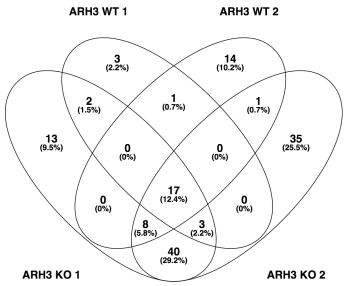

D

Gene name	Protein name	ARH3 WT 1	ARH3 WT 2	ARH3 KO 1	ARH3 KO 2
Gale	UDP-glucose 4-epimerase	1	2	3	1
Gapdh	Glyceraldehyde-3-phosphate dehydrogenase	1	1	1	1
Gm28062	Heterogeneous nuclear ribonucleoprotein U	5	1	8	10
H2afx	Histone H2AX	2	2	20	23
H3f3c	Histone H3.3C	1	1	1	4
Hba-a1	Hemoglobin subunit alpha	10	9	3	8
Hbbt1	Beta-globin	7	7	3	3
Hist1h1e	Histone H1.4	1	2	22	25
Hist1h2bb	Histone H2B type 1-B	2	3	8	11
Hist1h2bf	Histone H2B type 1-F/J/L	4	10	7	19
Hist1h2bm	Histone H2B type 1-M	3	4	6	6
Hist2h2bb	Histone H2B type 2-B	2	3	6	7
Hist2h3b	Histone H3.2	5	11	15	18
Hist3h2bb	Histone H2B type 3-B	1	1	1	1
Hnrnpa1	Heterogeneous nuclear ribonucleoprotein A1	1	1	2	3
Parp1	Poly [ADP-ribose] polymerase 1	6	2	23	26
Parp14	Poly [ADP-ribose] polymerase 14	1	3	2	1

E

Gene name	Protein name	ARH3 KO 1	ARH3 KO 2	Gene name	Protein name	ARH3 KO 1	ARH3 KO 2
N/A	Uncharacterized protein C1orf131 homolog	2	2	Kifc5b	Kinesin-like protein KIFC1	1	1
N/A	Uncharacterized protein C11orf98 homolog	1	3	Lbr	Lamin-B receptor	8	9
C1qb	Complement C1q subcomponent subunit B	2	1	Limd2	LIM domain-containing protein 2	2	2
Cbx3	Chromobox protein homolog 3	1	2	Lmna	Prelamin-A/C	3	7
Cbx5	Chromobox protein homolog 5	8	7	Mecp2	Methyl-CpG-binding protein 2	4	2
Cenpv	Centromere protein V	1	1	Mybbp1a	Myb-binding protein 1A	3	3
Chd1l	Chromodomain-helicase-DNA-binding protein 1-like	1	1	Npm1	Nucleophosmin	5	9
Cherp	Calcium homeostasis endoplasmic reticulum protein	1	2	Pola1	DNA polymerase alpha catalytic subunit	1	1
D8Ertd738e	Leydig cell tumor 10 kDa protein homolog	1	2	Rfc1	Replication factor C subunit 1	2	3
Ddx21	Nucleolar RNA helicase 2	2	1	Sarnp	SAP domain-containing ribonucleoprotein	1	3
Edf1	Endothelial differentiation-related factor 1	3	4	Senp3	Sentrin-specific protease 3	1	1
Gm16494	Predicted gene 16494	2	2	Ssb	Lupus La protein homolog	2	2
Gtf3c2	General transcription factor 3C polypeptide 2	1	1	Tcof1	Treacle protein	4	5
H1f0	Histone H1.0	2	2	Thumpd1	THUMP domain-containing protein 1	2	3
Heatr1	Heatr1 protein	1	1	Top2a	DNA topoisomerase 2-alpha	3	6
Hist1h1c	Histone H1.2	4	4	Trip12	E3 ubiquitin-protein ligase TRIP12	1	2
Hmga1	High mobility group protein HMG-I/HMG-Y	3	5	Wiz	Protein Wiz	2	2
Hmgb3	High mobility group protein B3	3	2	Yy1	Transcriptional repressor protein YY1	1	2
Hnrnpa2b1	Heterogeneous nuclear ribonucleoproteins A2/B1	1	1	Zfp800	Zinc finger protein 800	1	4
Ifi204	Interferon-activable protein 204	4	5	Znf22	Zinc finger protein 22	3	2

F

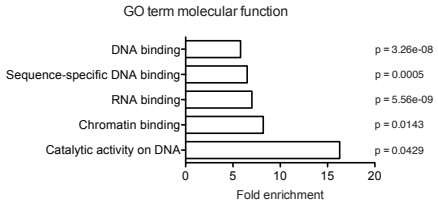

G

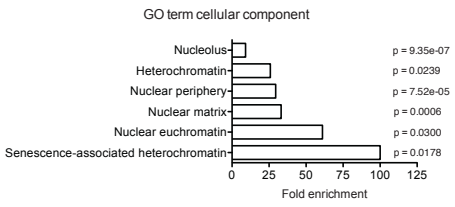

H

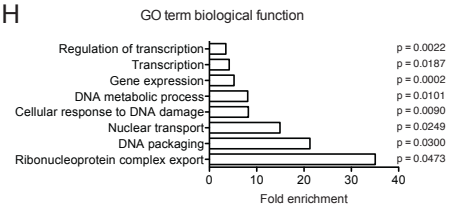

Figure 10: The basal spleen ADP-ribosylome consists of histones mainly and deficiency of ARH3 leads to an enhanced ADP-ribosylome of proteins involved in nuclear export and DNA packaging. Venn diagram of ADP-ribosylated proteins identified in A) both WT and B) both *ARH3* KO spleens. C) Venn diagram of all four measured spleen samples. D) List of the 17 proteins detected in all spleen samples and their corresponding PSM counts. E) List of the 40 proteins found exclusively in the spleens of KO mice and their number of identified PSMs. Genome ontology terms for F) molecular function, G) cellular component, and H) biological function.

Next, a gene ontology (GO) analysis for the molecular function including the 40 proteins exclusively modified in *ARH3* KO spleens compared to the entire mouse proteome was performed and revealed enriched terms in DNA- and RNA-binding proteins (Figure 10F). The cellular component analysis revealed highly significant enrichments for proteins of the nuclear periphery and the nucleolus, and both eu- and heterochromatin (Figure 10G). We also analyzed the GO terms for biological function, which revealed an enrichment in ribonucleoprotein complex export, nuclear export as well as DNA packaging, DNA-damage response proteins and proteins involved in transcription (Figure 10H).

Together, this data hints at ARH3 being responsible for the basal de-ADP-ribosylation of mainly nuclear, chromatin-associated and regulating proteins, suggesting that ARH3 functions in the regulation of heterochromatin assembly to the nuclear lamina and regulates the ADP-ribosylation state of proteins involved in general nuclear export, and potentially also of ribosome export. Additionally, the increase in ADP-ribosylated proteins of the DNA damage response in absence of ARH3 suggests a role of ARH3 as regulator of stress-induced ARTD1 ADP-ribosylation.

The total level of H3 lysine 27 trimethylation is reduced in *ARH3* KO MEFs

Considering the high number of ADP-ribosylation sites of core histones and linker histone 1 in *ARH3* KO MEFs (Abplanalp et al., manuscript submitted, and previous subchapter), we hypothesized that increased histone ADP-ribosylation might interfere with other known histone marks in this context. Since recombinant ARH3 is a potent hydrolase of ARTD1-modified H3-tail, we focused on other known H3 modifications. We prepared whole cell lysates of WT and *ARH3* KO MEFs and performed Western blots detecting H3 (Figure 11A, next page), acetylated H3 (Figure 11B), and H3 specifically dimethylated at position K9 (Figure 11C) or trimethylated at K27 (Figure 11D). While global levels of total H3, acetylated H3 as well as H3K9me2 were not altered, we observed a decrease in the repressive histone mark H3K27me3 in *ARH3* KO MEFs compared to WT cells, suggesting that ARH3 is required for either the establishment or the maintenance of H3K27me3 in the context of MEF cells.

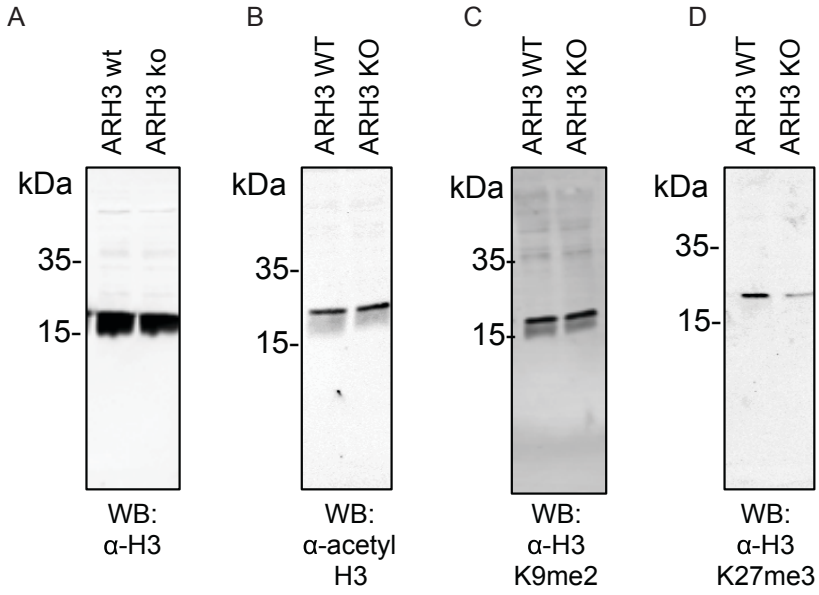

Figure 11: ARH3 promotes the repressive histone mark H3K27me3. Western blot analysis of 50 ug whole cell lysate of WT and *ARH3* KO MEF cells. A) H3, B) Acetyl-H3, C) H3K9me2, and D) H3K27me3. Representative images out of three independent experiments are shown.

ARH3 binds nuclear proteins

Besides finding potential targets of ARH3 that are demodified, we were also interested in identifying other binding partners that might regulate ARH3 (e.g. cofactors). As no commercially available antibody for direct immunoprecipitation of ARH3 was available, we generated a FLAG-tagged version of ARH3, which can be easily enriched and further analyzed using FLAG-beads. To confirm that an N-terminal tag would not interfere with physiological localization of ARH3, we overexpressed GFP-, HA-, and FLAG-tagged ARH3 in 3T3 mouse fibroblast cells (Figure 12 A-C, next page). All constructs localized to the nucleus, which is in line with our previous results (Abplanalp *et* al., submitted manuscript), confirming that an N-terminal tag does not interfere with the physiological nuclear localization of ARH3.

To identify potential binding partners of ARH3, we next overexpressed an empty vector (EV) or a vector containing FLAG-ARH in 3T3 cells. Cells were lyzed and the lysates incubated with FLAG-beads. After several washing steps, a FLAG-peptide was used to elute the proteins that bound to the FLAG-beads. Silver staining of an SDS-PAGE gel of the eluates revealed that FLAG-ARH3 was successfully pulled down and eluted (Figure 12D, band at 40 kDa). Mass spectrometric analysis of the eluates allowed identifying proteins that only bound to FLAG-tagged ARH3

(Figure 12E). The most prominently identified proteins were nuclear proteins, e.g. heterogeneous nuclear ribonucleoprotein K (Hnrnpk), Ras GTPase-activating protein-binding protein 1 (G3bp1) and Exportin-2 (Xpo2). Interestingly, these proteins were not found to be modified in our MS analysis and will need further validation, but still suggest that ARH3 is localized to the nucleus and plays a role in DNA- and RNA-associated processes or might be regulated by these proteins.

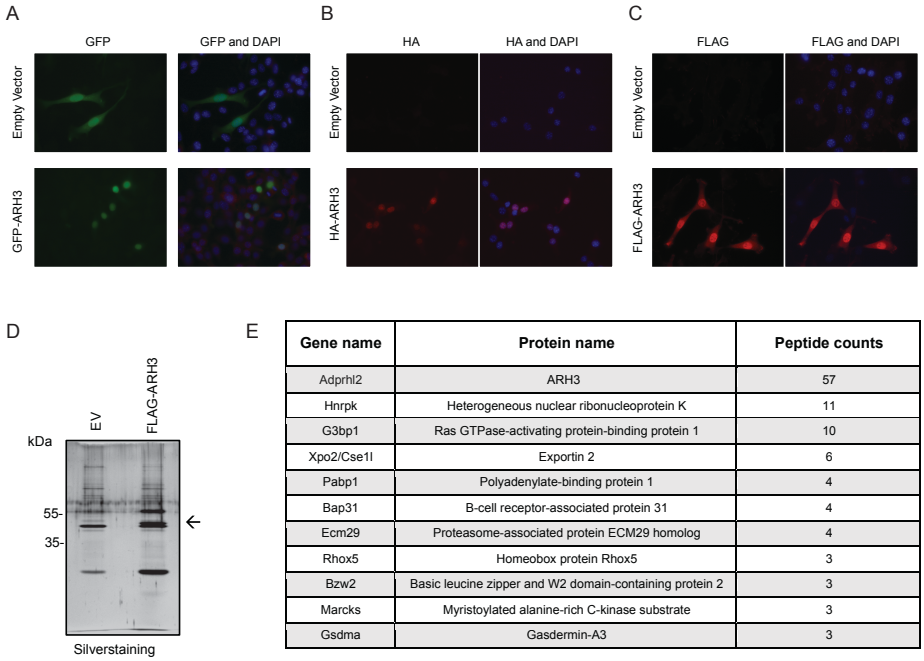

Gene name	Protein name	Peptide counts
Adprhl2	ARH3	57
Hnrpk	Heterogeneous nuclear ribonucleoprotein K	11
G3bp1	Ras GTPase-activating protein-binding protein 1	10
Xpo2/Cse1l	Exportin 2	6
Pabp1	Polyadenylate-binding protein 1	4
Bap31	B-cell receptor-associated protein 31	4
Ecm29	Proteasome-associated protein ECM29 homolog	4
Rhox5	Homeobox protein Rhox5	3
Bzw2	Basic leucine zipper and W2 domain-containing protein 2	3
Marcks	Myristoylated alanine-rich C-kinase substrate	3
Gsdma	Gasdermin-A3	3

Figure 12: FLAG-ARH3 localizes to the nucleus and binds to nuclear proteins. A) Immunofluorescence pictures of 3T3 cells transfected with A) GFP-, B) HA-, or C) FLAG-tagged ARH3. D) Silverstaining of proteins eluted from FLAG-beads upon binding of cell lysates from empty vector (EV) or FLAG-ARH3-transfected 3T3 cells. E) List of potential ARH3 binding proteins.

ARH3 represses *iNos* expression, yet enhances its activity upon LPS stimulation

Considering the function of ARH3 as a mono- and poly-ADP-ribosylhydrolase that demodifies many chromatin components (i.e. histones), and knowing that both MARylation and PARylation play important roles in inflammatory responses (see 2.1.4), we investigated a potential regulatory role of ARH3 in LPS-induced inflammation. LPS-treatment of cells and binding of LPS to the toll-like receptor 4 (TLR4) induces a well understood signaling cascade as part of the specific innate immune response[135]. Intracellularly, this signaling leads to the phosphorylation of

IκB, which is thereafter ubiquitinated and degraded, exposing the nuclear localization signal of NF-κB a heterodimeric interaction partner of IκB. This subsequently leads to the translocalization of NF-κB to the nucleus, where it activates the expression of different genes including those of cytokines. This transcriptional activity can easily be monitored by qPCR. To investigate a potential involvement of ARH3 in LPS-induced cytokine signaling, we first assessed whether transcription of ARH3 itself is regulated upon LPS-induced NF-κB activation. We isolated cells from the bone marrow of WT mice and differentiated them to bone marrow-derived macrophages (BMDM). The cells were treated with LPS for 1h, 4h, 8h, 12h, or 24h, respectively, RNA was isolated, reverse transcribed and the cDNA analyzed by qPCR (cDNA kindly provided by Friedrich Kunze). Interestingly, while the mRNA levels of the housekeeping gene *RPS12* were relatively stable over the course of the treatment (Figure 13A, next page), *ARH3* mRNA was upregulated 10-fold after 8h and 12h of LPS treatment (Figure 13B), suggesting *ARH3* expression itself is regulated by the LPS-signaling.

To investigate how ARH3 might influence the inflammatory response, we knocked down *ARH3* in 3T3 cells by siRNA and assessed the expression of NF-κB-target genes such as *IL6*, *IP10*, and *iNos* after 4h of LPS treatment. Levels of the housekeeping gene *RPS12* were comparable for siMock- and siARH3-treated 3T3 cells, suggesting that ARH3 deficiency does not affect cell viability (Figure 13C). The expression levels of *ARH3* were reduced to 65% when applying siARH3, indicating that the siRNA treatment worked (Figure 13D). The expression of the inflammatory genes *IL6* (Figure 13E) and *IP10* (Figure 13F) were both induced upon LPS treatment, however remained unchanged in siMock to siARH3 cells. However, the inflammatory gene *iNOS* was upregulated upon ARH3 knockdown and LPS treatment, suggesting a regulatory role of ARH3 in its expression (Figure 13G).

To confirm this finding in another cell line, we repeated the experiments with RAW macrophages. As this cell type is not easily transfectable with siRNA, we transduced cells with shMock and shARH3 retroviral constructs. Similar to the siRNA treatment, shMock and shARH3 did not affect the expression of the housekeeping gene *RPS12* (Figure 13H). *ARH3* levels were again downregulated to approximately one third comparing shARH3 to shMock RAW cells (Figure 13I). As observed before for 3T3 cells, *iNOS* expression was upregulated upon LPS treatment in shARH3 cells

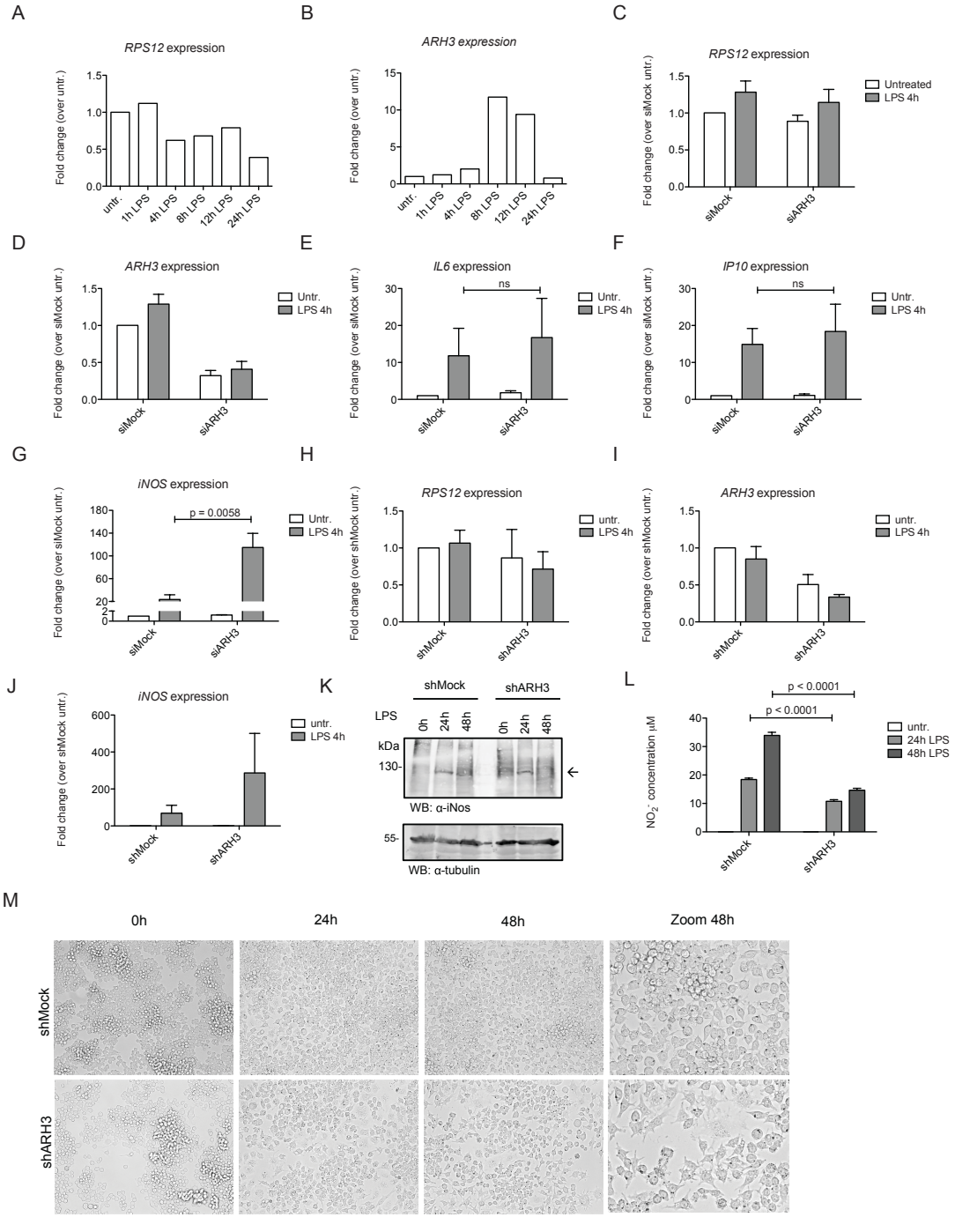

Figure 13: ARH3 regulates the transcription and activity of *iNOS* upon LPS stimulation of 3T3 and RAW cells. Bone marrow-derived macrophages were isolated and stimulated with 10 ng/ml LPS for the indicated time points and mRNA levels of A) *RPS12* and B) *ARH3* measured. 3T3 cells were treated with siMock or siARH3 for 48-72h and treated with 100 ng/ml LPS. C) *RPS12*, D) *ARH3*, E) *IL6*, F) *IP10*, and G) *iNOS* mRNA levels were assessed. n = 6 for C), D), and G) and n = 3 for E) and F). Mean ± SEM, ns = not significant, p = p-value, two-tailed Student's t-test. RAW cells stably expressing an shMock or shARH3 construct were treated with 100 ng/ml LPS for 4h and expression of H) *RPS12,* I) *ARH3*, and J) *iNOS* measured by qPCR. K) Western blot of iNOS protein levels upon 24h and 48h of 10 ng/ml LPS treatment of shMock and shARH3 RAW cells. n = 2, no statistical analysis performed. L) Griess assay measuring iNOS catalytic activity of these cells. n = 4, mean ± SEM, p = p-value, two-tailed Student's t-test. M) Bright-field microscopy (10x) pictures of shMock and shARH3 RAW cells 24h and 48h treated with LPS.

compared to shMock (Figure 13J), suggesting that ARH3 dampens the expression of *iNOS* in 3T3 and RAW cells.

In addition, we assessed the protein levels of iNOS in shMock and shARH3 cells upon 24h and 48h treatments with LPS. After 24h, iNOS was equally expressed in both shMock and shARH3 RAW cells (Figure 13K), suggestion that the observed transcription differences did not affect the translation efficiency of iNOS. Next, we characterized also the iNOS catalytic activity using the Griess assay. Surprisingly, a significant drop in iNOS activity was observed in shARH3 cells both after 24h and 48h of LPS treatment (Figure 13L), suggesting that ARH3 directly or indirectly regulates iNOS activity, potentially by binding or via modulating its ADP-ribosylation state. Due to the mainly cytoplasmic localization of iNOS, we assume a rather indirect effect of ARH3 on iNOS. Moreover, we also observed an interesting morphological change in shARH3 RAW cells upon treatment with LPS, which might indicate more drastic expression changes arising through the knockdown of ARH3 (Figure 13M).

Together, all this data suggests an inhibitory role of ARH3 for the expression of *iNOS* upon LPS stimulation in 3T3 and RAW cells, and a direct or indirect stimulating role on iNOS catalytic activity.

ARH3 differentially regulates *iNOS* expression upon LPS-stimulation in various cell types

To assess ARH3 function in inflammation at a more physiological level, we directly characterized the LPS response of BMDMs from WT and *ARH3* KO mice. 8-week-old males (n = 5 each genotype) were sacrificed and their bone marrow pooled. After differentiation, the macrophages were treated with LPS for 4h and their *RPS12*, *ARH3*, and *iNOS* mRNA expression levels measured using qPCR. *RPS12* levels were comparable between WT and *ARH3* KO macrophages (Figure 14A, next page) and as expected, *ARH3* levels were undetectable in the *ARH3* KO cells (Figure 14B). Interestingly, compared to the results from siARH3 3T3 and shARH3 RAW cells, macrophages isolated from *ARH3* KO animals did not show an altered *iNOS* transcription (Figure 14C).

We also used the BMDMs for a Griess assay to monitor iNOS activity. Here, similar to the shRAW cells, the enzymatic activity of iNOS from *ARH3* KO mouse

cells was undetectable 24h after the addition of LPS, while iNOS activity was easily observed in the WT cells (Figure 14D), suggesting that ARH3 indeed regulates the iNOS activity even in this context.

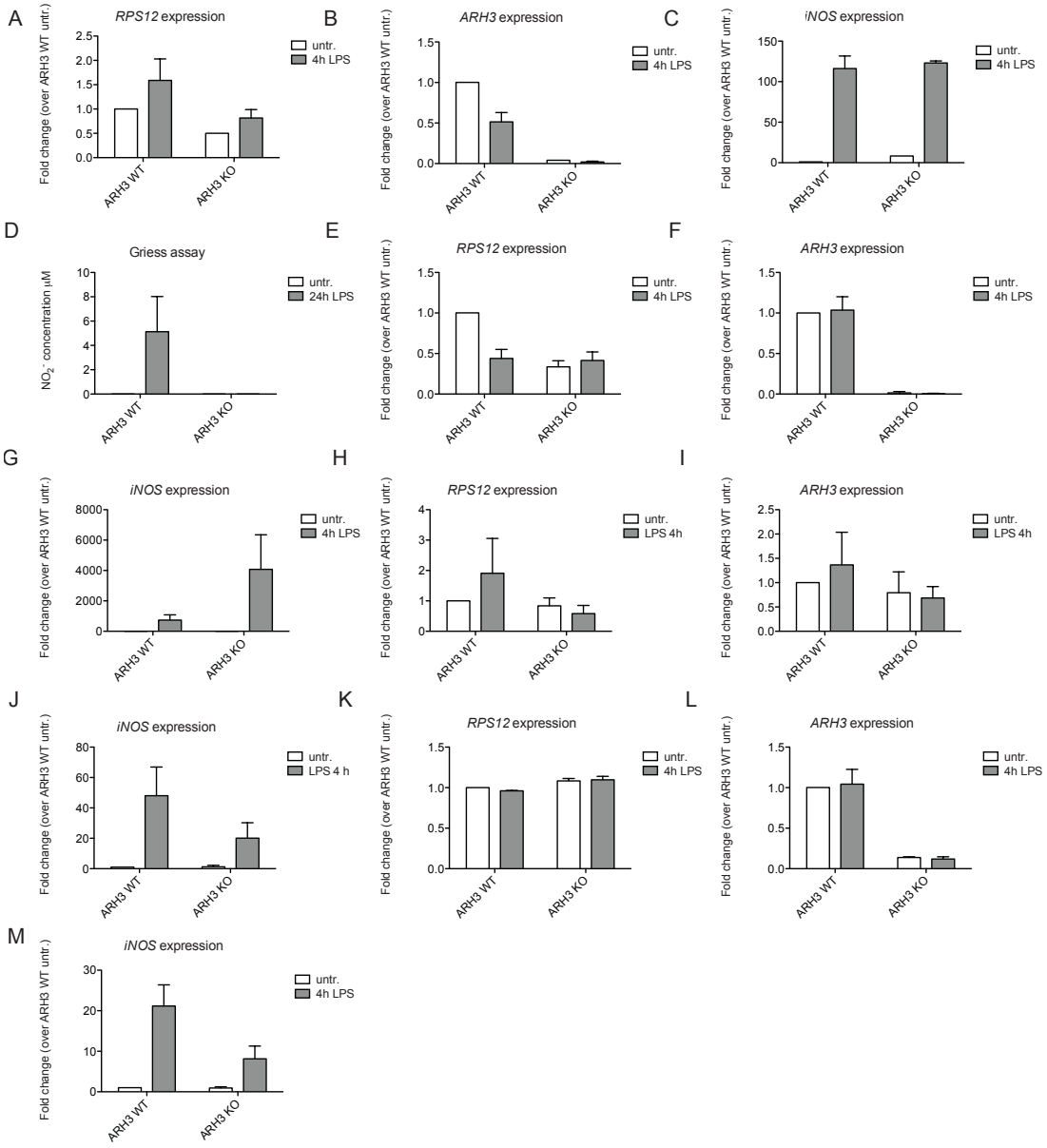

Figure 14: *iNOS* upregulation is differently regulated by ARH3 depending on the cell type. BMDMs from *ARH3* WT and KO mice were isolated and treated with 10 ng/ml LPS for 4h and A) *RPS12*, B) *ARH3*, and C) *iNOS* levels assessed by qPCR. D) Griess assay of BMDM after 24 h of 10 ng/ml LPS stimulation. Mouse ear fibroblasts from wt and *ARH3* ko mice were treated with 100 ng/ml LPS for 4 h and E) *RPS12*, F) *ARH3*, and G) *iNOS* levels quantified by qPCR. MLFs from *ARH3 WT* and KO mice were treated with 100 ng/ml LPS for 4 h and H) *RPS12*, I) *ARH3*, and J) *iNOS* levels assessed by qPCR. MEFs were treated with 100 ng/ml LPS for 4 h and K) *RPS12*, L) *ARH3*, and M) *iNOS* levels assessed by qPCR.

Additionally to the macrophages, we also isolated fibroblasts of the ear, lung and skin. Ears or lungs of two animals from each genotype were pooled and cultured for several passages, then treated with LPS for 4h. Similar to 3T3 cells, ear fibroblasts showed comparable *RPS12* levels (Figure 14E), and *ARH3* was undetectable in the *ARH3* KO cells (Figure 14F). *iNOS* was upregulated upon LPS stimulation and its expression further increased in the *ARH3* KO cells (Figure 14G). However, for the mouse lung fibroblasts (MLF), the results looked surprisingly different. While the *RPS12* levels were fairly equal (Figure 14H), the MLF *ARH3* KO cells expressed basal levels of *ARH3* (Figure 14I) and showed a decrease in *iNOS* expression upon 4h LPS treatment (Figure 14J). In MEFs (provided by Joel Moss), *RPS12* levels were comparable (Figure 14K), and the *ARH3* KO cells also showed detectable levels of *ARH3* (Figure 14L). Comparable to MLFs, the MEF cells showed a decrease of *iNOS* expression upon LPS stimulation in the *ARH3* KO compared to the WT (Figure 14M). Taken together, although the effect of ARH3 on iNOS activity was reproducible, the transcription analysis involving different cell types were inconclusive and did not allow an assessment of the function of *ARH3* in this regard.

3.4 Methods to unpublished results

Animals

Breeding pairs for the ARH3 KO mouse strain C57BL/6N-Adprhl2<em2Wtsi>/Wtsi were purchased from Genome Research Limited, Wellcome Trust Sanger Institute (Cambridge, UK). All mice were bred at the animal facility of the University of Zurich and maintained on a 12-h light–dark cycle with regular unrestricted diet. All animal experiments were carried out in accordance with the Swiss and EU ethical guidelines and have been approved by the local animal experimentation committee of the Canton of Zurich under license #ZH207/15 and following the 3R guidelines. Giovanni Pellegrini from the laboratory for animal model pathology, University of Zurich, carried out necropsies and histopathological phenotyping.

Mouse genotyping

DNA isolation. Toe biopsies from mice were taken and stored at 4 °C until further used. For DNA isolation, 85 µl of lysis buffer (25 mM NaOH, 0.2 mM EDTA) were added to each biopsy and incubated at 95 °C for at least 45 min (or until most tissue was dissolved). 85 µl of neutralization buffer (40 mM Tris HCl, pH 8) was added and the DNA concentration measured using a NanoDrop (Thermo Fisher Scientific).

Genotyping PCR. In a total reaction volume of 50 µl, 1x green Go-TAQ® Flexi buffer (Promega), 0.2 mM dNTP mix (Sigma), 0.2 µM of each primer (Microsynth), 1.5 mM $MgCl_2$ (Promega) (for wildtype PCR) or 2 mM $MgCl_2$ (for KO PCR), 100 ng template DNA and 1.25 u Go-TAQ® Flexi DNA polymerase (Promega) were mixed. To detect the wildtype allele, primers Adprhl2_DF1 (5'-3' GGTTTGGGAAGCAATTTCAAAAAGG) and Adprhl2_ER1 (5'-3' TTGGACGCCAAGGAGTGAGTAT) were used, leading to an expected PCR product size of 326 bp. For the detection of the mutant allele containing the exon deletion, primer Adprhl2_DF1 and primer Adprhl2_DR1 (5'-3' GAAAGTTTCCCTTCAGAAATCAGGG) were used, leading to an expected PCR product size of 532 bp, and the potential amplification of the endogenous wildtype allele appearing as a larger band. The PCR program used for both PCRs was initial denaturation at 95°C for 2 min, 35-40 cycles of denaturation at 95°C for 30 s,

annealing at 58°C for 30 s and extension at 72°C for 1 min, and a final extension at 72°C for 10 min.

Mouse organ processing for protein isolation and Western blotting

Protein isolation. Excised mouse organs were snap frozen in liquid nitrogen and stored at -80°C. For tissue lysis, ice-cold modified RIPA buffer (50 mM Tris HCl pH 7.4, 400 mM NaCl, 1% NP-40, 0.1% Na-deoxycholate, 1 mM EDTA, 1x EDTA-free protease inhibitor cocktail (Roche)) was freshly prepared, and supplemented with 40 μM PJ34 and 75 μM tannic acid to inhibit potential ARTD or PARG/ARH3 activity during lysis. RIPA buffer was added to frozen organs and lysis performed on a Tissue Lyser II (Qiagen) at 30 Hz for at least 1x 30 s, further cycles were added until respective tissues were fully lyzed. The lysate was incubated on a roller for 30 min at 4°C, sonicated 3 x 30 s and cleared by high-speed centrifugation. The supernatant was supplemented with glycerol to a final concentration of 20%. Protein concentration was measured using a Bradford assay (Biorad).

Western blotting. Proteins were separated by sodium dodecyl sulfate-polyacrylamide gel electrophoresis and bands visualized by using IR-Dye-conjugated antibodies (1:15'000, LI-COR) and detection by the Odyssey infrared imaging system (LI-COR). Antibodies used for Western blotting were diluted in 1% milk in TBST (0.05% Tween 20) as follows: α-MAR (1:1'000, homemade, raised in rabbits against a chemically ADP-ribosylated H2B-like peptide), α-tubulin (1:10'000, Sigma), α-ARH3 (1:1'000, custom made, Genosphere Biotech), α-H3 (1:5'000, Abcam), α-H3K27me3 (1:1'000, Cell Signaling).

Mouse organ processing for mass spectrometric analysis

Protein isolation. Lysis buffer (6 M guanidine-hydrochloride (Gnd-HCl), 5 mM tris (2-carboxyethyl)phosphine (TCEP), 10 mM 2-chloroacetamide CAA**,** 100 mM Tris pH 8) was preheated to 95°C and directly added to frozen tissue. Upon lysis using a Tissue Lyser II (Qiagen) as described above, sample concentration was measured using a Bradford assay (Biorad), the samples were diluted with 25 mM Tris, pH 8, and digested with trypsin (Promega). The peptide mixture was treated with PARG to obtain only MARylated peptides, and the peptides were enriched using a macrodomain affinity pulldown as described previously[23-25]. However, instead of the

conventional Af1521, we used an Af1521 mutant from a phage display shown to bind ADP-ribosylated peptides with higher affinity (data not shown). Data analysis was performed as described in (Abplanalp et al.), using the UniProtKB mouse database (taxonomy 256 10090, version 20160902). Mascot 2.5.1.3 (Matrix Science) was used for peptide sequence identification. S, R, K, D, E and Y residues were set as variable ADP-ribose acceptor sites. Peptides were considered correctly identified only when a Mascot score >20 and an expectation value >95% was reached. Venn diagrams were plotted using the online tool Venny 2.1.0 (Oliveros, J.C. (2007-2015) Venny. An interactive tool for comparing lists with Venn's diagrams, http://bioinfogp.cnb.csic.es/tools/venny/index.html). Gene ontology analysis was performed using the PANTHER database[136].

Cells

MEF cells from WT and *ARH3* KO mice (kindly provided by Joel Moss, described in[65]), mouse ear fibroblasts and MLFs isolated from our WT and *ARH3* KO mice, as well as 3T3, RAW, and HEK cells (all ATCC) were all cultured in DMEM (GIBCO) supplemented with 5% penicillin/streptomycin (P/S) and 10% fetal calf serum (FCS).

Cloning of mouse ARH3 constructs

cDNA of mouse *ARH3* was kindly provided by Joel Moss. The ARH3 sequence was amplified with primers (Microsynth) and cloned into the mammalian expression vectors pHA-MEX, pcDNA3.1 or pEGFP using restriction enzymes BamHI and XhoI (NEB). Plasmids were sequenced by Microsynth and purified using the NucleoBond Xtra kit (Macherey-Nagel) before transfection into 3T3 cells.

Transfection

Overexpression constructs. 3T3 cells were transfected at 40% confluency. 2x BES (50 mM *N,N*-bis(2-hydroxyethyl)-2-amino-ethanesulfonic acid (BES), pH 6.95, 280 mM NaCl, 1.5 mM Na_2HPO_4 in ddH_2O) was added dropwise to a mix of plasmid DNA and $CaCl_2$, yielding a final concentration of 1x BES, 10 µg/ml DNA and 150 mM $CaCl_2$), incubated for 3 min at room temperature (RT) and added to the cells

dropwise without swirling. Medium was changed after 6h and cells incubated for a total of 48-72h.

siRNA. 3T3 cells were transfected at 60% with 10 nM final concentration of siMock (Allstar Negative Control) or Mm_Adprhl2_1 or Mm_Adprhl2_5 siRNA (all from Qiagen) using the Lipofectamine® RNAiMAX Reagent (Invitrogen). The transfection solution was prepared according to the manufacturer's protocol) and cells incubated for 48-72h.

Immunofluorescence

3T3 cells were grown in 24-well plates on coverslips to a confluency of 80-90% confluency. Cells were fixed with 4% paraformaldehyde in PBS (PFA) for 15 min at RT and permeabilized with 0.2% Triton X-100 (in PBS) for 10 min at RT. After washing with PBS three times, cells were blocked in blocking solution (2% BSA, 0.1% Triton X-100 in PBS) for 45 min at RT. Primary antibody α-FLAG (M2) (1:1'000, Sigma) or α-HA (1:250, Covance) was incubated for 1h at RT in blocking solution. Cells were washed with PBS three times before the addition of secondary antibody Cy™3 AffiniPure Goat Anti-Mouse IgG (1:250, Jackson ImmunoResearch) in blocking solution for 1h at RT. Cells were washed three times again, and incubated for 2.5 min with Hoechst (1:500, Sigma), washed once with PBS, and mounted onto a glass slide using VECTASHIELD® mounting medium and fixed with nail polish. Images were acquired using an inverted fluorescence microscope at 40×, oil immersion (Leica).

FLAG-immunoprecipitation and mass spectrometry

Immunoprecipitation. Flag-tagged proteins were immunoprecipitated using ANTI-FLAG M2 agarose beads (Sigma). Slurry beads were washed three times in binding buffer (250 mM HEPES pH 7.9, 2 mM $MgCl_2$, 0.2 mM EGTA, 10% glycerol, 0.1 mM PMSF, 2 mM DTT, 140 mM NaCl, 0.1 % NP-40, 1 μg/ml leupeptin, 1 μg/ml pepstatin, 1 μg/ml bestatin). 500 μg cell lysate was incubated with 30 μl beads in 1 ml binding buffer for 2h at 4°C. Beads were washed four times with 1 ml binding buffer. Elution was carried out using binding buffer supplemented with 0.150 μg/μl FLAG peptide (Sigma) and incubation for 30 min at 4°C.

Sample digest and cleanup. Per 30 µl of elution, 200 µl of 8M urea (UA, in 100 mM Tris, pH 8.0) were added. Samples were loaded onto Amicon Ultra-0.5 ml centrifugal filters (Merck) according to the manufacturer's manual. Once the entire sample was loaded, several washing steps were applied. First, 200 µl UA were added, then the sample was incubated with 100 µl 0.05 M iodoacetamide for 5 min, then washed twice with UA, twice with 0.5 M NaCl, before transferring the filter to a new collection tube. Samples were digested on the filter overnight in 0.05 M triethylammonium bicarbonate containing trypsin in a 1:50 ratio to protein before centrifugation and final acidification to 0.5% trifluoroacetic acid the next day. The Functional Genomics Center Zurich (FGCZ) further processed samples.

Silver staining

Proteins were separated by sodium dodecyl sulfate-polyacrylamide gel electrophoresis. All following incubations were carried out at RT. The gel was fixed for 30 min in 50% methanol and 10% acetic acid. One wash for 15 min in 5% methanol was followed by three washes with H_2O for 5 min each. The gel was sensitized for 2 min in tetrathionate sensitizing solution (0.2 g $Na_2S_2O_3$ in 1 l of H_2O) and washed again three times with H_2O. The gel was stained with 200 mg $AgNO_3$ in 100 ml H_2O for 25 min. After three 1 min washes with H_2O, the gel was developed for 5-10 min in developing solution (3 g Na_2CO_3, 50 µl formaldehyde (37%) and 2 ml of tetrathionate sensitizing solution in 100 ml H_2O). The reaction was stopped for 10 min in stopping solution (0.05 M EDTA), and the gel washed and stored in H_2O.

Viral transduction

Lentivirus production. A 10 cm dish of HEK cells was transfected using the above protocol with 3.5 µg of the envelope-encoding plasmid pMD.G and 6.5 µg of the packaging plasmid CMV delta R8.91 and either 10 µg of the shMock empty pLKO.1 plasmid or a construct containing a shRNA targeting murine ARH3 (pLKO.1, shARH3, TRC0000340923, Sigma). After 6h, 6ml of fresh medium was added to the cells. The medium containing the virus was collected after 24h by centrifugation through a 0,45 µm cellulose acetate filter.

Transduction of target cells. RAW cells were infected at a confluency of 50%. 2 ml medium containing the virus and 4 µg/ml polybrene was added to a 6-well of

RAW cells. After 12 h, cells were split and selected using puromycin (3 μg/ml). In order to guarantee the knockdown, cells were continuously cultured in the presence of puromycin.

Isolation of bone marrow-derived macrophages

Femur and tibia from WT and *ARH3* KO mice were isolated. The bones were sterilized with ethanol and both ends cut with a scalpel. Bone marrow cells were flushed out using a syringe filled with PBS pH 7.4 containing 10 mM EDTA and 10% FCS. Cells were centrifuged for 3 min at 500 g and the pellet resuspended in 1 ml ACK Lysis buffer (Gibco), kept on ice for 2 min and centrifuged again. The pellet was resuspended in RPMI (Gibco) supplemented with 5% P/S and 10% FCS and 20 ng/ml mouse m-CSF for five days to stimulate macrophage differentiation.

Ear and lung fibroblast isolation

Ears and lungs of euthanized WT and *ARH3* KO mice were isolated and washed with ethanol or PBS, respectively. After drying the tissues, they were cut into small pieces and incubated for 90 min at 37 °C in 4 ml (lungs) or 2 ml (ears) lysis buffer (150 mM NaCl, 10 mM HEPES, 2 mM $CaCl_2$, 0.1% collagenase and 2.4 U/ml dispase, sterile filtered). Cells were centrifuged after addition of 2 ml 0.05 M EDTA in PBS for 5 min at 500 g, the pellet resuspended in 5 ml DMEM supplemented with 5% P/S and 10% FCS and plated. Cells were continuously observed and split when getting to 80-90% confluency.

RNA isolation and qPCR analysis

Cells were washed with PBS once before performing RNA extraction with the NucleoSpin RNA II kit (Macherey-Nagel). RNA was quantified with a NanoDrop (Thermo Fisher Scientific) and reverse transcribed according to the supplier's protocol (High Capacity cDNA Reverse Transcription Kit, Applied Biosystems). Quantitative real-time polymerase chain reactions (qPCR) were performed with KAPA SYBR fast (Kapa Biosystems) and a Rotor-Gene Q 2plex HRM System (Qiagen).

Griess assay

The amount of NO_2^- secreted into the cell medium was measured by mixing 100 µl sample with 100 µl 1% sulfanilamide in 2.5% phosphoric acid (H_3PO_4) and 100 µl naphthylethylenediamine dihydrochloride in 2.5% H_3PO_4. Absorbance at 550 nm was measured and the amount of NO_2^- calculated by using measurements of $NaNO_3$ standard samples.

4 Discussion

4.1 Summary of the results

The aim of this thesis was to identify and characterize a ADP-ribosylhydrolase able to cleave the linkage between ADP-ribose and the amino acids serine and/or lysine, and to characterize this hydrolase in the cellular and organismal context.

With these studies, we provide evidence that ARH3 is a mono-ADP-ribosylhydrolase that cleaves the serine-ADP-ribose linkage. ARH3 deficiency (i.e. KO of ARH3) increased the basal ADP-ribosylome in MEF cells or the spleen (Abplanalp *et al*., submitted manuscript, and unpublished results, Figures 8 and Figure 9). The main targets of ARH3 were nuclear proteins involved in DNA packaging, chromatin remodeling and nuclear export (Abplanalp *et al*., submitted manuscript, and unpublished results, Figure 10). Moreover, ARH3 was required for the establishment and/or maintenance of the histone modification H3K27me3 in MEF cells (unpublished results, Figure 11) and transcriptionally regulated the *iNos* expression, and stimulated the catalytic activity of iNos (unpublished results, Figure 13 and Figure 14). Initial analyses of the *ARH3* KO mouse revealed that ARH3 is dispensable for viability and fertility (unpublished results, Figure 5), and that these mice have no obvious phenotype, except for a weight gain evidently observed for 16 week-old mice (unpublished results, Figure 6 and Figure 7).

4.2 ARH3 has OAADPR-, PAR-, and newly also MAR-hydrolase activity

Previous work reported a PAR- and OAADPR-activity for ARH3[55,56]. A mono-ARH activity of ARH3 was excluded, although ARH3 was only tested to demodify ADP-ribose-cysteine, -asparagine, and diphtamide[56]. Here, we identified ARH3 as mono-ADP-ribosylhydrolase able to demodify serine residues (Abplanalp *et al*., submitted manuscript). Considering the high degree of homology of ARH3 with ARH1 and DRAG, which are both mono-ARHs, it is however not surprising that ARH3 is also able to release the terminal protein-bound ADP-ribose additional to its PAR- and OAADPR-hydrolase activity. So far, we were not able to dissect a distinct amino acids or regions of ARH3 that regulate either the MAR- or the PAR-degrading activity.

The three enzymatic activities of ARH3 could be viewed as ‘enzymatic promiscuity’, that is regulated by e.g. PTM of the respective enzyme, substrate

binding and/or conformational changes[137]. To define which ARH3activity is the most physiologically most relevant will require further studies. These include the crystallization or *in silico* modeling of ARH3 together with the respective substrates to identify specific residues important for binding and/or catalytic activity. Site-directed mutagenesis followed by *in vitro* activity assays using recombinant ARH3 will help solving the structural basis for ARH3's catalytic activity. Assays to assess enzyme kinetics and binding affinity will help resolving which substrates (MAR, PAR or OAADPR) are most likely the major targets of ARH3.

4.3 ARH3 is a nuclear serine-mono-ADP-ribosylhydrolase

Regarding the amino acid specificity of ARH3, we found S to be the major demodified ADP-ribose acceptor site in *in vitro* and *in vivo*, although we observed also a slight increase in lysine and glutamic acid ADP-ribosylation *in ARH3* KO MEFs and *ARH3* KO spleen, the only organ, where we were able to detect an increase in MARylation upon *ARH3* KO (Abplanalp *et al*., submitted manuscript, and unpublished results, Figure 9). Another group recently also reported that ARH3 demodifies ADP-ribosylated S, but not ADP-ribosylated E or K *in vitro*[134]. Based on our data, we do not exclude the possibility that *in vivo*, ARH3 demodifies additional ADP-ribosylated amino acids. Our mass spectrometry workflow might be biased towards the detection of serine-ADP-ribosylation, as other groups have shown mainly glutamic and aspartic acids to be modified, however using a different enrichment method[22]. Characterising ARH3 and other mono-ADP-ribosylhydrolases on samples enriched according to this E/D specific method in combination with label-free quantification mass spectrometry, will reveal which hydrolases are capable of reverting MARylated glutamic and aspartic acid residues.

As serine sites are mainly modified by ARTD1 in complex with its auxiliary factor HPF1[26,138], we assume ARH3 as only serine-specific ADP-ribosylhydrolase known so far, to be the main regulator of ARTD1-mediated ADP-ribosylation. We can however not exclude that potentially other hydrolases are also capable of releasing ADP-ribose from serines. Considering the chemical similarities of serines to tyrosines (both containing an alcohol group), we speculate that ARH3 is not only able to hydrolyze ADP-ribosylated serine residues, but also ADP-ribosylated tyrosines. The same should also be considered for the hydrolysis of the ADP-ribose-glutamic

acid linkage. Hydrolysis of ADP-ribose from lysines, which harbor an amino-group, is more difficult to explain. As lysines are known to be also non-enzymatically modified by free ADP-ribose, i.e. glycation[139], further experiments investigating *in vitro* demodification of specific peptides modified at lysine residues will be required. Additionally, additional evidence for the functional relevance of lysine ADP-ribosylation *in vivo* are still required, and studies including KO animals for the different mono-ARHs will reveal whether and to which extent, a certain hydrolase is responsible for lysine demodification. The specificity of ARH3 (or other potential ADP-ribosylhydrolases) towards a specific amino acid might be tightly regulated comparable to the different activities in ARH3 described above, e.g. by other posttranslational modifications of the ADP-ribosylhydrolases itself, which might influence the conformation of the protein. Alternatively, a co-factor might regulate the hydrolase activity, comparable to the HPF1 interaction with ARTD1.

In our studies, ARH3 primarily localized to the nucleus, more specifically to chromatin, when investigated by Western blot of endogenous or immunofluorescence of overexpressed tagged ARH3 (Abplanalp *et al.*, submitted manuscript, and unpublished results, Figure 12A-12C). The identification of mainly nuclear ADP-ribosylated proteins in the *ARH3* KO spleen samples and the identification of nuclear interaction partners strongly support this finding (unpublished results, Figure 10). Recently, the Human Protein Atlas Project (HPA) has mapped all human proteins to their respective subcellular localization by immunofluorescence, and validated their findings using mass spectrometry studies[140]. These data strongly correlate with our findings, confirming that ARH3 is localized in the nucleoplasm in several cell lines and with several tested antibodies (www.proteinatlas.org). Other groups provided evidence that endogenous ARH3 is localized mainly to the cytoplasm, as well as to the nucleus and mitochondria, but to a lesser extent[65]. Yet, other experiments showed that a C-terminally FLAG-tagged ARH3 localized to the mitochondria, due to a potential N-terminal mitochondrial signaling peptide present in ARH3[141]. In the same studies, however, immunofluorescence-stainings using a FLAG antibody indicated that the main portion of ARH3 resides in the nucleus and not in the mitochondria, which was not further discussed by the authors, neither did they confirm co-localization of ARH3-FLAG with a mitochondrial marker[141]. Since we did not perform an overexpression with C-terminally flagged ARH3 constructs, we cannot

fully exclude its mitochondrial localization. Potentially, the N-terminal signaling peptide might be required to redirect ARH3 to the mitochondria under specific conditions. Based on our findings investigating both endogenous and tagged ARH3 together with the data from the HPA, a nuclear localization of ARH3 under basal conditions is most likely.

4.4 ARH3 demodifies nucleosomes and chromatin-associated proteins

Unfortunately, not much is known about the cellular function of ARH3, except for its involvement in the oxidative stress response[65,141]. In our studies, ARH3 demodified ARTD1-ADP-ribosylated histones *in vitro*, and depletion of ARH3 in the spleen resulted in an increased ADP-ribosylation of core histone variants and especially H1 (Abplanalp *et al*., submitted manuscript, unpublished results, Figure 10). Histones were long known to be ADP-ribosylated[18-20,26], however, full reversal of this modification has so far not been shown. The mono-ARH activity of ARH3 on *in vitro* modified histone tails provides evidence for a full reversibility of histone ADP-ribosylation. The molecular role of histone ADP-ribosylation is poorly understood. Upon H_2O_2-treatment histone ADP-ribosylation rather seemed to decondense chromatin structures, and was mainly found *in vivo* associated with heterochromatin [36,128]. It is tempting to speculate that similar to histone methylation or acetylation, ADP-ribosylation regulates DNA accessibility or recruits proteins with an ADPr-binding domain and thus needs to be considered as a new important player in chromatin remodeling, subsequently regulating DNA associated processes such as transcription, replication and repair. ChIP analysis using an ARH3 antibody or an overexpressed tagged ARH3 version would reveal the genomic loci at which ARH3 resides. Together with ADP-ribose ChAP (i.e. identification of chromatin ADP-ribosylation), this would reveal at which loci ARH3 activity is most likely important. Global changes in the chromatin landscape, specifically targeting active and repressive histone marks, could be further investigated by ChIP in WT and *ARH3* KO cells. ATAC-seq of *ARH3* cells would reveal how the accessibility of chromatin is regulated by ADP-ribosylation at a genome wide level.

We identified in the spleen Cbx5 and Lbr as novel targets of ARH3 (unpublished results, Figure 10). Moreover, we observed a decrease in global H3K27me3 in *ARH3* KO MEFs, linking ARH3 and potentially its enzymatic activity

to heterochromatin formation and/or maintenance (unpublished results, Figure 11). Cbx5 and Lbr are part of a complex, although not directly interacting, that binds core histones H3 and H4 and anchors them to the nuclear lamina, an interaction lost upon acetylation of the histones[142]. We hypothesize that ADP-ribosylation of either Cbx5, Lbr, or the histones might, comparable to acetylation, interfere with their binding to the nuclear lamina. ARH3 might thus as part of the Cbx5-Lbr-histone complex, demodify the protein complex and regulate binding to the nuclear lamina thus assuring the formation and maintenance of H3K27me3. Interestingly, ADP-ribosylation has already been associated with lamina-associated domains (LADs), where ARTD1 interplays with CTCF to associate genomic regions to the lamina for controlling their expression dependent on the circadian clock[143]. Co-IP studies, ChIP and ChAP experiments and immunofluorescence imaging for distinct chromatin regions might shed light on the exact nuclear localization of ARH3 and its potential association with LADs.

In addition, we identified another newly emerging potential function of ARH3 in nuclear export, specifically for ribonuclear proteins, since several ARH3 target proteins are involved in nuclear export, such as Npm1, found to drive nuclear export of ribosomes, as well as ribonucleoproteins itself (unpublished results, Figure 10). Additionally, we identified exportin-2, which mediates importin-α re-export from the nucleus after cargo substrate release into the nucleoplasm as a binding partner of (unpublished results, Figure 12). *In vitro* studies using recombinant ARH3 would reveal whether it is indeed able to demodify the identified targets. Co-IP experiments would additionally show whether ARH3 really binds to exportin-2 and other identified potential binders.

4.5 Cellular function of ARH3

The downregulation or depletion of ARH3 in different cell types has provided opposite data on LPS-induced *iNOS* mRNA expression (unpublished results, Figure 12 and Figure 13). We assume that either ARH3 itself acts as a direct regulator of transcription, or as cofactor of a transcription factor. Genetic complementation experiments overexpressing the WT or catalytic inactive form of ARH3 in an *ARH3* KO context would reveal whether these effects are dependent on the enzymatic

activity of ARH3 or whether ARH3 is an important transcriptional regulator independent of its catalytic activity.

Both shARH3 Raw cells and BMDM from *ARH3* KO mice showed a decreased or complete loss of iNOS activity (unpublished results, Figure 12 and Figure 13). Interestingly, NOS activity has been shown previously to be regulated by conformational changes induced by binding to calmodulin[144]. We hypothesize that ARH3 might either bind iNOS directly or might interfere with binding of other binding partners of iNOS, e.g. upon removal of the ADP-ribose. ADP-ribosylome analysis upon LPS stimulation of shMock and shARH3 RAW cells might reveal whether iNOS itself or potential binding partners are ADP-ribosylated and whether this is dependent on the presence of ARH3. Additionally, direct binding of ARH3 to iNOS could be investigated by co-IP experiments.

RAW cell changed their morphology upon LPS treatment, in particular by flattening their shape, building vacuoles and protruding processes. These changes were more dramatic in shARH3-treated cells compared to shMock (unpublished results, Figure 13) and are in line with already published data, where treatment of RAW cells with LPS caused similar morphological effects[145]. Further investigations are required to address, what function these vacuoles have and how they are regulated by ARH3. As the stimulation of RAW cells was shown to enhance accumulation of triglycerides[146], vacuoles observed in our cells might contain fat, which could be confirmed by checked markers for lipid accumulation, such as oil red staining.

4.6 The functional role of ARH3 at the organismal level

While an initial necropsy of *ARH3* KO and WT mice did not point at specific abnormalities, at 16 weeks of age, we observed female *ARH3* KO mice to be significantly heavier compared to their WT counterparts (unpublished results, Figure 7). Interestingly, ADP-ribosylation has been implicated as a regulator of adipogenesis. ARTD1 inhibition or *ARTD1* KO impaired adipocyte differentiation (i.e. adipogenesis) under a high-fat diet[147]. Moreover, ARTD1 stimulated *in vitro* the differentiation of fibroblasts to adipocytes by binding to and PARylating PPARγ2, leading to PPARγ2-target gene expression and terminal adipocyte differentiation[111]. Consequently, we hypothesize that feeding *ARH3* KO mice with a high-fat diet would further accelerate the phenotype observed under conventional chow diet resulting in

even stronger increased body weight gain and fat content of these mice. ARH3 might directly demodify PPARγ2 and repress PPARγ2-target gene expression, thereby counteracting ARTD1's function and act as a repressor of adipogenesis. Further analyses using the *ARH3* KO mouse and si- or shRNA-mediated knockdown of *ARH3* during *in vitro* differentiation will reveal whether ARH3 is the main player counteracting ARTD1 in the context of adipogenesis. A recent study has linked regulatory T cells (Treg) to adipogenesis in that Tregs were shown to be induced upon high-calorie diet or cold exposure and were necessary to keep the adipose tissue functional[148]. It would be interesting to see how adipose tissue of *ARH3* KO mice would react to these stimuli.

Single gene expression analysis using *ARH3* KO MEFs and fibroblast of different tissues, revealed that ARH3 regulates, besides other genes, also *iNOS* expression, an NF-κB target gene. On the one hand, ARH3 repressed *iNOS* transcription upon LPS treatment in several cell lines (i.e. 3T3 and RAW cells, as well as BMDM and mouse ear fibroblasts), but on the other hand stimulated iNOS catalytic activity (i.e. RAW cells and BMDM) (Figure 13 and Figure 14). This might be due to two independent mechanisms. ARTD1 has been implicated in the regulation of the TLR4-mediated response to LPS via NF-κB[88,109], and considering the MAR and PAR-degrading function of ARH3 and its involvement in *iNOS* regulation, we speculate that ARH3 hydrolyzes ARTD1-mediated ADP-ribosylation in TLR4-mediated LPS signaling. We speculate that in animal models of e.g. LPS-induced septic shock or *Salmonella typhimurium* infection, where *ARTD1* KO mice showed a rather protective (i.e. slow response) phenotypes[106,149], *ARH3* KO mice, due to enhanced ADP-ribosylation levels, might show a stronger and enhanced reaction compared to *ARTD1* KO mice.

4.7 The *ARH3* KO mouse does not phenocopy the PARG KO mouse

Our necropsy of organs and tissues of adult *ARH3* KO mice revealed no major morphological differences. Also, we were only able to detect by Western blotting ARH3 protein in the lymph node and the spleen (Figure 8). Considering the published RNA sequencing data from mice, ARH3 mRNA is ubiquitously expressed, with the highest expression levels in immune cells, e.g. in myeloid progenitor cells and macrophages (biogps.org). This observation fits well with our observation, as these

cell types reside in spleen and lymph nodes, indicating a potential function of ARH3 in immunity. ARH3 protein was not detected with our antibody in the liver, the kidneys, and the heart, indicating that either, our antibody is not specific enough, or that the half-life time of the mRNA or the protein is altered in these organs.

ARH3 KO mice are viable, fertile and do not show any obvious differences from WT mice in the first few weeks after birth. Considering that both ARH3 and PARG localize to the nucleus and both degrade PAR, it seems likely that their KO would lead to similar phenotypic outcomes. Accordingly, it has been reported that a KO mouse missing the nuclear 110 kDa PARG isoform is viable[150]. It would be interesting to test whether a complete KO of nuclear PAR-degrading enzymes, i.e. a double KO of ARH3 and the 110kDa PARG isoform, would be viable. Considering the massive accumulation of PAR expected in these mice, potentially leading to a massive depletion of NAD^+, we would expect these mice to be embryonically lethal. Except for the *ARH1* KO mouse, which is viable, but shows an enhanced occurrence of different tumors compared to WT mice[60], no other model of a mono-ARH has been described so far. Little is known about the *in vivo* degradation of OAADPR, and although mammalian nucleoside diphosphates linked to x (NUDIX) hydrolases as well as macrodomains are known to hydrolase OAADPR *in vitro*, no known NUDIX or macrodomain member has been identified to degrade OAADPR *in vivo,* except for the NUDIX hydrolase Ysa1 from *Saccharomyces cerevisiae*[151].

We reason that *ARH3* KO mice do not show major morphological differences when compared to WT for several reasons. The lack of ARH3 as mono-ADP-ribosylhydrolase, might be compensated by other nuclear mono-ARHs (e.g. macrodomains), while PARG would be able to compensate for the missing PAR hydrolase activity of ARH3. Additionally, considering its potentially restricted expression pattern on the protein level, ARH3 activity might only be physiologically relevant in specific tissues

Data from our and one other group show that a lack of ARH3 in cultured cells leads to enhanced ADP-ribosylation levels (Abplanalp *et al*., submitted manuscript, and[134]), however, data on *ARH3* KO tissue have so far been missing. Own initial mass spectrometric analysis of spleens isolated from WT and *ARH3* KO mice identified under basal levels 40 proteins to be only ADP-ribosylated in the absence of ARH3 (Figure 10). Although there is also an extensive basal ADP-ribosylome observed in

ARH3 KO spleens, the spleen morphology seemed macroscopically not to be affected, indicating that an enhanced basal ADP-ribosylome does not alter the cell fitness drastically, and that organ and tissue function is likely independent of ARH3 enzymatic activity. Moreover, it seems that neither PARG nor any other mono-ADP-ribosylhydrolase would compensate ARH3's function under basal conditions in the mouse. Assuming a potential role of ARH3 in chromatin modeling (see above), it might be that under basal conditions, presence or absence of ARH3 does not functionally contribute in a fully differentiated and developed cell. However, we would assume that upon stress, those mice might suddenly show differences compared to WT (see also above). Different experiments, such as high-fat diet or bacterial challenges as mentioned above, might reveal a pathophysiological role of ARH3.

4.8 Clinical relevance

Based on our submitted and unpublished data ARH3 seems to play a much broader role and has so far been underestimated in various ways. Potentially, the role of ARH3 in both physiological and pathological conditions is more important than so far expected and further studies specifically targeting the aspects described above might help to further elucidate how ARH3 regulates ADP-ribosylation and cellular processes. With a potential function in adipogenesis and the immune response, ARH3 might be an interesting target for therapeutic intervention. Additionally, having in mind that several other MAR erasers as well as ARTD1 are implicated in various cancers, it is not unlikely that ARH3 might plays a role in cancer development as well. Whether ARH3 has an additional role as a structural component, e.g. by being part of protein complexes, fulfilling a function independent of its enzymatic activities needs further analyzed. Dissecting these two possibilities (ARH3 activity vs. ARH3 presence only) could be achieved by genetic complementation of cells with WT and enzymatic ARH3 mutants or by generating mice expressing an inactive ARH3 using CRISPR/Cas9 knockin models.

We observed that ARH3 is inhibited by the known PARG-inhibiting agent tannic acid (Abplanalp *et al.*, submitted manuscript). Several rhodanine-based PARG inhibitors (RBPI) were published to selectively inhibit PARG but not ARH3, whereas adenosine diphosphate (hydroxymethyl)pyrrolidinediol (ADP-HPD) inhibits PARG

and ARH3 PAR-degradation, with a higher affinity for ARH3[152]. To dissect which cellular function of ARH3 depends on its hydrolase activity, it will be crucial and important to develop a specific ARH3 inhibitor. Screening available compound libraries and identifying small molecules against ARH3 *in vitro*, e.g. in radioactivity assays or a cell-based assay using an immunofluorescence readout, could help to identify a potent ARH3 inhibitor. Some of them maybe even inhibit either the PAR-, MAR, or OAADPR-degrading function separately and allow dissecting their contribution in the cellular context.

5 Literature

1. Prabakaran, S., Lippens, G., Steen, H. & Gunawardena, J. Post-translational modification: nature's escape from genetic imprisonment and the basis for dynamic information encoding. *Wiley Interdisciplinary Reviews-Systems Biology and Medicine* **4**, 565-583 (2012).
2. Leung, A.K. Poly(ADP-ribose): An organizer of cellular architecture. *J Cell Biol* **205**, 613-619 (2014).
3. Gupte, R., Liu, Z.Y. & Kraus, W.L. PARPs and ADP-ribosylation: recent advances linking molecular functions to biological outcomes. *Genes Dev* **31**, 101-126 (2017).
4. Chambon, P., Weill, J. & Mandel, P. Nicotinamide mononucleotide activation of new DNA-dependent polyadenylic acid synthesizing nuclear enzyme. *Biochem Biophys Res Commun* **11**, 39-43 (1963).
5. Collier, R.J. & Pappenheimer, A.M., Jr. Studies on the Mode of Action of Diphtheria Toxin. Ii. Effect of Toxin on Amino Acid Incorporation in Cell-Free Systems. *The Journal of experimental medicine* **120**, 1019-39 (1964).
6. Canto, C., Menzies, K.J. & Auwerx, J. NAD(+) Metabolism and the Control of Energy Homeostasis: A Balancing Act between Mitochondria and the Nucleus. *Cell Metabolism* **22**, 31-53 (2015).
7. Sazanov, L.A. A giant molecular proton pump: structure and mechanism of respiratory complex I. *Nat Rev Mol Cell Biol* **16**, 375-88 (2015).
8. Houtkooper, R.H., Canto, C., Wanders, R.J. & Auwerx, J. The Secret Life of NAD(+): An Old Metabolite Controlling New Metabolic Signaling Pathways. *Endocrine Reviews* **31**, 194-223 (2010).
9. Malavasi, F. et al. Evolution and function of the ADP ribosyl cyclase/CD38 gene family in physiology and pathology. *Physiological Reviews* **88**, 841-886 (2008).
10. Dang, W. The controversial world of sirtuins. *Drug discovery today. Technologies* **12**, e9-e17 (2014).
11. Hottiger, M.O., Hassa, P.O., Luscher, B., Schuler, H. & Koch-Nolte, F. Toward a unified nomenclature for mammalian ADP-ribosyltransferases. *Trends Biochem Sci* **35**, 208-19 (2010).
12. Laing, S., Unger, M., Koch-Nolte, F. & Haag, F. ADP-ribosylation of arginine. *Amino Acids* **41**, 257-269 (2011).
13. Glowacki, G. et al. The family of toxin-related ecto-ADP-ribosyltransferases in humans and the mouse. *Protein Sci* **11**, 1657-70 (2002).
14. Vyas, S. et al. Family-wide analysis of poly(ADP-ribose) polymerase activity. *Nat Commun* **5**, 4426 (2014).
15. Schreiber, V., Dantzer, F., Ame, J.-C. & De Murcia, G. Poly(ADP-ribose): novel functions for an old molecule. *Nat Rev Mol Cell Biol* **7**, 517-28 (2006).
16. Butepage, M., Eckei, L., Verheugd, P. & Luscher, B. Intracellular Mono-ADP-Ribosylation in Signaling and Disease. *Cells* **4**, 569-95 (2015).
17. Matic, I., Ahel, I. & Hay, R.T. Reanalysis of phosphoproteomics data uncovers ADP-ribosylation sites. *Nat Methods* **9**, 771-772 (2012).
18. Ogata, N., Ueda, K. & Hayaishi, O. ADP-ribosylation of histone H2B. Identification of glutamic acid residue 2 as the modification site. *J Biol Chem* **255**, 7610-5 (1980).
19. Ogata, N., Ueda, K., Kagamiyama, H. & Hayaishi, O. ADP-ribosylation of histone H1. Identification of glutamic acid residues 2, 14, and the COOH-terminal lysine residue as modification sites. *J Biol Chem* **255**, 7616-20 (1980).
20. Messner, S. et al. PARP1 ADP-ribosylates lysine residues of the core histone tails. *Nucleic Acids Res* **38**, 6350-62 (2010).
21. Rosenthal, F. et al. Macrodomain-containing proteins are new mono-ADP-ribosylhydrolases. *Nat Struct Mol Biol* **20**, 502-7 (2013).
22. Zhang, Y., Wang, J., Ding, M. & Yu, Y. Site-specific characterization of the Asp- and Glu-ADP-ribosylated proteome. *Nat Methods* (2013).
23. Martello, R. et al. Proteome-wide identification of the endogenous ADP-ribosylome of mammalian cells and tissue. *Nature Communications* **in press**(2016).
24. Larsen, S.C. et al. Proteome-Wide Identification of In Vivo ADP-Ribose Acceptor Sites by Liquid Chromatography-Tandem Mass Spectrometry. *Methods Mol Biol* **1608**, 149-162 (2017).
25. Bilan, V., Leutert, M., Nanni, P., Panse, C. & Hottiger, M.O. Combining Higher-Energy Collision Dissociation and Electron-Transfer/Higher-Energy Collision Dissociation

Fragmentation in a Product-Dependent Manner Confidently Assigns Proteomewide ADP-Ribose Acceptor Sites. *Analytical Chemistry* **89**, 1523-1530 (2017).
26. Leidecker, O. et al. Serine is a new target residue for endogenous ADP-ribosylation on histones. *Nature chemical biology* (2016).
27. Bonfiglio, J.J., Colby, T. & Matic, I. Mass spectrometry for serine ADP-ribosylation? Think o-glycosylation! *Nucleic Acids Res* **45**, 6259-6264 (2017).
28. Teloni, F. & Altmeyer, M. Readers of poly(ADP-ribose): designed to be fit for purpose. *Nucleic Acids Res* **44**, 993-1006 (2016).
29. Allen, M.D., Buckle, A.M., Cordell, S.C., Lowe, J. & Bycroft, M. The crystal structure of AF1521 a protein from Archaeoglobus fulgidus with homology to the non-histone domain of macroH2A. *J Mol Biol* **330**, 503-11 (2003).
30. Karras, G. et al. The macro domain is an ADP-ribose binding module. *EMBO J* **24**, 1911-1920 (2005).
31. Han, W., Li, X. & Fu, X. The macro domain protein family: structure, functions, and their potential therapeutic implications. *Mutat Res* **727**, 86-103 (2011).
32. Sharifi, R. et al. Deficiency of terminal ADP-ribose protein glycohydrolase TARG1/C6orf130 in neurodegenerative disease. *EMBO J* **32**, 1225-1237 (2013).
33. Jankevicius, G. et al. A family of macrodomain proteins reverses cellular mono-ADP-ribosylation. *Nat Struct Mol Biol* **20**, 508-514 (2013).
34. Wang, Z. et al. Recognition of the iso-ADP-ribose moiety in poly(ADP-ribose) by WWE domains suggests a general mechanism for poly(ADP-ribosyl)ation-dependent ubiquitination. *Genes Dev* **26**, 235-240 (2012).
35. Aravind, L. The WWE domain: a common interaction module in protein ubiquitination and ADP ribosylation. *Trends Biochem Sci* **26**, 273-5 (2001).
36. Bartolomei, G., Leutert, M., Manzo, M., Baubec, T. & Hottiger, M.O. Analysis of Chromatin ADP-Ribosylation at the Genome-wide Level and at Specific Loci by ADPr-ChAP. *Mol Cell* **61**, 474-485 (2016).
37. Pleschke, J., Kleczkowska, H., Strohm, M. & Althaus, F. Poly(ADP-ribose) binds to specific domains in DNA damage checkpoint proteins. *J Biol Chem* **275**, 40974-80 (2000).
38. Gagné, J.-P. et al. Proteome-wide identification of poly(ADP-ribose) binding proteins and poly(ADP-ribose)-associated protein complexes. *Nucleic Acids Res* **36**, 6959-76 (2008).
39. Eustermann, S. et al. Solution structures of the two PBZ domains from human APLF and their interaction with poly(ADP-ribose). *Nat Struct Mol Biol* **17**, 241-3 (2010).
40. Oberoi, J. et al. Structural basis of poly(ADP-ribose) recognition by the multizinc binding domain of checkpoint with forkhead-associated and RING Domains (CHFR). *J Biol Chem* **285**, 39348-58 (2010).
41. Ahel, I. et al. Poly(ADP-ribose)-binding zinc finger motifs in DNA repair/checkpoint proteins. *Nature* **451**, 81-5 (2008).
42. Min, W. et al. Poly(ADP-ribose) binding to Chk1 at stalled replication forks is required for S-phase checkpoint activation. *Nat Commun* **4**(2013).
43. Li, M., Lu, L.Y., Yang, C.Y., Wang, S. & Yu, X. The FHA and BRCT domains recognize ADP-ribosylation during DNA damage response. *Genes Dev* **27**, 1752-68 (2013).
44. Loerch, S. & Kielkopf, C.L. Dividing and Conquering the Family of RNA Recognition Motifs: A Representative Case Based on hnRNP L. *J Mol Biol* **427**, 2997-3000 (2015).
45. Shepard, P.J. & Hertel, K.J. The SR protein family. *Genome biology* **10**, 242 (2009).
46. Thandapani, P., O'Connor, T.R., Bailey, T.L. & Richard, S. Defining the RGG/RG Motif. *Mol Cell* **50**, 613-623 (2013).
47. Flynn, R.L. & Zou, L. Oligonucleotide/oligosaccharide-binding fold proteins: a growing family of genome guardians. *Critical reviews in biochemistry and molecular biology* **45**, 266-75 (2010).
48. Zhang, F., Shi, J., Chen, S.H., Bian, C. & Yu, X. The PIN domain of EXO1 recognizes poly(ADP-ribose) in DNA damage response. *Nucleic Acids Res* **43**, 10782-94 (2015).
49. Barkauskaite, E., Jankevicius, G., Ladurner, A.G., Ahel, I. & Timinszky, G. The recognition and removal of cellular poly(ADP-ribose) signals. *FEBS J* **280**, 3491-3507 (2013).
50. Moss, J., Jacobson, M.K. & Stanley, S.J. Reversibility of arginine-specific mono(ADP-ribosyl)ation: identification in erythrocytes of an ADP-ribose-L-arginine cleavage enzyme. *Proc Natl Acad Sci USA* **82**, 5603-7 (1985).
51. Moss, J., Oppenheimer, N.J., West, R.E., Jr. & Stanley, S.J. Amino acid specific ADP-ribosylation: substrate specificity of an ADP-ribosylarginine hydrolase from turkey erythrocytes. *Biochemistry* **25**, 5408-14 (1986).

52. Pope, M.R., Murrell, S.A. & Ludden, P.W. Covalent Modification of the Iron Protein of Nitrogenase from Rhodospirillum-Rubrum by Adenosine Diphosphoribosylation of a Specific Arginine Residue. *Proc Natl Acad Sci U S A* **82**, 3173-3177 (1985).
53. Saari, L.L., Triplett, E.W. & Ludden, P.W. Purification and Properties of the Activating Enzyme for Iron Protein of Nitrogenase from the Photosynthetic Bacterium Rhodospirillum-Rubrum. *Journal of Biological Chemistry* **259**, 5502-5508 (1984).
54. Moss, J. et al. Molecular and immunological characterization of ADP-ribosylarginine hydrolases. *J Biol Chem* **267**, 10481-8 (1992).
55. Ono, T., Kasamatsu, A., Oka, S. & Moss, J. The 39-kDa poly(ADP-ribose) glycohydrolase ARH3 hydrolyzes O-acetyl-ADP-ribose, a product of the Sir2 family of acetyl-histone deacetylases. *Proc Natl Acad Sci U S A* **103**, 16687-91 (2006).
56. Oka, S., Kato, J. & Moss, J. Identification and characterization of a mammalian 39-kDa poly(ADP-ribose) glycohydrolase. *J Biol Chem* **281**, 705-13 (2006).
57. Konczalik, P. & Moss, J. Identification of critical, conserved vicinal aspartate residues in mammalian and bacterial ADP-ribosylarginine hydrolases. *Journal of Biological Chemistry* **274**, 16736-16740 (1999).
58. Zhu, J., Lv, Y., Han, X., Xu, D. & Han, W. Understanding the differences of the ligand binding/unbinding pathways between phosphorylated and non-phosphorylated ARH1 using molecular dynamics simulations. *Scientific reports* **7**, 12439 (2017).
59. Kato, J., Zhu, J., Liu, C. & Moss, J. Enhanced sensitivity to cholera toxin in ADP-ribosylarginine hydrolase-deficient mice. *Mol Cell Biol* **27**, 5534-43 (2007).
60. Kato, J. et al. ADP-ribosylarginine hydrolase regulates cell proliferation and tumorigenesis. *Cancer Res* **71**, 5327-35 (2011).
61. Kato, J. et al. Mutations of the functional ARH1 allele in tumors from ARH1 heterozygous mice and cells affect ARH1 catalytic activity, cell proliferation and tumorigenesis. *Oncogenesis* **4**, e151 (2015).
62. Smith, S.J. et al. The cardiac-restricted protein ADP-ribosylhydrolase-like 1 is essential for heart chamber outgrowth and acts on muscle actin filament assembly. *Developmental Biology* **416**, 373-388 (2016).
63. Mueller-Dieckmann, C. et al. The structure of human ADP-ribosylhydrolase 3 (ARH3) provides insights into the reversibility of protein ADP-ribosylation. *Proc Natl Acad Sci USA* **103**, 15026-31 (2006).
64. Kasamatsu, A. et al. Hydrolysis of O-acetyl-ADP-ribose isomers by ADP-ribosylhydrolase 3. *J Biol Chem* **286**, 21110-7 (2011).
65. Mashimo, M., Kato, J. & Moss, J. ADP-ribosyl-acceptor hydrolase 3 regulates poly (ADP-ribose) degradation and cell death during oxidative stress. *Proc Natl Acad Sci U S A* **110**, 18964-9 (2013).
66. Niere, M. et al. ADP-ribosylhydrolase 3 (ARH3), not poly(ADP-ribose) glycohydrolase (PARG) isoforms, is responsible for degradation of mitochondrial matrix-associated poly(ADP-ribose). *J Biol Chem* **287**, 16088-16102 (2012).
67. Ovaska, K. et al. Integrative analysis of deep sequencing data identifies estrogen receptor early response genes and links ATAD3B to poor survival in breast cancer. *PLoS computational biology* **9**, e1003100 (2013).
68. Xi, H.Q., Zhao, P. & Han, W.D. Clinicopathological significance and prognostic value of LRP16 expression in colorectal carcinoma. *World journal of gastroenterology* **16**, 1644-8 (2010).
69. Mohseni, M. et al. MACROD2 overexpression mediates estrogen independent growth and tamoxifen resistance in breast cancers. *Proc Natl Acad Sci U S A* **111**, 17606-17611 (2014).
70. Miwa, M. & Sugimura, T. Splitting of the ribose-ribose linkage of poly(adenosine diphosphate-robose) by a calf thymus extract. *J Biol Chem* **246**, 6362-4 (1971).
71. Hatakeyama, K., Nemoto, Y., Ueda, K. & Hayaishi, O. Purification and characterization of poly(ADP-ribose) glycohydrolase. Different modes of action on large and small poly(ADP-ribose). *J Biol Chem* **261**, 14902-11 (1986).
72. Slade, D. et al. The structure and catalytic mechanism of a poly(ADP-ribose) glycohydrolase. *Nature* **477**, 616-20 (2011).
73. Meyer-Ficca, M.L., Meyer, R.G., Coyle, D.L., Jacobson, E.L. & Jacobson, M.K. Human poly(ADP-ribose) glycohydrolase is expressed in alternative splice variants yielding isoforms that localize to different cell compartments. *Exp Cell Res* **297**, 521-32 (2004).
74. Koh, D. et al. Failure to degrade poly(ADP-ribose) causes increased sensitivity to cytotoxicity and early embryonic lethality. *Proc Natl Acad Sci USA* **101**, 17699-704 (2004).

75. Boehler, C. et al. Poly(ADP-ribose) polymerase 3 (PARP3), a newcomer in cellular response to DNA damage and mitotic progression. *Proc Natl Acad Sci USA* **108**, 2783-8 (2011).
76. Beck, C. et al. PARP3 affects the relative contribution of homologous recombination and nonhomologous end-joining pathways. *Nucleic Acids Res* **42**, 5616-5632 (2014).
77. Grundy, G.J. et al. PARP3 is a sensor of nicked nucleosomes and monoribosylates histone H2B(Glu2). *Nat Commun* **7**(2016).
78. Zheng, C.L. et al. Characterization of MVP and VPARP assembly into vault ribonucleoprotein complexes. *Biochem Biophys Res Commun* **326**, 100-107 (2005).
79. Raval-Fernandes, S., Kickhoefer, V.A., Kitchen, C. & Rome, L.H. Increased susceptibility of vault poly(ADP-ribose) polymerase-deficient mice to carcinogen-induced tumorigenesis. *Cancer Res* **65**, 8846-52 (2005).
80. Ikeda, Y. et al. Germline PARP4 mutations in patients with primary thyroid and breast cancers. *Endocrine-related cancer* **23**, 171-179 (2016).
81. Aguiar, R.C., Takeyama, K., He, C., Kreinbrink, K. & Shipp, M.A. B-aggressive lymphoma family proteins have unique domains that modulate transcription and exhibit poly(ADP-ribose) polymerase activity. *J Biol Chem* **280**, 33756-65 (2005).
82. Walford, H.H. & Doherty, T.A. STAT6 and lung inflammation. *JAK-STAT* **2**, e25301 (2013).
83. Goenka, S. & Boothby, M. Selective potentiation of Stat-dependent gene expression by collaborator of Stat6 (CoaSt6), a transcriptional cofactor. *Proc Natl Acad Sci U S A* **103**, 4210-5 (2006).
84. Mehrotra, P. et al. PARP-14 functions as a transcriptional switch for Stat6-dependent gene activation. *J Biol Chem* **286**, 1767-76 (2011).
85. Goenka, S., Cho, S.H. & Boothby, M. Collaborator of Stat6 (CoaSt6)-associated poly(ADP-ribose) polymerase activity modulates Stat6-dependent gene transcription. *J Biol Chem* **282**, 18732-18739 (2007).
86. Yang, C.S. et al. Ubiquitin Modification by the E3 Ligase/ADP-Ribosyltransferase Dtx3L/Parp9. *Mol Cell* **66**, 503-+ (2017).
87. Feijs, K.L. et al. ARTD10 substrate identification on protein microarrays: regulation of GSK3beta by mono-ADP-ribosylation. *Cell communication and signaling : CCS* **11**, 5 (2013).
88. Verheugd, P. et al. Regulation of NF-kappaB signalling by the mono-ADP-ribosyltransferase ARTD10. *Nat Commun* **4**, 1683 (2013).
89. Carter-O'Connell, I. et al. Identifying Family-Member-Specific Targets of Mono-ARTDs by Using a Chemical Genetics Approach. *Cell Reports* **14**, 621-631 (2016).
90. Welsby, I. et al. PARP12, an Interferon-stimulated Gene Involved in the Control of Protein Translation and Inflammation. *Journal of Biological Chemistry* **289**, 26642-26657 (2014).
91. Ma, Q., Baldwin, K.T., Renzelli, A.J., McDaniel, A. & Dong, L.Q. TCDD-inducible poly(ADP-ribose) polymerase: A novel response to 2,3,7,8-tetrachlorodibenzo-p-dioxin. *Biochem Biophys Res Commun* **289**, 499-506 (2001).
92. Ma, Q. Induction and superinduction of 2,3,7,8-tetrachlorodibenzo-p-dioxin-inducible poly(ADP-ribose) polymerase: Role of the aryl hydrocarbon receptor/aryl hydrocarbon receptor nuclear translocator transcription activation domains and a labile transcription repressor. *Archives of Biochemistry and Biophysics* **404**, 309-316 (2002).
93. MacPherson, L. et al. 2,3,7,8-Tetrachlorodibenzo-p-dioxin poly(ADP-ribose) polymerase (TiPARP, ARTD14) is a mono-ADP-ribosyltransferase and repressor of aryl hydrocarbon receptor transactivation. *Nucleic Acids Res* **41**, 1604-1621 (2013).
94. Ahmed, S. et al. Loss of the Mono-ADP-ribosyltransferase, Tiparp, Increases Sensitivity to Dioxin-induced Steatohepatitis and Lethality. *J Biol Chem* **290**, 16824-40 (2015).
95. Jwa, M. & Chang, P. PARP16 is a tail-anchored endoplasmic reticulum protein required for the PERK- and IRE1alpha-mediated unfolded protein response. *Nat Cell Biol* **14**, 1223-1230 (2012).
96. Huang, J.Y., Wang, K., Vermehren-Schmaedick, A., Adelman, J.P. & Cohen, M.S. PARP6 is a Regulator of Hippocampal Dendritic Morphogenesis. *Scientific Reports* **6**(2016).
97. Wang, H.P. et al. Knockdown of PARP6 or survivin promotes cell apoptosis and inhibits cell invasion of colorectal adenocarcinoma cells. *Oncology Reports* **37**, 2245-2251 (2017).
98. Alvarezgonzalez, R. & Jacobson, M.K. Characterization of Polymers of Adenosine-Diphosphate Ribose Generated Invitro and Invivo. *Biochemistry* **26**, 3218-3224 (1987).
99. Dziadkowiec, K.N., Gasiorowska, E., Nowak-Markwitz, E. & Jankowska, A. PARP inhibitors: review of mechanisms of action and BRCA1/2 mutation targeting. *Menopause Review-Przeglad Menopauzalny* **15**, 215-219 (2016).

100. Wei, H.T. & Yu, X.C. Functions of PARylation in DNA Damage Repair Pathways. *Genomics Proteomics & Bioinformatics* **14**, 131-139 (2016).
101. Ali, A.A.E. et al. The zinc-finger domains of PARP1 cooperate to recognize DNA strand breaks. *Nat Struct Mol Biol* **19**, 685-+ (2012).
102. Langelier, M.F., Ruhl, D.D., Planck, J.L., Kraus, W.L. & Pascal, J.M. The Zn3 Domain of Human Poly(ADP-ribose) Polymerase-1 (PARP-1) Functions in Both DNA-dependent Poly(ADP-ribose) Synthesis Activity and Chromatin Compaction. *Journal of Biological Chemistry* **285**, 18877-18887 (2010).
103. Caldecott, K.W. Single-strand break repair and genetic disease. *Nature reviews. Genetics* **9**, 619-31 (2008).
104. Helleday, T. The underlying mechanism for the PARP and BRCA synthetic lethality: clearing up the misunderstandings. *Molecular oncology* **5**, 387-93 (2011).
105. Rouleau, M., Patel, A., Hendzel, M.J., Kaufmann, S.H. & Poirier, G.G. PARP inhibition: PARP1 and beyond. *Nat Rev Cancer* **10**, 293-301 (2010).
106. Liaudet, L. et al. Activation of poly(ADP-Ribose) polymerase-1 is a central mechanism of lipopolysaccharide-induced acute lung inflammation. *American journal of respiratory and critical care medicine* **165**, 372-7 (2002).
107. Rosado, M.M., Bennici, E., Novelli, F. & Pioli, C. Beyond DNA repair, the immunological role of PARP-1 and its siblings. *Immunology* **139**, 428-37 (2013).
108. Hassa, P.O., Buerki, C., Lombardi, C., Imhof, R. & Hottiger, M.O. Transcriptional coactivation of nuclear factor- κ B-dependent gene expression by p300 is regulated by poly(ADP)-ribose polymerase-1. *J Biol Chem* **278**, 45145-53 (2003).
109. Hassa, P.O. et al. Acetylation of poly(ADP-ribose) polymerase-1 by p300/CREB-binding protein regulates coactivation of NF- κ B-dependent transcription. *J Biol Chem* **280**, 40450-64 (2005).
110. Lehmann, M. et al. ARTD1-induced poly-ADP-ribose formation enhances PPARgamma ligand binding and co-factor exchange. *Nucleic Acids Res* **43**, 129-42 (2015).
111. Erener, S., Hesse, M., Kostadinova, R. & Hottiger, M.O. Poly(ADP-ribose)polymerase-1 (PARP1) controls adipogenic gene expression and adipocyte function. *Mol Endocrinol* **26**, 79-86 (2012).
112. Fujiki, K. et al. PPARgamma-induced PARylation promotes local DNA demethylation by production of 5-hydroxymethylcytosine. *Nat Commun* **4**, 2262 (2013).
113. Nie, J. et al. Interaction of Oct-1 and automodification domain of poly(ADP-ribose) synthetase. *FEBS Lett* **424**, 27-32 (1998).
114. Gao, F., Kwon, S.W., Zhao, Y. & Jin, Y. PARP1 poly(ADP-ribosyl)ates Sox2 to control Sox2 protein levels and FGF4 expression during embryonic stem cell differentiation. *J Biol Chem* **284**, 22263-73 (2009).
115. Tulin, A. & Spradling, A. Chromatin loosening by poly(ADP)-ribose polymerase (PARP) at Drosophila puff loci. *Science* **299**, 560-562 (2003).
116. Van Holde, K.E., Sahasrabuddhe, C.G. & Shaw, B.R. A model for particulate structure in chromatin. *Nucleic Acids Res* **1**, 1579-86 (1974).
117. Olins, A.L. & Olins, D.E. Spheroid chromatin units (v bodies). *Science* **183**, 330-2 (1974).
118. Bednar, J. et al. Nucleosomes, linker DNA, and linker histone form a unique structural motif that directs the higher-order folding and compaction of chromatin. *Proc Natl Acad Sci U S A* **95**, 14173-8 (1998).
119. Ou, H.D. et al. ChromEMT: Visualizing 3D chromatin structure and compaction in interphase and mitotic cells. *Science* **357**, 370-+ (2017).
120. Clapier, C.R. & Cairns, B.R. The biology of chromatin remodeling complexes. *Annu Rev Biochem* **78**, 273-304 (2009).
121. Bannister, A.J. & Kouzarides, T. Regulation of chromatin by histone modifications. *Cell research* **21**, 381-95 (2011).
122. Richards, E.J. & Elgin, S.C. Epigenetic codes for heterochromatin formation and silencing: rounding up the usual suspects. *Cell* **108**, 489-500 (2002).
123. Adamietz, P., Bredehorst, R. & Hilz, H. ADP-ribosylated histone H1 from HeLa cultures. Fundamental differences to (ADP-ribose)n-histone H1 conjugates formed into vitro. *Eur J Biochem* **91**, 317-26 (1978).
124. Burzio, L., Riquelme, P. & Koide, S. ADP ribosylation of rat liver nucleosomal core histones. *J Biol Chem* **254**, 3029-37 (1979).
125. Kleine, H. et al. Substrate-assisted catalysis by PARP10 limits its activity to mono-ADP-ribosylation. *Mol Cell* **32**, 57-69 (2008).

126. Rulten, S.L. et al. PARP-3 and APLF function together to accelerate nonhomologous end-joining. *Mol Cell* **41**, 33-45 (2011).
127. Poirier, G., de Murcia, G., Jongstra-Bilen, J., Niedergang, C. & Mandel, P. Poly(ADP-ribosyl)ation of polynucleosomes causes relaxation of chromatin structure. *Proc Natl Acad Sci USA* **79**, 3423-7 (1982).
128. de Murcia, G. et al. Modulation of chromatin superstructure induced by poly(ADP-ribose) synthesis and degradation. *J Biol Chem* **261**, 7011-7017 (1986).
129. Perez-Lamigueiro, M.A. & Alvarez-Gonzalez, R. Polynucleosomal synthesis of poly(ADP-ribose) causes chromatin unfolding as determined by micrococcal nuclease digestion. *Ann N Y Acad Sci* **1030**, 593-8 (2004).
130. Petesch, S.J. & Lis, J.T. Activator-induced spread of poly(ADP-ribose) polymerase promotes nucleosome loss at Hsp70. *Mol Cell* **45**, 64-74 (2012).
131. Bisceglie, L., Bartolomei, G. & Hottiger, M.O. ADP-ribose-specific chromatin-affinity purification for investigating genome-wide or locus-specific chromatin ADP-ribosylation. *Nature protocols* **12**, 1951-1961 (2017).
132. Subbarayan, S., Marimuthu, S.K., Nachimuthu, S.K., Zhang, W. & Subramanian, S. Characterization and cytotoxic activity of apoptosis-inducing pierisin-5 protein from white cabbage butterfly. *International journal of biological macromolecules* **87**, 16-27 (2016).
133. Abplanalp, J. & Hottiger, M.O. Cell fate regulation by chromatin ADP-ribosylation. *Seminars in Cell & Developmental Biology* **63**, 114-122 (2017).
134. Fontana, P. et al. Serine ADP-ribosylation reversal by the hydrolase ARH3. *Elife* **6**(2017).
135. Lu, Y.C., Yeh, W.C. & Ohashi, P.S. LPS/TLR4 signal transduction pathway. *Cytokine* **42**, 145-51 (2008).
136. Thomas, P.D. et al. PANTHER: a library of protein families and subfamilies indexed by function. *Genome research* **13**, 2129-41 (2003).
137. Khersonsky, O. & Tawfik, D.S. Enzyme promiscuity: a mechanistic and evolutionary perspective. *Annu Rev Biochem* **79**, 471-505 (2010).
138. Bonfiglio, J.J. et al. Serine ADP-Ribosylation Depends on HPF1. *Mol Cell* **65**, 932-+ (2017).
139. Ansari, N.A., Moinuddin & Ali, R. Glycated lysine residues: a marker for non-enzymatic protein glycation in age-related diseases. *Disease markers* **30**, 317-24 (2011).
140. Thul, P.J. et al. A subcellular map of the human proteome. *Science* **356**(2017).
141. Niere, M., Kernstock, S., Koch-Nolte, F. & Ziegler, M. Functional localization of two poly(ADP-ribose)-degrading enzymes to the mitochondrial matrix. *Mol Cell Biol* **28**, 814-24 (2008).
142. Polioudaki, H. et al. Histones H3/H4 form a tight complex with the inner nuclear membrane protein LBR and heterochromatin protein 1. *EMBO Rep* **2**, 920-925 (2001).
143. Zhao, H.L. et al. PARP1-and CTCF-Mediated Interactions between Active and Repressed Chromatin at the Lamina Promote Oscillating Transcription. *Mol Cell* **59**, 984-997 (2015).
144. Piazza, M., Guillemette, J.G. & Dieckmann, T. Dynamics of nitric oxide synthase-calmodulin interactions at physiological calcium concentrations. *Biochemistry* **54**, 1989-2000 (2015).
145. Roy, S., Bonfield, T. & Tartakoff, A.M. Non-apoptotic toxicity of Pseudomonas aeruginosa toward murine cells. *PLoS ONE* **8**, e54245 (2013).
146. Funk, J.L., Feingold, K.R., Moser, A.H. & Grunfeld, C. Lipopolysaccharide stimulation of RAW 264.7 macrophages induces lipid accumulation and foam cell formation. *Atherosclerosis* **98**, 67-82 (1993).
147. Erener, S. et al. ARTD1 deletion causes increased hepatic lipid accumulation in mice fed a high-fat diet and impairs adipocyte function and differentiation. *FASEB J* **26**, 2631-8 (2012).
148. Kalin, S. et al. A Stat6/Pten Axis Links Regulatory T Cells with Adipose Tissue Function. *Cell metabolism* **26**, 475-492 e7 (2017).
149. Altmeyer, M. et al. Absence of Poly(ADP-Ribose) Polymerase 1 Delays the Onset of Salmonella enterica Serovar Typhimurium-Induced Gut Inflammation. *Infection and Immunity* **78**, 3420-3431 (2010).
150. Cortes, U. et al. Depletion of the 110-kilodalton isoform of poly(ADP-ribose) glycohydrolase increases sensitivity to genotoxic and endotoxic stress in mice. *Mol Cell Biol* **24**, 7163-78 (2004).
151. Tong, L. & Denu, J.M. Function and metabolism of sirtuin metabolite O-acetyl-ADP-ribose. *Biochim Biophys Acta* **1804**, 1617-25 (2010).
152. Finch, K.E., Knezevic, C.E., Nottbohm, A.C., Partlow, K.C. & Hergenrother, P.J. Selective small molecule inhibition of poly(ADP-ribose) glycohydrolase (PARG). *ACS Chem Biol* **7**, 563-70 (2012).

6 Abbreviations

ADP	Adenosine diphosphate
ADP-HPD	Adenosine diphosphate (hydroxymethyl)pyrrolidinediol
AHR	Aryl hydrocarbon receptor
AMP	Adenosine monophosphate
APLF	Aprataxin and PNK-like factor
ARH1	ADP-ribosylarginine hydrolase
ARH3	ADP-ribosylhydrolase 3
ARNT	AHR nuclear translocator
ART	Adenosine diphosphate ribosyltransferases
ARTC	Adenosine diphosphate ribosyltransferase, cholera-toxin like
ARTD	Adenosine diphosphate ribosyltransferases, diphtheria toxin-like
BAL	B-aggressive-lymphoma
bp	Base pair
BRCA1/2	Breast cancer 1/2
BRCT domain	Breast cancer gene 1 C-terminal domain
cADPR	Cyclic adenosine diphosphate ribose
ChAP	Chromatin affinity precipitation
ChIP	Chromatin immunoprecipitation
CHFR	Checkpoint with forkhead and ring finger domains
CHK1	Checkpoint kinase 1
CoaSt6	Collaborator of STAT6
DNA	Deoxyribonucleic acid
DRAG	Dinitrogenase-activating glycohydrolase
DRAT	Dinitrogenase reductase ADP-ribosyltransferase
DSB	Double-strand break
DTT	Dithiothreitol
E	Glutamic acid
EThCD	Electron-transfer/higher-energy collision dissociation
FHA domain	Fork-head associated domain
H	Histidine
H1	Histone 1
H2A	Histone 2A

H2B	Histone 2B
H3	Histone 3
H4	Histone 4
HCD	Higher-energy collision dissociation
HDAC	Histone deacetylase
K	Lysine
LPS	Lipopolysaccharide
MACROD1	Macrodomain containing 1
MACROD2	Macrodomain containing 2
MAR	Mono-ADP-ribose
MARylation	Mono-ADP-ribosylation
MEF	Mouse embryonic fibroblasts
MLF	Mouse lung fibroblasts
mRNA	Messenger ribonucleic acid
MS	Mass spectrometry
MVP	Major vault protein
NA	Nicotinic acid
NAD+	Nicotinamide adenine dinucleotide
NAM	Nicotinamide
NAMPT	Nicotinamide phosphoribosyltransferase
NF-κB	Nuclear factor kappa-light-chain-enhancer of activated B cells
NHEJ	Non-homologous end joining
NMNAT	Nicotinamide mononucleotide adenylyltransferase
NR	Nicotinamide riboside
OAADPR	2'-*O*-acetyl adenosine diphosphate ribose
OB-fold	Oligonucleotide/oligosaccharide-binding fold
PAR	Poly-ADP-ribose
PARG	Poly-ADP-ribose glycohydrolase
PARP	Poly-ADP-ribose polymerase
PARPi	PARP inhibitor
PARylation	Poly-ADP-ribosylation
PBM	Poly-ADP-ribose-binding motif
PBZ	PAR-binding zinc finger

PIN domain	PilT protein N-terminus domain
PPARγ2	peroxisome proliferator-activated receptor 2
PPRE	PPARγ2 response elements
PTM	Post-translational modification
R	Arginine
RBPI	Rhodanine-based PARG inhibitor
RNA	Ribonucleic acid
RRM	RNA recognition motif
S	Serine
shRNA	Short hairpin RNA
siRNA	Small hairpin RNA
SSB	Single-strand break
SUMO	Small ubiquitin-related modifier
TARG	Terminal ADP-ribose glycohydrolase
TCA	Trichloroacetic acid
TCCD	2,3,7,8-Tetrachlorodibenzo-*p*-dioxin
TEP1	Telomerase-associated protein 1
T_H2	T helper cell 2
TLR4	Toll-like receptor 4
UPR	Unfolded protein response
W	Tryptophan
Y	Tyrosine
ZF	Zinc finger

7 Acknowledgements

Firstly, I would like to thank my supervisor, Prof. Dr. Dr. Michael O. Hottiger, for trusting me with a challenging and rewarding PhD project and his constant valuable scientific input. Thanks also to my thesis committee members, Prof. Dr. Petr Cejka, Prof. Dr. Oliver Zerbe and Prof. Dr. Andreas Marx for their help during the course of my PhD. I would like to thank Tobias Suter for his advice and input during thesis and manuscript writing.

Secondly, I thank all our collaborators, which have put a lot of efforts into this project. Especially Emilie Frugier and Prof. Dr. Amedeo Caflisch, for performing *in silico* modeling and stimulating discussions.

Thirdly, I am very thankful for the great work environment at the DMMD, generated by all present and former members. Whether it is for technical help, scientific input, or the non-scientific apéros, poker nights, and after work beers, there was always someone around to count on. A special thank you goes to all the Hottiger lab members, for the nice group trips, the entertaining lunch and coffee breaks, scientific discussions during group meetings and a great lab atmosphere. Very special thanks to Ann-Katrin Hopp and Friedrich Kunze for all their help concerning the mouse experiments, and Vera Bilan, Mario Leutert and Kathrin Nowak for sharing their mass spectrometry expertise with me. Thanks also to my veterinary students, Anne Roentgen and Roxane Feurer, who had the tough task to work with me for their theses. I learned a lot from you!

Lastly, I want to thank my parents for always supporting me, as well as all my friends. You took my mind off work when I needed it, shared laughter with me, and kept me sane during stressful times. Thank you!

8 Curriculum Vitae

Personal Information

Name:	Jeannette Abplanalp
Address:	Leonhard-Ragaz-Weg 6 8055 Zürich
E-mail:	jeannette.abplanalp@dmmd.uzh.ch
Date of birth:	August 15, 1988
Nationality:	Swiss (Innertkirchen, BE) and Danish

Education

PhD program in Molecular Life Science, University of Zurich	2013-2017
Master in Biochemistry, ETH Zurich	2010-2012
Bachelor in Biology, ETH Zurich and ANU Canberra, Australia	2007-2010
High school degree, Gymnasium Interlaken, focus on Latin and philosophy	2004-2007

Professional Experience

University of Zurich — 09.2013 - 12.2017
Department of Molecular Mechanisms of Disease
Doctoral Researcher

Malcisbo AG — 01. - 06.2013
Biopharmaceutical company developing carbohydrate-based vaccines against parasitic and bacterial diseases
Research assistant

ETH Zurich — 09. - 12.2012
Institute of Microbiology
Intern

Publications

Research articles:
Proteomic analyses identify ARH3 as a serine mono-ADP-ribosylhydrolase
Abplanalp J., Leutert M., Frugier E., Feurer R., Kato J., Moss J., Caflisch A. and Hottiger M.O.
under revision

The cataract and glucosuria associated monocarboxylate transporter MCT12 is a new creatine transporter.
Abplanalp J., Laczko E., Philp NJ., Neidhardt J., Zuercher J., Braun P., Schorderet D.F., Munier F.L., Verrey F., Berger W., Camargo S.M., Kloeckener-Gruissem B., Hum Mol Genet. 2013

Book chapter:
Mono-ADP-ribosylhydrolase assays
Abplanalp J.*, Hopp A.K.* and Hottiger M.O.
* equal contribution
under revision

Review:
Cell fate regulation by chromatin ADP-ribosylation.
Abplanalp J. and M.O. Hottiger, Semin Cell Dev Biol. 2017
